KEK preprint 99-69
KEK-TH-639
August 1999
H

Muon Decay and Physics Beyond the Standard Model

Yoshitaka Kuno* and Yasuhiro Okada†
Institute of Particle and Nuclear Studies (IPNS),
High Energy Accelerator Research Organization (KEK),
Tsukuba, Ibaraki, Japan 305-0801

arXiv:hep-ph/9909265 v1 6 Sep 1999

Abstract

This article reviews the current theoretical and experimental status of the field of muon decay and its potential to search for new physics beyond the Standard Model. The importance of rare muon processes with lepton flavor violation is highly stressed, together with precision measurements of normal muon decay. Recent up-to-date motivations of lepton flavor violation based on supersymmetric models, in particular supersymmetric grand unified theories, are described along with other theoretical models. Future prospects of experiments and muon sources of high intensity for further progress in this field are also discussed.

submitted to Review of Modern Physics.

*yoshitaka.kuno@kek.jp

†yasuhiro.okada@kek.jp

Contents

I Introduction **4**

II Basic Properties of the Muon in the Standard Model **7**

A Muon in the Standard Model 7
1 The Standard Model 7
2 Interaction of the muon in the Standard Model 9
3 Neutrino mass and mixing 10
B Static properties of the muon 12
1 Mass and lifetime 12
2 Magnetic moment 13
C Decay modes of the muon 14
1 Normal muon decay 14
2 Radiative muon decay 17

III Lepton Flavor Violation and Physics beyond the Standard Model **20**

A Effective Lagrangians for lepton flavor violating processes 20
B Supersymmetric models 22
1 Introduction to supersymmetric models 22
2 Flavor problems in supersymmetric models 24
3 SUSY GUT and lepton flavor violation 25
4 Supersymmetric models with a right-handed neutrino 29
5 Other supersymmetric models 30
6 LFV in slepton production and decay 30
C Other theoretical models 31
1 Models with a massive neutrino 31
2 Models with a doubly charged Higgs 32
3 Supersymmetric models with R-parity violation 32
4 Models with Z' 33
5 Models with Lorentz non-invariance 33
D Lepton flavor violation with Polarized Muons 33
E $|\Delta L_i| = 2$ processes 34

IV Normal Muon Decay **37**

A Muon lifetime 37
1 Phenomenology 37
2 Experimental status 38
B Michel decay spectrum 39
1 Phenomenology 39
2 Experimental status 39
C Polarization of e^+ in $\mu^+ \to e^+\nu_e\overline{\nu}_\mu$ decay 40
1 Phenomenology 40
2 Experimental status 41

V Lepton Flavor Violating Muon Decays **42**
A $\mu^+ \to e^+\gamma$ decay . . . 42
1 Phenomenology of $\mu^+ \to e^+\gamma$ decay . . . 42
2 Event signature and backgrounds . . . 43
3 Physics background . . . 43
4 Accidental background . . . 44
5 Muon polarization . . . 45
6 Experimental status of $\mu^+ \to e^+\gamma$ decay . . . 47
B $\mu^+ \to e^+e^+e^-$ decay . . . 48
1 Phenomenology of $\mu^+ \to e^+e^+e^-$ decay . . . 48
2 Event signature and backgrounds . . . 50
3 Experimental status of $\mu^+ \to e^+e^+e^-$ decay . . . 50
C $\mu^- - e^-$ coherent conversion in a muonic atom . . . 51
1 Phenomenology of $\mu^- - e^-$ conversion . . . 51
2 Event signature and backgrounds . . . 56
3 Muon decay in orbit . . . 57
4 Experimental status of $\mu^- - e^-$ conversion . . . 58
D $\mu^- - e^+$ conversion in a muonic atom . . . 60
1 Phenomenology of $\mu^- - e^+$ conversion . . . 60
2 Event signature and backgrounds . . . 60
3 Experimental status of $\mu^- - e^+$ conversion . . . 61
E Muonium to anti-muonium conversion . . . 61
1 Phenomenology of $\mathrm{Mu} - \overline{\mathrm{Mu}}$ conversion . . . 61
2 Event signature and backgrounds . . . 63
3 Experimental status of $\mathrm{Mu} - \overline{\mathrm{Mu}}$ conversion . . . 63

VI Future Prospects **65**
A Towards new high-intensity muon sources . . . 65

VII Conclusions **68**

APPENDIXES **70**

A Radiative Muon Decay **70**

B MSSM Lagrangian **70**

C Differential Branching Ratio of the $\mu^+ \to e^+e^+e^-$ Decay **72**

I. INTRODUCTION

The muon was discovered in 1937 by Neddermeyer and Anderson (Neddermeyer and Anderson, 1937) in cosmic rays. The mass of the muon was found to be about 200 times the mass of the electron. The discovery was made just after Yukawa postulated the existence of the π meson, a force carrier of the strong interaction, in 1935 (Yukawa, 1935). But, it was demonstrated in 1947 that the muon did not react through the strong interaction, and thus it could not be the Yukawa π meson (Conversi, *et al.*, 1947). The famous comment by Rabi "Who ordered that ?" might indicate how puzzling the existence of a new lepton was at that time. By then, it was known that the muon decays into an electron and a neutral particle. It was thought that if the muon were a heavy electron, it would also decay into an electron and a γ-ray. The first search for $\mu^+ \to e^+\gamma$ was made by Hincks and Pontecorvo in 1947 using cosmic-ray muons (Hincks and Pontecorvo, 1947). Its negative result set an upper limit of less than 10%. This was the beginning of the search for lepton flavor violation, *i.e.* violation of the lepton number conservation for each generation. In 1948, the continuous spectrum of electrons was established, suggesting a three-body decay with an electron accompanied by two neutral particles (Steinberger, 1948). Soon after, the search for a neutrinoless muon nuclear capture process ($\mu^- N \to e^- N$, where N is a nucleus capturing the muon) was also carried out, but with a negative result (Lagarrigue and Peyrou, 1952). Such searches were significantly improved when muons became artificially produced at accelerators. In 1955, the upper limits of $B(\mu \to e\gamma) < 2 \times 10^{-5}$ (Lokonathan and Steinberger, 1955) and $B(\mu^- Cu \to e^- Cu) < 5 \times 10^{-4}$ (Steinberger and Wolfe, 1955) were set at the Columbia University Nevis cyclotron.

After the discovery of parity violation, it was suggested that the weak interaction takes place through the exchange of charged intermediate vector bosons (Feynman and Gell-Mann, 1958). In 1958, Feinberg pointed out that the intermediate vector boson, if it exists, would lead to $\mu^+ \to e^+\gamma$ at a branching ratio of 10^{-4} (Feinberg, 1958). The absence of any experimental observation of the $\mu^+ \to e^+\gamma$ process with $B(\mu \to e\gamma) < 2 \times 10^{-5}$ led directly to the two-neutrino hypothesis (Nishijima, 1957; Schwinger, 1957) in which the neutrino coupled to the muon is different from that coupled to the electron, and the $\mu^+ \to e^+\gamma$ process would be forbidden. The two-neutrino hypothesis was verified experimentally at Brookhaven National Laboratory (BNL) by confirming muon production, but no electron production from the scattering of neutrinos from pion decays (Danby, *et al.*, 1962). This introduced the concept of the separate conservation of lepton flavors, electron number (L_e) and muon number (L_μ).

Our understanding of modern elementary particle physics is based on the Standard Model (SM), which is a gauge theory of the strong and electroweak interactions. The formulation of the SM is based on many theoretical developments of gauge theory in the 1960s and 1970s. Since then, the SM has confronted various experimental tests and has had amazing success in explaining all measurements so far. In the minimal version of the SM, where only one Higgs doublet is included and massless neutrinos are assumed, lepton flavor conservation is an automatic consequence of gauge invariance and the renormalizability of the SM Lagrangian. It is the basis of a natural explanation for the smallness of lepton flavor violation (LFV) in the charged lepton process.

In extensions of the minimal SM, however, LFV could occur from various sources. In

fact, in most cases, new physics or interactions beyond the SM would predict LFV at some level. LFV processes with muons of major interest are such as $\mu^+ \to e^+\gamma$, $\mu^- - e^-$ conversion in a muonic atom ($\mu^- N \to e^- N$), $\mu^+ \to e^+e^+e^-$, and muonium to anti-muonium conversion (Mu$-\overline{\text{Mu}}$ conversion). Historical progress in various LFV searches in muon and kaon decays is shown in Fig.1, in which the experimental upper limits have been continuously improved at a rate of about two orders of magnitude per decade for about 50 years since the first LFV experiment by Hincks and Pontecorvo. The current LFV searches with muons have reached a sensitivity on the order of $10^{-12} - 10^{-13}$ in their branching ratios. In general, searches for rare processes could probe new interactions at high energy. For example, in the four fermion interaction, the LFV branching ratios could be scaled by $(m_W/m_X)^4$, where m_X is the mass of an exotic heavy particle responsible for the LFV interaction and m_W is the mass of the W gauge boson. Thus, the present sensitivities for LFV searches in muon decays could explore a mass scale of several 100 TeV, which is not directly accessible by the present accelerators.

Recently, considerable interest in LFV processes has arisen based on supersymmetric (SUSY) extensions to the SM, in particular supersymmetric grand unified theories (SUSY GUT). Since the three gauge coupling constants of the strong, weak, and electromagnetic interactions, which were measured at LEP and SLC, are shown to be consistent with the assumption that they are unified to a single $SU(5)$ gauge coupling constant at the order of 10^{16} GeV scale in SUSY SM, the SUSY GUT model becomes a very attractive candidate for physics beyond the SM. In the SUSY models, in general, there is a new source of flavor mixing in the mass matrices of SUSY partners for leptons and quarks. This will induce LFV processes for charged leptons. The predictions of the branching ratios depend on flavor mixing in the mass matrix of sleptons, which are supersymmetric partners of leptons. In the SUSY-GUT scenario, the flavor mixing in the slepton sector is naturally induced at the GUT scale because leptons and quarks are in the same GUT multiplet (Hall, *et al.*, 1986). It has been shown (Barbieri and Hall, 1994; Barbieri, *et al.*, 1995a) that the surprisingly large top-quark mass determined recently has an impact on calculations of the branching ratios of $\mu^+ \to e^+\gamma$ and $\mu^- - e^-$ conversion in SUSY GUT. The predictions are as large as just one or two orders of magnitude lower than the present experimental limits.

There is considerable evidence for the existence of neutrino masses and their mixing based on the experimental results of the solar neutrino deficit (Cleveland, *et al.*, 1998; Fukuda, *et al.*, 1996; Hampel, *et al.*, 1999; Abdurashitov, *et al.*, 1996; Fukuda, *et al.*, 1998a) and the atmospheric neutrino anomaly (Fukuda, *et al.*, 1998b). Since neutrino oscillations imply that lepton flavor is certainly not conserved, LFV processes in muon decays are also expected to occur. In non-SUSY models, however, the neutrino mixing introduces only small effects on $\mu^+ \to e^+\gamma$. For example, the branching ratio of $\mu^+ \to e^+\gamma$ is on the order of 10^{-50} for a difference of the neutrino mass squared of $\Delta m_\nu^2 \sim 10^{-3}$ eV^2, since it is suppressed by $(\Delta m_\nu^2/m_W^2)^2$ (Petcov, 1977; Bilenky, *et al.*, 1977). The situation changes drastically in SUSY models. In SUSY models with a neutrino-mass generation mechanism of the see-saw type, the Yukawa coupling constants among the Higgs doublet, lepton doublets and right-handed neutrinos could induce large flavor mixing effects in the slepton sector (Borzumati and Masiero, 1986; Hisano, *et al.*, 1998a; Hisano and Nomura, 1999a). The resulting LFV rates can be as large as, or even larger than, the experimental upper bounds, depending on various parameters, especially on the Majorana mass of the right-handed neutrino. In such a case, the same Yukawa coupling constants for the right-handed neutrino are responsible

for both the neutrino oscillation and the LFV processes of charged leptons.

Thus, there are many theoretical scenarios under which the predicted branching ratios for the muon LFV processes can be close to their present experimental upper bounds, and therefore they could be accessible and tested by future experiments.

Experimentally, there has been much progress. First of all, several new experimental results have been obtained using the high-intensity muon beams now available, and on-going and proposed experiments are aiming at further improvements. Furthermore, in the long term, new attempts to create high-intensity muon sources have been initiated, based on the ideas arising from the $\mu^+\mu^-$ collider project. The muon beam intensity aimed at such a new muon source would be about $10^{12} - 10^{13}$ $\mu^{\pm}$/sec, several orders of magnitude higher than that presently available. With this increased muon flux, significant improvements in experimental searches can be anticipated.

In this article, we review the current theoretical and experimental status of the field of muon decay and its potential for new physics beyond the Standard Model. We highly stress the importance of rare LFV processes of muons, especially within the framework of SUSY models. In addition, we cover precision measurements of normal muon decay. There have been many excellent review articles on muon decay and lepton flavor violation (Frankel, 1975; Scheck, 1978; Vergados, 1986; Engfer and Walter, 1986; Depommier, 1987; Van der Schaaf, 1993; Depommier and Leroy, 1995). However, reflecting current renewed interest, this article has been written to bring up to date recent topics on muon decay and physics beyond the SM. The phenomenology and experimental status of some of the important muon processes are described in detail.

This article is organized as follows. In Chapter 2, we give a short summary of the SM and the muon properties within the SM. In Chapter 3, LFV is discussed based on various theoretical models, including the SUSY models. Chapter 4 deals with the current status of precision measurements in normal muon decay, such as the muon lifetime, the Michel decay spectrum and its asymmetry, and e^+ polarization. In Chapter 5, the phenomenology and status of the most recent experiments on various lepton flavor violating muon decay modes, such as $\mu^+ \to e^+\gamma$, $\mu^+ \to e^+e^+e^-$, $\mu^- - e^-$ and $\mu^- - e^+$ conversions in a muonic atom, and $\mathrm{Mu} - \overline{\mathrm{Mu}}$ conversion, are described. In Chapter 6, prospects on future experiments and high-intensity muon sources are briefly discussed. Some useful formulas are collected in the Appendices.

II. BASIC PROPERTIES OF THE MUON IN THE STANDARD MODEL

A. Muon in the Standard Model

1. The Standard Model

The current view of elementary particle physics is based on a gauge theory of quarks and leptons. In the Standard Model (SM), three fundamental interactions, the strong, electromagnetic and weak interactions, are described as a $SU(3)_C \times SU(2)_L \times U(1)_Y$ gauge theory. Quarks and leptons are classified in three generations. The three quarks of $\frac{2}{3}e$ electric charge are the *up* quark (u), *charm* quark (c) and *top* quark (t), and those of $-\frac{1}{3}e$ charge are the *down* quark (d), *strange* quark (s) and *bottom* quark (b). Correspondingly, there are three charged leptons of $-e$ electric charge, electron (e), muon (μ) and tau (τ), and three species of neutrinos of neutral charge are introduced, *i.e.* electron neutrino (ν_e), muon neutrino (ν_μ) and tau neutrino (ν_τ). These six quarks and six leptons are given in Table I.

TABLE I. Quarks and leptons in the Standard Model

Electric charge	1st generation	2nd generation	3rd generation
$\frac{2}{3}e$	u	c	t
$-\frac{1}{3}e$	d	s	b
0	ν_e	ν_μ	ν_τ
-1	e	μ	τ

In the SM, ferminonic fields, gauge fields, and a $SU(2)_L$ doublet Higgs field are introduced as an elementary field. They are listed along with their quantum numbers in Table II, where the $SU(3)_C$, $SU(2)_L$ and $U(1)_Y$ gauge fields are denoted as G_μ, A_μ and B_μ, respectively. The subscripts of L and R represent left-handed and right-handed chirality projections ($P_L \equiv (1-\gamma_5)/2$ and $P_R \equiv (1+\gamma_5)/2$), respectively. H represents the Higgs doublet field. The suffix i ($= 1-3$) for the quark and lepton fields is the generation index. The $SU(2)_L$ doublet fields, such as q_{iL}, l_{iL}, and H, have field components given by

$$q_{iL} = \begin{pmatrix} u_{iL} \\ d_{iL} \end{pmatrix}, \quad l_{iL} = \begin{pmatrix} \nu_{iL} \\ e_{iL} \end{pmatrix}, \quad H = \begin{pmatrix} \phi^+ \\ \phi^0 \end{pmatrix}. \tag{1}$$

The SM Lagrangian, $\mathcal{L}_{SM}$, consists of three parts, which are for the gauge interaction, the Higgs potential, and the Yukawa interaction. It is given as

$$\mathcal{L}_{SM} = \mathcal{L}_{gauge} + \mathcal{L}_{Higgs} + \mathcal{L}_{Yukawa}. \tag{2}$$

The Lagrangian for the gauge interaction, $\mathcal{L}_{gauge}$, is presented by

$$\mathcal{L}_{gauge} = \sum_{SU(3)_C, SU(2)_L, U(1)_Y} F^{(a)}_{\mu\nu} F^{(a)\mu\nu} + \sum_{quarks,\ leptons} i\overline{\psi}_{iL(R)} \gamma^\mu \mathcal{D}_\mu \psi_{iL(R)} + |\mathcal{D}_\mu H|^2, \tag{3}$$

where $F_{\mu\nu}$ is the gauge-field strength, and $\mathcal{D}_\mu$ is a covariant derivative defined as

TABLE II. Quantum numbers of elementary fields in the minimal Standard Model. The $SU(3)_C$, $SU(2)_L$ representation and $U(1)_Y$ charge are given.

	G_μ	A_μ	B_μ	q_{iL}	u_{iR}	d_{iR}	l_{iL}	e_{iR}	H
$SU(3)_C$	**8**	**1**	**1**	**3**	**3**	**3**	**1**	**1**	**1**
$SU(2)_L$	**1**	**3**	**1**	**2**	**1**	**1**	**2**	**1**	**2**
$U(1)_Y$	0	0	0	$\frac{1}{6}$	$\frac{2}{3}$	$-\frac{1}{3}$	$-\frac{1}{2}$	-1	$\frac{1}{2}$

$$\mathcal{D}_\mu = \partial_\mu + ig_s\frac{\lambda^a}{2}G^a_\mu + ig\frac{\tau^a}{2}A^a_\mu + ig'Q_Y B_\mu \tag{4}$$

for the representations with $SU(3)_C$-triplet and $SU(2)_L$-doublet and Q_Y-$U(1)_Y$ charge quantum numbers. g_s, g, and $g^{'}$ are the gauge coupling constants for $SU(3)_C$, $SU(2)_L$, and $U(1)_Y$, respectively. λ^a $(a = 1-8)$ is the Gell-Mann matrix for a $SU(3)$ group, and τ^a $(a = 1-3)$ is the Pauli matrix for a $SU(2)$ group. The terms for a singlet representation for either the $SU(3)_C$ or $SU(2)_L$ gauge groups are absent in the definition of $\mathcal{D}_\mu$.

The Lagrangian for the Higgs potential, $\mathcal{L}_{Higgs}$, is given by

$$\mathcal{L}_{Higgs} = -(-\mu^2|H|^2 + \lambda|H|^4). \tag{5}$$

For $\mu^2 > 0$, the Higgs field develops the following vacuum expectation:

$$< H >= \begin{pmatrix} 0 \\ v/\sqrt{2} \end{pmatrix}, \tag{6}$$

where $v = \mu/\sqrt{\lambda}$ ($\cong$ 246 GeV). The physical Higgs mass is given by $m_H = \sqrt{2\lambda}v$. After electroweak symmetry breaking, the $SU(2)_L$ and $U(1)_Y$ gauge fields form a massless photon, and massive $W^\pm$ and Z^0 bosons. At the tree level, their masses are given as $m_W = \frac{1}{2}gv$ and $m_Z = \frac{1}{2}\sqrt{g^2 + g^{'2}}v$. The SU(3) gauge boson, gluon, remains massless.

The Yukawa interaction part of the Lagrangian is given by

$$\mathcal{L}_{Yukawa} = (y_e)_{ij}H^\dagger\overline{e_i}_R l_{j\,L} + (y_d)_{ij}H^\dagger\overline{d_i}_R q_{j\,L} + (y_u)_{ij}\tilde{H}^\dagger\overline{u_i}_R q_{j\,L} + H.c., \tag{7}$$

where $(y_e)_{ij}$, $(y_d)_{ij}$, and $(y_u)_{ij}$ are the Yukawa coupling constants for the charged leptons, the down-type quarks, and the up-type quarks respectively, and,

$$\tilde{H} = i\tau_2 H^* = \begin{pmatrix} \phi^{0*} \\ -\phi^- \end{pmatrix}. \tag{8}$$

Substituting the vacuum expectation value for the Higgs field, the Yukawa interaction in Eq.(7) generates the mass terms for quarks and leptons, as follows:

$$\mathcal{L}_{mass} = -\left(\overline{e_i}_R(m_e)_{ij}e_{j\,L} + \overline{d_i}_R(m_d)_{ij}d_{j\,L} + \overline{u_i}_R(m_u)_{ij}u_{j\,L}\right) + H.c., \tag{9}$$

where $(m_e)_{ij} = -(y_e)_{ij}(v/\sqrt{2})$, $(m_d)_{ij} = -(y_d)_{ij}(v/\sqrt{2})$ and $(m_u)_{ij} = -(y_u)_{ij}(v/\sqrt{2})$. Each mass matrix is diagonalized by unitary transformations for the left-handed fermions and the

right-handed fermions with the same charge. Since the unitary matrices for the left-handed up-type quark and the left-handed down-type quark are generally different, flavor mixing is induced in the charged weak current interaction for quarks. It is given by

$$\mathcal{L}_{W\overline{q}q} = -\frac{g}{\sqrt{2}}\Big(\overline{u}_{iL}\gamma^{\mu}(V_{CKM})_{ij}d_{jL}W^{+}_{\mu} + \overline{d}_{iL}\gamma^{\mu}(V_{CKM})^{*}_{ji}u_{jL}W^{-}_{\mu}\Big), \tag{10}$$

where the $(V_{CKM})_{ij}$ represents the flavor mixing matrix for the quark sector, *i.e.* Cabibbo-Kobayashi-Maskawa (CKM) matrix (Kobayashi and Maskawa, 1973). In this equation and hereafter, the quark fields are presented in the mass-diagonalized basis.

On the other hand, the charged lepton mass matrix in Eq.(9), equivalently the lepton Yukawa coupling constant, is fully diagonalized by unitary transformations on the lepton doublet fields (l_{iL}) and the lepton singlet fields (e_{jR}). In the mass-diagonalized basis, the charged weak current interaction for leptons remain diagonal, as follows:

$$\mathcal{L}_{W\overline{\nu}e} = -\frac{g}{\sqrt{2}}\Big(\overline{\nu_i}_{L}\gamma^{\mu}e_{iL}W^{+}_{\mu} + \overline{e_i}_{L}\gamma^{\mu}\nu_{iL}W^{-}_{\mu}\Big). \tag{11}$$

In the above basis, the lepton flavors can be defined for each generation, and are thus conserved. They are the electron number (L_e), the muon number (L_μ), and the tau number (L_τ), as defined in Table III.

TABLE III. Assignment of lepton flavors, the electron (L_e), the muon number (L_μ), and the tau number (L_τ).

	e^-	ν_e	μ^-	ν_μ	τ^-	ν_τ	e^+	$\overline{\nu_e}$	μ^+	$\overline{\nu_\mu}$	τ^+	$\overline{\nu_\tau}$
L_e	+1	+1	0	0	0	0	−1	−1	0	0	0	0
L_μ	0	0	+1	+1	0	0	0	0	−1	−1	0	0
L_τ	0	0	0	0	+1	+1	0	0	0	0	−1	−1

2. Interaction of the muon in the Standard Model

At the tree level of the SM Lagrangian, the muon has three gauge interactions, namely those with the photon, the $W^{\pm}$ and Z^0 bosons, and also the Higgs interaction. They are given by

$$\begin{aligned}\mathcal{L} = {} & e\overline{\mu}\gamma^{\mu}\mu A_{\mu} - \frac{g}{\sqrt{2}}(\overline{\nu_{\mu}}_{L}\gamma^{\mu}\mu_{L}W^{+}_{\mu} + \overline{\mu_L}\gamma^{\mu}\nu_{\mu}{}_{L}W^{-}_{\mu}) \\ & - \sqrt{g^2+g'^2}\Big\{\overline{\mu_L}\gamma^{\mu}(-\frac{1}{2}+\sin^2\theta_W)\mu_L + \overline{\mu_R}\gamma^{\mu}\sin^2\theta_W\mu_R\Big\}Z^0_{\mu} - \frac{m_\mu}{v}\overline{\mu}\mu H,\end{aligned} \tag{12}$$

where the Weinberg angle θ_W is defined by $\sin\theta_W \equiv g'/\sqrt{g^2+g'^2}$, and also $e = g\sin\theta_W$ at the tree level. H denotes the physical Higgs boson field. In addition to the electromagnetic interaction, the second and third terms describe, respectively, the charged weak-current interaction mediated by the $W^{\pm}$ boson and the neutral weak-current interaction mediated by the Z^0 boson. The other charged leptons, electron and tau, have the same gauge interaction

as the above, and the coupling constant to the Higgs boson is proportional to their lepton masses.

The muon decay in the SM is described by a charged weak-current interaction mediated by the $W^{\pm}$ gauge boson. The four fermion interaction is given by

$$\mathcal{L}_{Fermi} = -\frac{G_F}{\sqrt{2}}[\overline{\nu_\mu}\gamma^\mu(1-\gamma_5)\mu\overline{e}\gamma_\mu(1-\gamma_5)\nu_e + \overline{\nu_e}\gamma^\mu(1-\gamma_5)e\overline{\mu}\gamma_\mu(1-\gamma_5)\nu_\mu], \tag{13}$$

where G_F is the Fermi coupling constant. At the tree level of the SM, this is given by

$$G_F = \frac{g^2}{4\sqrt{2}m_W^2}, \tag{14}$$

where m_W is the $W^{\pm}$ boson mass. This interaction describes the normal muon decays, $\mu^+ \to e^+\nu_e\overline{\nu}_\mu$ and $\mu^- \to e^-\overline{\nu}_e\nu_\mu$.

Lepton universality is a fundamental property of the gauge interaction. The universality in charged weak currents has been tested from the combination of leptonic and semi-leptonic decays of τ, and leptonic decays of μ, π and K mesons. The constraints on the ratio of the charged weak current coupling constants for electron (g_e) and muon (g_μ) are obtained from the ratios of $B(\tau^- \to e^-\overline{\nu_e}\nu_\tau)/B(\tau^- \to \mu^-\overline{\nu}_\mu\nu_\tau)$ and $B(\pi^- \to e^-\overline{\nu}_e)/B(\pi^- \to \mu^-\overline{\nu}_\mu)$. For the ratio of the charged weak current coupling of tau (g_τ) and g_μ, $\Gamma(\tau^- \to e^-\overline{\nu}_e\nu_\tau)/\Gamma(\tau^- \to \mu^-\overline{\nu}_\mu\nu_\tau)$, $\Gamma(\tau^- \to \nu_\tau\pi^-)/\Gamma(\pi^- \to \mu^-\overline{\nu}_\mu)$ and $\Gamma(\tau^- \to \nu_\tau K^-)/\Gamma(K^- \to \mu^-\overline{\nu}_\mu)$ were used. These ratios give a test of the equality of the relevant coupling constants at the level of 0.1 - 0.5 %, except for those decays involving kaons, where the sensitivity is at the 2% level (Pich, 1997). A similar test can be performed for leptonic decays of the W boson at Tevatron and LEP. A recent measurement of leptonic branching ratios of W gives $B(W \to e\nu) = 10.9 \pm 0.4\%$, $B(W \to \mu\nu) = 10.2 \pm 0.5\%$ and $B(W \to \tau\nu) = 11.3 \pm 0.8\%$ (Particle Data Group, 1998). Thus, the sensitivity for the coupling ratio is a few %. The lepton universality for neutral weak currents has been tested at the Z^0 boson pole. At LEP experiments, the measurements of partial leptonic widths, leptonic forward-backward asymmetries, tau polarization and its angular distributions are sensitive to the vector and axial vector coupling constants for different lepton species. At SLC, the left-right asymmetry and forward-backward left-right asymmetry are also measured using a polarized beam. Lepton universality is now treated at the level of 5-10% for vector couplings and less than 0.2% for axial vector couplings (Pich, 1997). The difference in sensitivity is due to the fact that the lepton vector coupling is very small compared to the axial coupling.

3. Neutrino mass and mixing

Although the minimal SM does not allow massive neutrinos, there is increasing evidence for the masses of neutrinos from the solar-neutrino deficit (Cleveland, *et al.*, 1998; Fukuda, *et al.*, 1996; Hampel, *et al.*, 1999; Abdurashitov, *et al.*, 1996; Fukuda, *et al.*, 1998a) and the atmospheric-neutrino anomaly (Fukuda, *et al.*, 1998b). If the solar-neutrino deficit is explained by neutrino oscillations, the mass-square difference is in the range of $\Delta m_\nu^2 \approx 10^{-6} - 10^{-5}$ eV^2 for the MSW solution (Wolfenstein, 1978; Mikheyev and Smirnov, 1985) or $\Delta m_\nu^2 \approx 10^{-11}$ eV^2 for the vacuum oscillation (or "just-so" oscillation) (Glashow and

Krauss, 1987; Glashow, *et al*, 1999). Also, the atmospheric-neutrino anomaly suggests that the mass-square difference between the muon neutrino and the tau (or sterile) neutrino is on the order of $\Delta m_\nu^2 \approx 10^{-3} - 10^{-2}$ eV^2 (Fukuda, *et al.*, 1998b). In addition, the LSND (Liquid Scintillator Neutrino Detector) experiment has reported the $\overline{\nu}_\mu(\nu_\mu) \rightarrow \overline{\nu}_e(\nu_e)$ oscillation, suggesting $|m_{\nu_\mu}^2 - m_{\nu_e}^2| \approx 10^{-1} - 10^{0}$ eV^2 (Athanassopoulos, *et al.*, 1998), although the KARMEN experiment has seen no evidence of such an oscillation (Eitel, *et al.*, 1999). If neutrino mixing is the true interpretation of the anomalies, the SM must be extended. On the other hand, there are direct upper bounds on the neutrino mass for each species, which is 15 eV/c^2 for the electron neutrino, 170 keV/c^2 for the muon neutrino, and 18.2 MeV/c^2 for the tau neutrino (Particle Data Group, 1998). Recently, improved measurements of the electron neutrino mass have been reported with a much better sensitivity of a few eV/c^2 (Lobashev, 1998; Otten and Weinheimer, 1998).

It is possible to accommodate the Dirac mass terms for the neutrinos if $SU(2)$ singlet fields of the right-handed neutrinos ν_{iR} $(i = 1 - 3)$ are included in the minimal SM field contents. Then, the following interaction can be added to Eq.(7):

$$\mathcal{L}_{\nu_R} = (y_\nu)_{ij} \tilde{H}^\dagger \overline{\nu_i}_R l_{j_L} + H.c., \tag{15}$$

where $(y_\nu)_{ij}$ is the Yukawa coupling for neutrinos. If it is very small, the small masses of neutrinos can be explained. For example, the Yukawa coupling constant should be $O(10^{-11})$ for a neutrino mass of 1 eV/c^2. Note that the total lepton number is conserved in this scenario, whereas the lepton flavor could be generally violated.

A more natural explanation for the small neutrino masses is provided by the "see-saw mechanism" (Yanagida, 1979; Gell-Mann, *et al.*, 1979). In this scenario, the Majorana mass term is also included for the right-handed neutrino,

$$\mathcal{L}_{\nu_R} = (y_\nu)_{ij} \tilde{H}^\dagger \overline{\nu_i}_R l_{j_L} - \frac{1}{2} \overline{\nu_i}_R (M_R)_{ij} \nu_{j_R}^c + H.c., \tag{16}$$

where the charge-conjugation field is defined as $\overline{\psi}^c = -\psi^T C^{-1}$ and the charge-conjugation matrix (C) satisfies $C^{-1}\gamma^\mu C = -\gamma^{\mu T}$. $(M_R)_{ij}$ is the right-handed Majorana neutrino matrix. Substituting the vacuum expectation value for the Higgs field, the neutrino mass terms become

$$\mathcal{L}_{\nu\ mass} = -\frac{1}{2} \left(\overline{(\nu_{iL})^c}\, , \overline{\nu_i}_R \right) \begin{pmatrix} 0 & m_D^T \\ m_D & M_R \end{pmatrix} \begin{pmatrix} \nu_{j_L} \\ (\nu_{j_R})^c \end{pmatrix} + H.c., \tag{17}$$

where the Dirac mass term is $(m_D)_{ij} = -(y_\nu)_{ij}(v/\sqrt{2})$. When the Majorana mass scale is much larger than the Dirac masses, the lighter neutrino masses are given by

$$\mathcal{L}_{\nu\ mass} \approx -\frac{1}{2} \overline{(\nu_{iL})^c} (m_\nu)_{ij} \nu_{jL} + H.c. \tag{18}$$

and

$$m_\nu = m_D^T (M_R)^{-1} m_D. \tag{19}$$

For example, if M_R is 10^{15} GeV and the Dirac mass is in the range of 100 GeV, then the neutrino mass becomes naturally $O(10^{-2})$ eV.

By diagonalization of the charged lepton and neutrino mass matrices, lepton flavor mixing is induced in the charged weak current interaction, as follows:

$$\mathcal{L}_{W\nu e} = -\frac{g}{\sqrt{2}}\left[\overline{\nu_i}_L\gamma^\mu(V_{MNS})^*_{ji}e_{jL}W^+_\mu + \overline{e_i}_L\gamma^\mu(V_{MNS})_{ij}\nu_{jL}W^-_\mu\right], \tag{20}$$

where the $(V_{MNS})_{ij}$ is the flavor mixing matrix for the lepton sector, *i.e.* Maki-Nakagawa-Sakata (MNS) matrix (Maki, *et al.*, 1962). Note that as in the case of quarks, the lepton fields in Eq.(20) are written in the mass-diagonalized basis. The $(V_{MNS})_{ij}$ matrix element represents neutrino mixing which can be studied by neutrino oscillations. For a review on the neutrino mass and mixing, please see other references (Bilenky and Petcov, 1987; Fukugita and Yanagida, 1994; Mohapatra and Pal, 1998; Fisher, Kayser, and McFarland, 1999).

B. Static properties of the muon

1. Mass and lifetime

The mass and lifetime of the muon are the fundamental inputs of the SM. The muon mass is given by (Particle Data Group, 1998)

$$m_\mu = 106.658389(34)\ \text{MeV}. \tag{21}$$

It is derived from the ratio of the muon mass to the electron mass, m_μ/m_e, which is measured in a muonium (μ^+e^- atom) with QED corrections (Cohen and Taylor, 1987).

The experimental value of the muon lifetime is

$$\tau_\mu = 2.19703(4) \times 10^{-6}\ \text{sec}. \tag{22}$$

In the framework of the SM, the muon lifetime (τ_μ) is related to the Fermi coupling constant (G_F), by including QED corrections, as follows (Kinoshita and Sirlin, 1959; Marciano and Sirlin, 1988):

$$\tau_\mu^{-1} = \frac{G_F^2 m_\mu^5}{192\pi^3}F(\frac{m_e^2}{m_\mu^2})(1+\frac{3}{5}\frac{m_\mu^2}{m_W^2})\Big[1+\frac{\alpha(m_\mu)}{2\pi}(\frac{25}{4}-\pi^2)\Big], \tag{23}$$

where $F(x) = 1 - 8x + 8x^3 - x^4 - 12x^2\ln x$. m_μ and m_e are masses of the muon and the electron, respectively. The α value at the m_μ scale, $\alpha(m_\mu)$, is given by

$$\alpha(m_\mu)^{-1} = \alpha^{-1} - \frac{2}{3\pi}\ln\Big(\frac{m_\mu}{m_e}\Big) + \frac{1}{6\pi} \approx 136. \tag{24}$$

From Eq.(23), the Fermi coupling constant of $G_F = 1.16639(1) \times 10^{-5}\text{GeV}^{-2}$ is determined (Particle Data Group, 1998). The higher order two-loop corrections to the muon lifetime have been calculated (Van Ritbergen and Stuart, 1999).

2. Magnetic moment

Since the muon is a Dirac particle, the g factor of its magnetic moment is 2, if radiative corrections are ignored. A deviation from 2, namely $g-2$, is very important to investigate quantum corrections. The present experimental value of $a_\mu = (g_\mu - 2)/2$ is given by (Particle Data Group, 1998)

$$a_\mu^{exp} = 11659230(84) \times 10^{-10} \quad (\pm 7\text{ppm}). \tag{25}$$

A new experiment, E821, is on-going at Brookhaven National Laboratory (BNL) and the experimental error is aimed to be improved by a factor of 20. The result from the first run gives $a_\mu^{exp} = 1165925(15) \times 10^{-9}$ (± 13 ppm) (Carey, *et al.*, 1999a).

Theoretically, this quantity is calculated very precise (Hughes and Kinoshita, 1999). The correction is divided into higher-order QED corrections, hadronic contributions and the electroweak (EW) contributions. A recent update of theoretical calculations for them gives (Czarnecki and Marciano, 1998)

$$a_\mu^{QED} = 11658470.56(0.29) \times 10^{-10}, \tag{26}$$

$$a_\mu^{hadron} = 673.9(6.7) \times 10^{-10}, \tag{27}$$

$$a_\mu^{EW} = 15.1(0.4) \times 10^{-10}. \tag{28}$$

By adding them, the SM prediction is

$$\begin{aligned} a_\mu^{SM} &= a_\mu^{QED} + a_\mu^{hadron} + a_\mu^{EW} \\ &= 11659159.6(6.7) \times 10^{-10}. \end{aligned} \tag{29}$$

The theoretical prediction is in good agreement with the experimental value.

To calculate the QED correction, the fine structure constant is needed as an input. Eq.(26) was estimated by using the fine structure constant obtained from the Quantum Hall effect, which gives $\alpha^{-1}(qH) = 137.03600370(270)$. It is consistent with that determined from the electron anomalous magnetic moments (a_e) by assuming a theoretical evaluation based on the SM. It is $\alpha^{-1}(a_e) = 137.03599959(38)$, where the experimental values of the electron anomalous magnetic moments are $a_{e^-}^{ext} = 1159652188.4(4.3) \times 10^{-12}$ and $a_{e^+}^{ext} = 1159652187.9(4.3) \times 10^{-12}$.

Although the electron $g-2$ factor is better determined than the muon $g-2$ factor, the latter is much more sensitive to short-distance physics. For example, the EW correction to a_e is $O(10^{-14})$ level compared the a_μ^{EW} quoted in Eq.(28). Therefore, the muon $g-2$ experiment is much more important to search for the effects of new physics. For example, the on-going experiment E821 is expected to put very strong constraints on supersymmetric (SUSY) models, since SUSY models could contribute to the muon $g-2$ factor significantly when the slepton, charginos, and neutralinos exist in the mass range of a few hundred GeV (Lopez, *et al.*, 1994; Chattopadhyay and Nath, 1996; Moroi, 1996; Carena, *et al.*, 1997; Gabrielli and Sarid, 1997).

TABLE IV. Decay modes of muons.

Decay mode	Branching ratio	References
$\mu^- \to e^- \overline{\nu}_e \nu_\mu$	$\sim 100\%$	
$\mu^- \to e^- \overline{\nu}_e \nu_\mu \gamma$	$1.4 \pm 0.4\%$ (for $E_\gamma > 10$ MeV)	Crittenden, *et al.* (1961)
$\mu^- \to e^- \overline{\nu}_e \nu_\mu e^+ e^-$	$(3.4 \pm 0.4) \times 10^{-5}$	Bertl, *et al.* (1985)
$\mu^- \to e^- \nu_e \overline{\nu}_\mu$	$< 1.2\%$	Freedman, *et al.* (1993)
$\mu^- \to e^- \gamma$	$< 1.2 \times 10^{-11}$	Brooks, *et al.* (1999)
$\mu^- \to e^- e^- e^+$	$< 1.0 \times 10^{-12}$	Bellgardt, *et al.* (1988)
$\mu^- \to e^- \gamma\gamma$	$< 7.2 \times 10^{-11}$	Bolton, *et al.* (1988)

C. Decay modes of the muon

The measured decay modes of muons are $\mu^- \to e^- \overline{\nu}_e \nu_\mu$ (Michel decay), $\mu^- \to e^- \overline{\nu}_e \nu_\mu \gamma$ (radiative muon decay), and $\mu^- \to e^- \overline{\nu}_e \nu_\mu e^+ e^-$. The branching ratios for these modes and the upper bounds on the other exotic decay modes at 90% confidence level (C.L.) are summarized in Table IV. Although these branching fractions have been measured in experiments with positive muon decays, they are listed for negative muons by assuming CP invariance. Since $\mu^- \to e^- \overline{\nu}_e \nu_\mu \gamma$ cannot be clearly separated from $\mu^- \to e^- \overline{\nu}_e \nu_\mu$ with a soft photon, the branching ratio for the radiative decay is shown for $E_\gamma > 10$ MeV. There is no evidence of lepton flavor violating processes, such as $\mu^- \to e^- \gamma$, $\mu^- \to e^- e^- e^+$ and $\mu^- \to e^- \gamma\gamma$. Also, an upper bound is set for those with $|\Delta L_i| = 2$, such as $\mu^- \to e^- \nu_e \overline{\nu}_\mu$ decay, which is allowed if the lepton flavor is conserved multiplicatively instead of additively.

1. Normal muon decay

In the SM, the normal muon decay is described by the V−A interaction. In extensions to the SM, the energy spectrum of a decay electron (positron), its angular distribution if muons are polarized, and its spin polarization in $\mu^- \to e^- \overline{\nu}_e \nu_\mu$ (or $\mu^+ \to e^+ \nu_e \overline{\nu}_\mu$) decay are sensitive to the type of interaction on muon decays, including new possible interactions besides the V−A interaction. If the general four fermion interactions with no derivatives are assumed, the muon differential decay rate is given with a few parameters by (Fetscher and Gerber, 1998)

$$\frac{d^2\Gamma(\mu^\pm \to e^\pm \nu\overline{\nu})}{dx\, d\cos\theta_e} = \frac{m_\mu}{4\pi^3} W_{e\mu}^4 G_F^2 \sqrt{x^2 - x_0^2} \Big(F_{IS}(x) \pm P_\mu \cos\theta_e F_{AS}(x) \Big) \Big(1 + \vec{P}_e(x, \theta_e) \cdot \hat{\zeta} \Big), \quad (30)$$

where $W_{e\mu} = (m_\mu^2 + m_e^2)/(2m_\mu)$, $x = E_e/W_{e\mu}$ and $x_0 = m_e/W_{e\mu} (= 9.7 \times 10^{-3}) \le x \le 1$. E_e is the energy of the $e^\pm$. m_e and m_μ are the masses of the positron and the muon, respectively. The plus (minus) sign corresponds to $\mu^+(\mu^-)$ decay. θ_e is the angle between the muon polarization ($\vec{P}_\mu$) and the electron (or positron) momentum, and $\hat{\zeta}$ is the directional vector of the measurement of the $e^\pm$ spin polarization. $\vec{P}_e(x, \theta_e)$ is the polarization vector of the $e^\pm$. The functions $F_{IS}(x)$ and $F_{AS}(x)$ are the isotropic and anisotropic parts of the $e^\pm$ energy spectrum, respectively. They are given by

$$F_{IS}(x) = x(1-x) + \frac{2}{9}\rho(4x^2 - 3x - x_0^2) + \eta x_0(1-x), \tag{31}$$

$$F_{AS}(x) = \frac{1}{3}\xi\sqrt{x^2 - x_0^2}\Big[1 - x + \frac{2}{3}\delta(4x - 3 + (\sqrt{1 - x_0^2} - 1))\Big], \tag{32}$$

where ρ, η, ξ, and δ are called Michel parameters (Michel, 1950; Bouchiat and Michel, 1957).

In the SM, these parameters are given as $\rho = \frac{3}{4}$, $\eta = 0$, $\xi = 1$ and $\delta = \frac{3}{4}$. When the electron (positron) polarization is not measured and x_0 is ignored, the differential branching ratio in the SM in Eq.(30) leads to a simple form of

$$\frac{d^2\Gamma(\mu^{\pm} \to e^{\pm}\nu\overline{\nu})}{dx\, d\cos\theta_e} = \frac{m_\mu^5 G_F^2}{192\pi^3} x^2[(3 - 2x) \pm P_\mu \cos\theta_e(2x - 1)]. \tag{33}$$

Fig.2 shows the e^+ energy spectrum in $\mu^+ \to e^+\nu_e\overline{\nu}_\mu$ decay in the SM, for the cases of $\cos\theta = 0$, $\cos\theta_e = +1$, and $\cos\theta_e = -1$ with 100% polarized positive muons. As can be seen, the spectrum is high at $x \approx 1$, and the sign of $e^{\pm}$ asymmetry changes at $x = 1/2$.

If the SM is not assumed, the muon lifetime in Eq.(23) should be replaced by (Scheck, 1978; Fetscher and Gerber, 1995; Pich and Silva, 1995)

$$\tau_\mu^{-1} = \frac{G_F^2 m_\mu^5}{192\pi^3}\Big[F(\frac{m_e^2}{m_\mu^2}) + 4\eta\frac{m_e}{m_\mu}G(\frac{m_e^2}{m_\mu^2}) - \frac{32}{3}(\rho - \frac{3}{4})\frac{m_e^2}{m_\mu^2}(1 - \frac{m_e^4}{m_\mu^4})\Big] \times$$
$$(1 + \frac{3}{5}\frac{m_\mu^2}{m_W^2})[1 + \frac{\alpha(m_\mu)}{2\pi}(\frac{25}{4} - \pi^2)], \tag{34}$$

where $G(x) = 1 + 9x - 9x^2 - x^3 + 6x(1+x)\ln x$. Regarding radiative corrections, since it can be assumed that the SM contribution dominates in the normal muon decay process, those based on the SM, as in Eq.(23), are used. From Eq.(34), the correction from the η parameter is proportional to $O(m_e/m_\mu)$, whereas that from the ρ parameter is very small, in the order of $O(m_e^2/m_\mu^2)$. Since the present experimental accuracy of the η parameter is about 1%, the uncertainty from the η correction is about on the order of 10^{-4} to the estimation of the muon lifetime in the non-SM case.

When the spin polarization of $e^+(e^-)$ in the $\mu^+ \to e^+\nu_e\overline{\nu}_\mu$ ($\mu^- \to e^-\nu_\mu\overline{\nu}_e$) decay is detected, $\vec{P}_e(x, \theta_e)$ in Eq.(30) can be measured. It is given by

$$\vec{P}_e(x, \theta_e) = P_{T1} \cdot \frac{(\vec{z} \times \vec{P}_\mu) \times \vec{z}}{|(\vec{z} \times \vec{P}_\mu) \times \vec{z}|} + P_{T2} \cdot \frac{\vec{z} \times \vec{P}_\mu}{|\vec{z} \times \vec{P}_\mu|} + P_L \cdot \frac{\vec{z}}{|\vec{z}|}, \tag{35}$$

where $\vec{z}$ is the direction of the $e^{\pm}$ momentum, and $\vec{P}_\mu$ is the muon spin polarization. P_L, P_{T1}, and P_{T2} are, respectively, the $e^{\pm}$ polarization component parallel to the $e^{\pm}$ momentum direction, that transverse to the $e^{\pm}$ momentum within the decay plane, and that transverse to the $e^{\pm}$ momentum and normal to the decay plane. A non-zero value of the triple T-odd correction, P_{T2}, would imply violation of time-reversal invariance. They are given by

$$P_{T1}(x, \theta_e) = \frac{P_\mu \sin\theta_e F_{T1}(x)}{F_{IS}(x) \pm P_\mu \cos\theta_e F_{AS}(x)}, \tag{36}$$

$$P_{T2}(x, \theta_e) = \frac{P_\mu \sin\theta_e F_{T2}(x)}{F_{IS}(x) \pm P_\mu \cos\theta_e F_{AS}(x)}, \tag{37}$$

$$P_L(x, \theta_e) = \frac{\pm F_{IP}(x) + P_\mu \cos\theta_e F_{AP}(x)}{F_{IS}(x) \pm P_\mu \cos\theta_e F_{AS}(x)}, \tag{38}$$

TABLE V. Experimental values of some of the Michel decay parameters.

Michel parameter	SM value	Experimental value	Sensitive observables
ρ	3/4	0.7518 ± 0.0026	F_{IS}
η	0	-0.007 ± 0.013	F_{IS} and P_{T1}
δ	3/4	0.7486 ± 0.0038	F_{AS} and P_L
ξ	1	1.0027 ± 0.0084	$F_{AS}^{\dagger}$ and P_L
$\xi^{'}$	1	1.00 ± 0.04	P_L
$\xi^{''}$	1	0.65 ± 0.36	P_L

† Only the product of ξP_{μ} is measured.

where the $\pm$ sign corresponds to $\mu^{\pm}$ decays, and

$$F_{T1}(x) = \frac{1}{12}\left\{-2\Big[\xi^{''} + 12(\rho - \frac{3}{4})\Big](1-x)x_0 - 3\eta(x^2 - x_0^2) + \eta^{''}(-3x^2 + 4x - x_0^2)\right\}, \quad (39)$$

$$F_{T2}(x) = \frac{1}{3}\sqrt{x^2 - x_0^2}\left\{3\frac{\alpha^{'}}{A}(1-x) + 2\frac{\beta^{'}}{A}\sqrt{1 - x_0^2}\right\}, \quad (40)$$

$$F_{IP}(x) = \frac{1}{54}\sqrt{x^2 - x_0^2}\left\{9\xi^{'}(-2x + 2 + \sqrt{1 - x_0^2}) + 4\xi(\delta - \frac{3}{4})(4x - 4 + \sqrt{1 - x_0^2})\right\}, \quad (41)$$

$$F_{AP}(x) = \frac{1}{6}\left\{\xi^{''}(2x^2 - x - x_0^2) + 4(\rho - \frac{3}{4})(4x^2 - 3x - x_0^2) + 2\eta^{''}(1-x)x_0\right\}. \quad (42)$$

where $\xi^{'}$, $\xi^{''}$, $\eta^{''}$, $(\alpha^{'}/A)$, and $(\beta^{'}/A)$ are newly defined Michel parameters (Kinoshita and Sirlin, 1957b; Fetscher and Gerber, 1998). In the SM, $\xi^{'} = \xi^{''} = 1$ and $\eta^{''} = (\alpha^{'}/A) = (\beta^{'}/A) = 0$.

The muon-decay Lagrangian for the general four-fermion couplings with ten complex parameters is expressed as (Fetscher, *et al.*, 1986)

$$\begin{aligned}
\mathcal{L}_{\mu\to e\nu\overline{\nu}} = -\frac{4G_F}{\sqrt{2}}\Big[\; & g_{RR}^S(\overline{e}_R\nu_{eL})(\overline{\nu_{\mu}}_L\mu_R) + g_{RL}^S(\overline{e}_R\nu_{eL})(\overline{\nu_{\mu}}_R\mu_L) \\
& + g_{LR}^S(\overline{e}_L\nu_{eR})(\overline{\nu_{\mu}}_L\mu_R) + g_{LL}^S(\overline{e}_L\nu_{eR})(\overline{\nu_{\mu}}_R\mu_L) \\
& + g_{RR}^V(\overline{e}_R\gamma^{\mu}\nu_{eR})(\overline{\nu_{\mu}}_R\gamma_{\mu}\mu_R) + g_{RL}^V(\overline{e}_R\gamma^{\mu}\nu_{eR})(\overline{\nu_{\mu}}_L\gamma_{\mu}\mu_L) \\
& + g_{LR}^V(\overline{e}_L\gamma^{\mu}\nu_{eL})(\overline{\nu_{\mu}}_R\gamma_{\mu}\mu_R) + g_{LL}^V(\overline{e}_L\gamma^{\mu}\nu_{eL})(\overline{\nu_{\mu}}_L\gamma_{\mu}\mu_L) \\
& + \frac{g_{RL}^T}{2}(\overline{e}_R\sigma^{\mu\nu}\nu_{eL})(\overline{\nu_{\mu}}_R\sigma_{\mu\nu}\mu_L) + \frac{g_{LR}^T}{2}(\overline{e}_L\sigma^{\mu\nu}\nu_{eR})(\overline{\nu_{\mu}}_L\sigma_{\mu\nu}\mu_R) + H.c.\;\Big],
\end{aligned} \quad (43)$$

where there is a normalization condition of

$$\begin{aligned}
\tfrac{1}{4}(|g_{RR}^S|^2 + |g_{LL}^S|^2 + |g_{RL}^S|^2 + |g_{LR}^S|^2) + (|g_{RR}^V|^2 + |g_{LL}^V|^2 + |g_{RL}^V|^2 + |g_{LR}^V|^2) \\
+ 3(|g_{RL}^T|^2 + |g_{LR}^T|^2) = 1.
\end{aligned} \quad (44)$$

Note that in the V$-$A interaction of the SM, $g_{LL}^V = 1$ and all the others are zero.

The Michel decay parameters of ρ, η, ξ and δ are given by

$$\rho = \frac{3}{16}(|g^S_{RR}|^2 + |g^S_{LL}|^2 + |g^S_{RL} - 2g^T_{RL}|^2 + |g^S_{LR} - 2g^T_{LR}|^2) + \frac{3}{4}(|g^V_{RR}|^2 + |g^V_{LL}|^2) \quad (45)$$

$$\eta = \frac{1}{2}Re[g^V_{RR}g^{S*}_{LL} + g^V_{LL}g^{S*}_{RR} + g^V_{RL}(g^{S*}_{LR} + 6g^{T*}_{LR}) + g^V_{LR}(g^{S*}_{RL} + 6g^{T*}_{RL})] \quad (46)$$

$$\xi = \frac{1}{4}(|g^S_{LL}|^2 - |g^S_{RR}|^2) - \frac{1}{4}(|g^S_{LR}|^2 - |g^S_{RL}|^2) + (|g^V_{LL}|^2 - |g^V_{RR}|^2) + 3(|g^V_{LR}|^2 - |g^V_{RL}|^2)$$
$$+5(|g^T_{LR}|^2 - |g^T_{RL}|^2) + 4Re(g^S_{LR}g^{T*}_{RL} - g^S_{RL}g^{T*}_{LR}) \quad (47)$$

$$\xi\delta = \frac{3}{16}(|g^S_{LL}|^2 - |g^S_{RR}|^2 + |g^S_{RL} - 2g^T_{RL}|^2 - |g^S_{LR} - 2g^T_{LR}|^2)) + \frac{3}{4}(|g^V_{LL}|^2 - |g^V_{RR}|^2) \quad (48)$$

Table V summarizes the present knowledge of the Michel decay parameters (Particle Data Group, 1998). Precise measurements of the Michel decay parameters would place constraints on various new physics, which would induce a small deviation from the V−A couplings. The current constraints on the general four-fermion couplings are summarized in Fetscher and Gerber (1998).

Among many theoretical models which can be studied by precise measurements of normal muon decay, one example is the left-right symmetric models of $SU(2)_L \times SU(2)_R \times U(1)$ symmetry (Herczeg, 1986; Langacker and Sankar, 1989). In this model, heavy right-handed gauge bosons (two charged $W^\pm_R$ and one neutral Z') are added. In general, they are mixed with each other, and form mass eigenstates $W^\pm_{1,2}$.

$$\begin{pmatrix} W^\pm_L \\ W^\pm_R \end{pmatrix} = \begin{pmatrix} \cos\zeta & -\sin\zeta \\ e^{i\omega}\sin\zeta & e^{i\omega}\cos\zeta \end{pmatrix} \begin{pmatrix} W^\pm_1 \\ W^\pm_2 \end{pmatrix}, \quad (49)$$

where ζ is a mixing angle, and ω is a CP-violating phase. One of the models is a manifest $SU(2)_L \times SU(2)_R \times U(1)$ model, which has the same gauge couplings and CKM quark mixing matrix elements for both the $SU(2)_L$ and $SU(2)_R$ sectors. It, however, can receive a strong constraint from the $K_L - K_S$ mass difference, yielding a limit of the mass of W_R, $m_R > 1.4$ TeV. The constraint can be much weaker in general cases (Langacker and Sankar, 1989). In the manifest $SU(2)_L \times SU(2)_R \times U(1)$ model, the Michel parameters of ρ and ξ would be related to ζ and the masses of $W^\pm_{1,2}$ as follows:

$$\frac{1}{2}(1 - \frac{4}{3}\rho) = \zeta^2, \quad (50)$$

$$\frac{1}{2}(1 - \xi) = \zeta^2 + (\frac{m_1}{m_2})^4, \quad (51)$$

where $m_{1,2}$ are the masses of $W^\pm_{1,2}$. The direct lower limit for the $W^\pm_2$ mass of $m_2 > 720$ GeV/c^2 is obtained from D0 (Abachi, *et al.*, 1996). Together with the previous measurement of ρ and ξ parameters (Jodidio, *et al.*, 1986), the constraint on the $\zeta - m_R$ plane is given in Fig.3.

2. Radiative muon decay

The spectrum of the radiative muon decay, $\mu^\pm \to e^\pm\nu\overline{\nu}\gamma$, has been calculated by several authors (Kinoshita and Sirlin, 1957a; Fronsdal and Überall, 1959; Eckstein and Pratt, 1959). Within the framework of the V−A interaction, the differential branching ratio of

the radiative muon decay, where final electron (positron) and photon are emitted to energy intervals of dx and dy at solid angles of $d\Omega_e$ and $d\Omega_\gamma$ respectively in the muon rest frame, is expressed by

$$dB(\mu^\pm \to e^\pm \nu\overline{\nu}\gamma) = \frac{\alpha}{64\pi^3}\beta dx\frac{dy}{y}d\Omega_e d\Omega_\gamma[F(x,y,d) \mp \beta\vec{P_\mu}\cdot\hat{p_e}G(x,y,d) \mp \vec{P_\mu}\cdot\hat{p_\gamma}H(x,y,d)]. \tag{52}$$

$\vec{P_\mu}$ is the muon polarization vector; $\vec{p_e}$ and $\vec{p_\gamma}$ are the momenta of an electron (positron) and a photon in the muon rest frame respectively; $\hat{p_e}$ and $\hat{p_\gamma}$ are their unit vectors defined by $\hat{p_e} \equiv \vec{p_e}/|\vec{p_e}|$, $\hat{p_\gamma} \equiv \vec{p_\gamma}/|\vec{p_\gamma}|$ respectively; β is defined as $\beta \equiv |\vec{p_e}|/E_e$; d is given by $d \equiv 1 - \beta\hat{p_e}\cdot\hat{p_\gamma}$; x and y are normalized electron and photon energies, $x = 2E_e/m_\mu$ and $y = 2E_\gamma/m_\mu$ in the muon rest frame. From the four-body kinematics, the ranges of x and y are given by

$$\begin{aligned} 2\sqrt{r} < x < 1 + r \quad for \quad 0 < y \le 1 - \sqrt{r}, \\ (1-y) + r/(1-y) \le x \le 1 + r \quad for \quad 1 - \sqrt{r} < y \le 1 - r, \end{aligned} \tag{53}$$

where $r = (m_e/m_\mu)^2$. $F(x,y,d)$, $G(x,y,d)$ and $H(x,y,d)$ in the SM are given in Appendix A.

The decay probability distribution in the x-y plane is shown in Fig.4. The probability is high for an energetic $e^\pm$ with a soft photon, namely $x \approx 1$ and $y \approx 0$. In the soft-photon limit ($y \to 0$), the distribution has an infrared singularity which is canceled by the radiative correction of the Michel decay.

The photon spectrum is obtained by integrating over the electron (positron) energy and angle variables. By neglecting the terms suppressed by m_e/m_μ, it is given by (Kuno, *et al.*, 1997a)

$$\frac{dB(\mu^\pm \to e^\pm \nu\overline{\nu}\gamma)}{dy\,d\cos\theta_\gamma} = \frac{1}{y}\Big[J_+(y)(1 \pm P_\mu\cos\theta_\gamma) + J_-(y)(1 \mp P_\mu\cos\theta_\gamma)\Big], \tag{54}$$

where $J_+(y)$ and $J_-(y)$ are defined by

$$\begin{aligned} J_+(y) = \frac{\alpha}{6\pi}(1-y)\Big[(3\ln\frac{1-y}{r} - \frac{17}{2}) + (-3\ln\frac{1-y}{r} + 7)(1-y) \\ +(2\ln\frac{1-y}{r} - \frac{13}{3})(1-y)^2\Big], \end{aligned} \tag{55}$$

$$\begin{aligned} J_-(y) = \frac{\alpha}{6\pi}(1-y)^2\Big[(3\ln\frac{1-y}{r} - \frac{93}{12}) + (-4\ln\frac{1-y}{r} + \frac{29}{3})(1-y) \\ +(2\ln\frac{1-y}{r} - \frac{55}{12})(1-y)^2\Big], \end{aligned} \tag{56}$$

and θ_γ is the angle between the muon spin polarization and the photon momentum. The photon spectrum for unpolarized muons is shown in Fig.5. Note that at the maximum photon energy ($y \sim 1$), the photon distribution is approximately given by $(1 + P_\mu\cos\theta_\gamma)$ for the $\mu^+ \to e^+\nu_e\overline{\nu}_\mu\gamma$ decay, because $J_+(y)$ has a first-order term in $(1-y)$, but $J_-(y)$ only contains the second and higher order terms. This fact is important for the suppression of accidental background in a $\mu^+ \to e^+\gamma$ search using polarized muons, as mentioned in Section V A 5.

In generalized interactions, the differential branching ratio of $\mu^{\pm} \to e^{\pm}\nu\overline{\nu}\gamma$ decay has been calculated (Lenard, 1953; Behrends, *et al.*, 1956; Fronsdal and Überall, 1959). Here, the spectra of $e^{\pm}$ and a photon depend not only on the Michel parameters of ρ and δ in the normal muon decay, but also on an additional parameter, $\overline{\eta}$, which should be zero in the V−A interaction in the SM. Also, the asymmetry of $e^{\pm}$ in $\mu^{\pm} \to e^{\pm}\nu\overline{\nu}\gamma$ from polarized muons is parameterized by another parameter, $\xi \cdot \kappa$ (Fetscher and Gerber, 1995). Measurements of these parameters would give additional constraints on the four fermion coupling constants (Eichenberger, *et al.*, 1984). Time-reversal violation in radiative muon decay was also discussed (Pratt, 1958), but it was concluded that the T-odd effects have to include either the $e^{\pm}$ polarization or those terms suppressed by the electron mass.

III. LEPTON FLAVOR VIOLATION AND PHYSICS BEYOND THE STANDARD MODEL

In the minimal SM with vanishing neutrino masses, lepton flavor is conserved separately for each generation. This is not necessarily true if new particles or new interactions beyond the SM are introduced. In this section, we discuss various theoretical models with LFV in the charged-lepton processes. In particular, we mention those in which LFV effects could be large enough to be detected in on-going or future experiments on $\mu^+ \to e^+\gamma$ decay, $\mu^+ \to e^+e^+e^-$ decay, $\mu^- - e^-$ conversion, and other LFV processes. Among the theoretical models which predict observable LFV effects, SUSY models have recently received much attention. In SUSY models, the origin of LFV could be interactions at a very high energy scale, such as the GUT scale or the mass scale of a heavy right-handed Majorana neutrino that appears in the sea-saw mechanism. Searches for rare muon decays, thereby, could provide a hint for physics at a very high energy scale. In the following, we first explain the effective Lagrangians for various muon LFV processes of $|\Delta L_i| = 1$, and then discuss LFV in SUSY models and other theoretical models. Finally, the muon LFV processes with $|\Delta L_i| = 2$ are discussed.

A. Effective Lagrangians for lepton flavor violating processes

The effective Lagrangians for muon LFV processes of $|\Delta L_i| = 1$, such as $\mu^+ \to e^+\gamma$ decay, $\mu^+ \to e^+e^+e^-$ decay, and $\mu^- - e^-$ conversion in a muonic atom, are discussed. Possible LFV contributions can be grouped into two types: photonic interaction and four fermion interaction.

First, the effective Lagrangian for $\mu^+ \to e^+\gamma$ process is given by

$$\mathcal{L}_{\mu\to e\gamma} = -\frac{4G_F}{\sqrt{2}}\Big[m_\mu A_R \overline{\mu_R}\sigma^{\mu\nu} e_L F_{\mu\nu} + m_\mu A_L \overline{\mu_L}\sigma^{\mu\nu} e_R F_{\mu\nu} + H.c.\Big], \tag{57}$$

where A_R and A_L are coupling constants that correspond to $\mu^+ \to e^+_R\gamma$ and $\mu^+ \to e^+_L\gamma$ processes, respectively.

For $\mu^+ \to e^+e^+e^-$ decay and $\mu^- - e^-$ conversion, off-shell photon emission also contributes. The general photonic $\mu - e$ transition amplitude is, then, written as

$$M_{photonic} = -\Big[eA^*_\mu(q)\overline{u}_e(p_e)\Big[(f_{E0}(q^2) + \gamma_5 f_{M0}(q^2))\gamma_\nu(g^{\mu\nu} - \frac{q^\mu q^\nu}{q^2}) + (f_{M1}(q^2) + \gamma_5 f_{E1}(q^2))\frac{i\sigma_{\mu\nu}q^\nu}{m_\mu}\Big]u_\mu(p_\mu)\Big], \tag{58}$$

where p_μ and p_e are the μ^- and e^- four momenta, and $q \equiv p_\mu - p_e$ is the four-momentum transfer. The electromagnetic form factors (f_{E0}, f_{E1}, f_{M0} and f_{M1}) are functions of q^2. For $\mu^+ \to e^+\gamma$ decay, only $f_{E1}(0)$ and $f_{M1}(0)$ can contribute, whereas all of the four form factors could contribute to $\mu^+ \to e^+e^+e^-$ decay and $\mu^- - e^-$ conversion. The coupling constants A_R and A_L are related to the dipole form factors as

$$A_R = -\frac{\sqrt{2}e}{8G_F^2 m_\mu^2}(f_{E1}^*(0) + f_{M1}^*(0)), \tag{59}$$

$$A_L = \frac{\sqrt{2}e}{8G_F^2 m_\mu^2}(f_{E1}^*(0) - f_{M1}^*(0)). \tag{60}$$

The direct four fermion interactions could introduce $\mu^+ \to e^+e^+e^-$ decay and $\mu^- - e^-$ conversion, in addition to the photonic $\mu - e$ transition in Eq.(58). For the $\mu^+ \to e^+e^+e^-$ decay, the general four fermion couplings are given by

$$\begin{aligned}\mathcal{L}_{\mu\to 3e}^{non-photo} = -\frac{4G_F}{\sqrt{2}}\Big[& g_1(\overline{\mu_R}e_L)(\overline{e_R}e_L) + g_2(\overline{\mu_L}e_R)(\overline{e_L}e_R) \\ & + g_3(\overline{\mu_R}\gamma^\mu e_R)(\overline{e_R}\gamma_\mu e_R) + g_4(\overline{\mu_L}\gamma^\mu e_L)(\overline{e_L}\gamma_\mu e_L) \\ & + g_5(\overline{\mu_R}\gamma^\mu e_R)(\overline{e_L}\gamma_\mu e_L) + g_6(\overline{\mu_L}\gamma^\mu e_L)(\overline{e_R}\gamma_\mu e_R) + H.c.\Big],\end{aligned} \tag{61}$$

where the Fierz rearrangement for the four fermion operators is used. For the $\mu^- - e^-$ conversion process, the relevant interactions are written as

$$\begin{aligned}\mathcal{L}_{\mu-e\ conv}^{non-photo} = -\frac{G_F}{\sqrt{2}}\sum_{q=u,d,s\ldots}\Big[& (g_{LS(q)}\overline{e_L}\mu_R + g_{RS(q)}\overline{e_R}\mu_L)\overline{q}q \\ & + (g_{LP(q)}\overline{e_L}\mu_R + g_{RP(q)}\overline{e_R}\mu_L)\overline{q}\gamma_5 q \\ & + (g_{LV(q)}\overline{e_L}\gamma^\mu\mu_L + g_{RV(q)}\overline{e_R}\gamma^\mu\mu_R)\overline{q}\gamma_\mu q \\ & + (g_{LA(q)}\overline{e_L}\gamma^\mu\mu_L + g_{RA(q)}\overline{e_R}\gamma^\mu\mu_R)\overline{q}\gamma_\mu\gamma_5 q \\ & + \frac{1}{2}(g_{LT(q)}\overline{e_L}\sigma^{\mu\nu}\mu_R + g_{RT(q)}\overline{e_R}\sigma^{\mu\nu}\mu_L)\overline{q}\sigma_{\mu\nu}q + H.c.\Big],\end{aligned} \tag{62}$$

where $g_{LX(q)}$ and $g_{RX(q)}$ are the coupling constants for the left-handed and right-handed lepton currents, respectively, and $X = S, P, V, A, T$ represent scalar, pseudoscalar, vector, axial vector, and tensor interactions, respectively. Here, the flavor-changing quark currents are not included. The four fermion coupling constants introduced in Eqs.(61) and (62) are determined by specific contributions in some theoretical models beyond the SM. For examples, they are box diagrams in supersymmetric models, tree diagrams of $Z^{'}$, supersymmetric models with $R-$parity breaking, and others.

The f_{E0} and f_{M0} form factors contribute to off-shell photons and not to real photon emission. Therefore, they vanish in the $q^2 \to 0$ limit. They could be rewritten by

$$f_{E0}(q^2) = \frac{q^2}{m_\mu^2}\tilde{f}_{E0}(q^2), \tag{63}$$

$$f_{M0}(q^2) = \frac{q^2}{m_\mu^2}\tilde{f}_{M0}(q^2), \tag{64}$$

where $\tilde{f}_{E0}(q^2)$ and $\tilde{f}_{M0}(q^2)$ are finite at $q^2 \to 0$. If these transitions are induced by loop diagrams including heavy particles, $\tilde{f}_{E0}(q^2)$ and $\tilde{f}_{M0}(q^2)$ are regarded as slowly varying functions of q^2. One example of such diagrams is shown in Fig.6(a). In such a case, these

form factors could be translated into additional contributions which should be added into the corresponding four-fermion coupling constants in Eqs.(61) and (62). Those additional contributions are

$$\Delta g_3 = \Delta g_5 = \frac{\sqrt{2}}{4G_F}\frac{e^2}{m_\mu^2}(\tilde{f}^*_{E0}(0) + \tilde{f}^*_{M0}(0)), \tag{65}$$

$$\Delta g_4 = \Delta g_6 = \frac{\sqrt{2}}{4G_F}\frac{e^2}{m_\mu^2}(\tilde{f}^*_{E0}(0) - \tilde{f}^*_{M0}(0)), \tag{66}$$

for g_3, g_4, g_5, and g_6, correspondingly, and

$$\Delta g_{LV(u)} = -2\Delta g_{LV(d)} = -\frac{2}{3}\frac{\sqrt{2}}{G_F}\frac{e^2}{m_\mu^2}(\tilde{f}_{E0}(0) + \tilde{f}_{M0}(0)), \tag{67}$$

$$\Delta g_{RV(u)} = -2\Delta g_{RV(d)} = -\frac{2}{3}\frac{\sqrt{2}}{G_F}\frac{e^2}{m_\mu^2}(\tilde{f}_{E0}(0) - \tilde{f}_{M0}(0)), \tag{68}$$

for $g_{LV(u)}$, $g_{LV(d)}$, $g_{RV(u)}$ and $g_{RV(d)}$ respectively.

If these form factors are generated by penguin diagrams with a photon coupled to an internal line of a light fermion, as seen in Fig.6(b), $\tilde{f}_{E0}(q^2)$ and $\tilde{f}_{M0}(q^2)$ have a logarithmic dependence of q^2 that is cut off by the light-fermion mass. Such examples are a model with a doubly charged Higgs boson and the SUSY models with R-parity violation, which are discussed later in Section III C. The logarithmic factor could enhance the rates of $\mu^+ \to e^+e^+e^-$ decay and $\mu^- - e^-$ conversion, but not that of $\mu^+ \to e^+\gamma$ decay.

If $f_{E1}(q^2)$ and $f_{M1}(q^2)$ dominate, the following simple relations among the branching ratios of $\mu^+ \to e^+\gamma$, $\mu^+ \to e^+e^+e^-$ and $\mu^- - e^-$ conversion can be derived:

$$\frac{\Gamma(\mu T_i \to eT_i)}{\Gamma(\mu T_i \to capture)} \simeq \frac{1}{200} B(\mu^+ \to e^+\gamma), \tag{69}$$

$$B(\mu^+ \to e^+e^+e^-) \simeq \frac{1}{160} B(\mu^+ \to e^+\gamma). \tag{70}$$

These relations hold in some models of SUSY GUT, which are discussed in the next subsection. Regarding $\mu^- - e^-$ conversion, more detailed discussions on Eq.(69), including the nuclear dependence, are given in Section V C 1.

B. Supersymmetric models

1. Introduction to supersymmetric models

Phenomenological applications of SUSY theories have been considered since the late 70's in connection with the naturalness problem (or the hierarchy problem) in the SM. The SM model can be regarded as being a low-energy approximation of a more complete theory, and is replaced by this at a high energy scale. Supposing that this high energy scale is close to the Planck scale ($\approx 10^{19}$ GeV), the quadratic divergence appearing in the radiative corrections to the Higgs scalar mass becomes problematic, because a precise fine tuning between the bare mass and the radiative corrections must be necessary to keep the electroweak scale well

below this high energy scale. This problem can be avoided if SUSY is introduced, since the quadratic divergence is canceled between the fermionic and bosonic loop contributions. For general reviews on SUSY models, see other references (Nilles, 1984; Haber and Kane, 1985).

The minimal SUSY extension of the SM is called the minimal supersymmetric Standard Model (MSSM). In MSSM, SUSY partners (which have a different spin by 1/2 from the corresponding ordinary particles) are introduced for each particle in the SM. For quarks and leptons, complex scalar fields, squark ($\tilde{q}$) and slepton ($\tilde{l}$), are introduced. The superpartner of the gauge boson is a gauge fermion (or a gaugino), and that of the Higgs field is called a higgsino($\tilde{H}$). The superpartners of gluon, $SU(2)$ and $U(1)$ gauge bosons are a gluino ($\tilde{G}$), a wino ($\tilde{W}$) and a bino ($\tilde{B}$), respectively. After electroweak symmetry breaking, the wino, bino and higgsino mix with each other and form two charged Dirac fermions, called charginos ($\tilde{\chi}_i^{\pm}$) ($i = 1, 2$), and four Majorana fermions, called neutralinos ($\tilde{\chi}_i^0$) ($i = 1 - 4$). As for the Higgs sector, the SUSY models contain at least two Higgs doublet fields. They are required separately for the mass terms for up-type quarks, and those for down-type quarks and charged leptons to eliminate any possible conflict with SUSY in the Yukawa couplings. The particle contents of the MSSM are listed in Table VI.

TABLE VI. Particle Contents in the MSSM.

Ordinary particles		SUSY particles	
Particle	Spin	Particle	Spin
quark (q)	$\frac{1}{2}$	squark ($\tilde{q}$)	0
lepton (l)	$\frac{1}{2}$	slepton ($\tilde{l}$)	0
gluon (G)	1	gluino ($\tilde{G}$)	$\frac{1}{2}$
$W^{\pm}$, Z^0, γ	1	chargino ($\tilde{\chi}_i^{\pm}$) ($i = 1 - 2$)	$\frac{1}{2}$
Higgs boson ($h, H, A, H^{\pm}$)	0	neutralino ($\tilde{\chi}_i^0$) ($i = 1 - 4$)	$\frac{1}{2}$

The MSSM Lagrangian consists of two parts. They are the SUSY invariant Lagrangian and the soft SUSY-breaking terms, as follows:

$$\mathcal{L} = \mathcal{L}_{SUSY\ inv} + \mathcal{L}_{SUSY\ breaking}, \tag{71}$$

The MSSM Lagrangian is described in more details in Appendix B. One of the important features of the SUSY invariant Lagrangian is that various bosonic and fermionic interactions are related to each other by the requirement of SUSY invariance. For example, the gauge coupling constants appear not only in the covariant derivative, but also in the gaugino-scalar-fermion interactions and the scalar self-couplings.

The ordinary Yukawa coupling constants are included in a scalar function called the superpotential ($W(\phi_i)$). The Lagrangian specified by the superpotential ($\mathcal{L}_{superpotential}$) contains a set of fermionic interactions and scalar potentials, as follows:

$$\mathcal{L}_{superpotential} = -\sum_i |\frac{W(\phi)}{\partial\phi_i}|^2 - \frac{1}{2}\frac{\partial^2 W(\phi)}{\partial\phi_i\partial\phi_j}\overline{(\psi_{iL})^c}\psi_{jL} + H.c., \tag{72}$$

where the scalar field (ϕ_i) and the left-handed Weyl field (ψ_{iL}) form a chiral multiplet of SUSY. The superpotential of the MSSM is given by

$$W_{MSSM} = (y_e)_{ij} H_1 E_i^c L_j + (y_d)_{ij} H_1 D_i^c Q_j + (y_u)_{ij} H_2 U_i^c Q_j - \mu H_1 H_2, \tag{73}$$

where E_i^c and L_i represent the supermultiplets of $SU(2)_L$ lepton singlets and doublets, respectively. Also, Q_i U_i^c and D_i^c are the supermultiplets for quark doublets, up-type quark singlets, and down-type quark singlets, respectively. H_1 and H_2 are two Higgs doublet fields. From this superpotential in Eq.(73), the following Yukawa couplings are induced:

$$\mathcal{L}_{Yukawa} = -\left[(y_e)_{ij} H_1 \overline{e_i}_R l_{jL} + (y_d)_{ij} H_1 \overline{d}_{iR} q_{jL} + (y_u)_{ij} H_2 \overline{u_i}_R q_{jL}\right] + H.c. \tag{74}$$

In addition to Eq.(74), the superpotential in Eq.(73) generates the higgsino mass term, various Yukawa-type couplings, and the three- and four-point scalar couplings, according to Eq.(72).

2. Flavor problems in supersymmetric models

In the MSSM, the masses of superparticles, *i.e.*, squarks, sleptons, and gaugino, are generated by the soft SUSY-breaking mass terms, which are defined as SUSY-breaking terms that do not induce quadratic divergence. In general, the soft SUSY-breaking mass terms become a new source of flavor mixing in the MSSM, which is not necessarily related to the flavor mixing in the Yukawa coupling constant in Eq.(73). For the slepton sector, the soft SUSY-breaking mass terms are given by

$$\mathcal{L}_{soft} = -(m_E^2)_{ij} \tilde{e}^*_{Ri} \tilde{e}_{Rj} - (m_L^2)_{ij} \tilde{l_{Li}}^* \tilde{l_{Lj}} - \{m_0 (A_e)_{ij} H_1 \tilde{e}^*_{Ri} \tilde{l}_{Lj} + H.c.\}, \tag{75}$$

where $(m_E)_{ij}$ and $(m_L)_{ij}$ are the mass matrices for the right-handed sleptons ($\tilde{e}_R$) and left-handed sleptons ($\tilde{l}_L$), respectively; m_0 is a SUSY-breaking parameter and A_e is a dimensionless scalar trilinear coupling matrix.

In the basis where the lepton mass matrix is diagonalized, if there exist non-zero off-diagonal matrix elements in the slepton mass matrix, LFV is introduced. From the diagram in Fig.7, the constraint on the off-diagonal elements on the slepton mass matrix, for instance the $\tilde{\mu} - \tilde{e}$ element ($\Delta m_{\tilde{\mu}\tilde{e}}$), can be placed from the present upper limit of $\mu^+ \to e^+\gamma$ decay as follows:

$$\frac{\Delta m^2_{\tilde{\mu}\tilde{e}}}{m^2_{\tilde{l}}} \lesssim 10^{-3} \left(\frac{m_{\tilde{l}}}{100GeV}\right)^2, \tag{76}$$

where $m_{\tilde{l}}$ is the mass of a slepton. Similar constraints on the squark mass matrix elements are obtained from the flavor-changing neutral current (FCNC) processes in the quark sector. For example, the observed $K^0 - \overline{K}^0$ mixing places constraints that the possible SUSY contribution must be small, resulting in that the squarks in the first and second generations must be degenerate at the level of a few % in the case that the squark mass is a few 100 GeV and that the squark mixing angle is of similar magnitude to the Cabibbo angle. These constraints from LFV and FCNC suggest that there should be a special suppression mechanism on the flavor mixing of sfermions (squarks and sleptons) from the dynamics of SUSY breaking. It is called the SUSY flavor problem.

There are several scenarios to solve the SUSY flavor problem:

- The soft SUSY-breaking mass terms have a universal structure at a very high energy scale, such as the Planck scale ($\approx 10^{19}$ GeV) (*Gravity mediated SUSY breaking scenario*) (Nilles, 1984).

- The SUSY-breaking effects are mediated by the SM gauge interaction so that squarks and sleptons with the same quantum numbers receive the same amount of the soft SUSY-breaking mass terms (*Gauge mediated SUSY breaking scenario*) (Dine and Nelson, 1993; Dine, *et al.*, 1995; Dine, *et al.*, 1996; Giudice and Rattazzi, 1998).

- There is some approximate flavor symmetry which produces nearly degenerate masses for squarks and sleptons, at least for the first two generations (*Flavor Symmetry Scenario*) (Barbieri, *et al.*, 1996).

- Squarks and sleptons can be diagonalized in the same basis as the quarks and lepons (*Alignment Scenario*) (Nir and Seiberg, 1993).

- The squark and slepton masses are heavy enough (10 -100 TeV) to avoid constraints from FCNC and LFV, at least for the sfermions in the first two generations (*Effective SUSY scenario*) (Cohen, *et al.*, 1996).

The minimal supergravity model (SUGRA) is a realization of the first scenario. There are many phenomenological analyses based on the supergravity model. In this model, all squarks and sleptons receive the same magnitudes of the soft SUSY-breaking mass terms through the coupling of supergravity at the Planck scale, so that the mass matrices are diagonal with the same diagonal elements. Therefore, there is neither FCNC nor LFV at that energy scale. This does not necessarily imply that LFV effects should not exist in this scenario. In fact, if there is some interaction which breaks lepton flavor conservation between the Planck ($\approx 10^{19}$ GeV) and the electroweak scales ($\approx 10^2$ GeV), the LFV effect could be induced in the slepton mass matrices through radiative corrections (Hall, *et al.*, 1986). In recent years, it has been noticed that such an effect can induce muon LFV processes at large branching ratios in some models of SUSY GUT (Barbieri and Hall, 1994; Barbieri, *et al.*, 1995a).

3. SUSY GUT and lepton flavor violation

In SUSY GUT (Dimopoulos and Georgi, 1981; Sakai, 1981), the SM gauge groups of $SU(3)_C$, $SU(2)_L$ and $U(1)_Y$ are assumed to be unified by a larger group at a high energy scale. In recent years, SUSY GUT has attracted much attention because the three gauge coupling constants determined at LEP and SLC are consistent with the $SU(5)$ GUT prediction if contributions from SUSY particles are taken into account in the evolution of the coupling constants. The three coupling constants are then unified at 2×10^{16} GeV (Amaldi, *et al.*, 1991; Langacker and Luo, 1991; Ellis, *et al.*, 1991). It suggests that SUSY GUTs with the $SU(5)$ group or other gauge groups which include $SU(5)$ could be a viable candidate of physics beyond the SM.

Let us first discuss how LFV would be induced in $SU(5)$ SUSY GUT. In this model, quarks and leptons are classified in the three generations of $\bar{\mathbf{5}}$ and **10** representations of the

$SU(5)$ group, where the $\bar{\mathbf{5}}$ representation ($\bar{F}_i$) contains d^c_{iL} and l_{iL} and their superpartners, and the **10** representation (T_i) contains q_{iL}, u^c_{iL}, and e^c_{iL} and their superpartners. The Yukawa coupling constants at the GUT scale are determined by the superpotential,

$$W_{SU(5)} = \frac{1}{8}(y_u)_{ij} T_i \cdot T_j \cdot H(5) + (y_d)_{ij} \bar{F}_i \cdot T_j \cdot \bar{H}(5), \tag{77}$$

where $H(5)$ and $\bar{H}(5)$ are two Higgs fields associated with the $\mathbf{5}$ and $\bar{\mathbf{5}}$ representations, respectively. By substituting the fermionic fields for $\bar{F}_i$ and T_i, and also the Higgs boson fields for $H(5)$ and $\bar{H}(5)$, the Yukawa couplings responsible to the quark and lepton masses are obtained. Here, the matrix $(y_u)_{ij}$ corresponds to the Yukawa coupling matrix for the up-type quarks, and $(y_d)_{ij}$ to that for the down-type quarks, and the leptons.

In the minimal supergravity model, all of the scalar partners of the quarks and leptons, namely squarks and sleptons, are assumed to have a common SUSY-breaking mass from the coupling of the gravity interaction. In addition to the mass terms, the scalar triple couplings also have a universal structure so that they are proportional to the corresponding Yukawa coupling constants. At the Planck scale, the soft SUSY-breaking mass terms are given by

$$\mathcal{L}_{soft} = -m_0^2 \{\tilde{T}_i^\dagger \tilde{T}_i + \tilde{\bar{F}}_i^\dagger \tilde{\bar{F}}_i\} - \left[m_0 A_0 \{\frac{1}{8}(y_u)_{ij} \tilde{T}_i \cdot \tilde{T}_j \cdot H(5) + (y_d)_{ij} \tilde{\bar{F}}_i \cdot \tilde{T}_j \cdot \bar{H}(5)\} + H.c. \right], \tag{78}$$

where m_0 is the universal scalar mass, and A_0 is the universal trilinear coupling. At this stage, there is no LFV in the slepton sector. When the lepton Yukawa coupling constants (in this case y_d) are diagonalized by unitary transformations on the bosons and fermions of $\bar{F}_i$ and T_i for each generation indices, the soft SUSY-breaking mass terms for the sleptons can also become diagonal in the same basis. This is no longer true if we take into account the radiative corrections to the soft SUSY-breaking mass terms due to the Yukawa coupling constants. In particular, since the Yukawa coupling constant corresponding to the top-quark mass is surprisingly large, its effects on the soft SUSY-breaking mass terms are expected to be sizeable. In the basis where the matrix of up-type Yukawa coupling constants is diagonal, all members of T_i, including the right-handed slepton masses, are obtained by

$$m_T^2 \simeq \begin{pmatrix} m^2 & & \\ & m^2 & \\ & & m^2 + \Delta m^2 \end{pmatrix} \quad \text{and} \tag{79}$$

$$\Delta m^2 \simeq -\frac{3}{8\pi^2} |(y_u)_{33}|^2 m_0^2 (3 + |A_0|^2) \ln(\frac{M_P}{M_G}), \tag{80}$$

where M_P and M_G denote the reduced Planck mass ($\sim 2 \times 10^{18}$GeV) and the GUT scale ($\sim 2 \times 10^{16}$GeV). Δm^2 arises from the evolution of the renormalization group equation between the Planck and the GUT scales through the diagrams in Fig.8.

Since the physical LFV effect is induced by a mismatch of the lepton and slepton diagonalization, the off-diagonal terms of the slepton mass matrix can be examined in the basis where the Yukawa coupling constant for leptons is diagonalized. If it is diagonalized by

$$V_R y_e V_L^\dagger = diagonal, \tag{81}$$

the off-diagonal elements of the right handed slepton mass matrix in this new basis are given by

$$(m^2_{\tilde{e}_R})_{ij} \simeq -\frac{3}{8\pi^2}(V_R)_{i3}(V_R)^*_{j3}|y_u^{33}|^2 m_0^2(3+|A_0|^2)\ln(\frac{M_P}{M_G}). \tag{82}$$

It becomes a source of $\mu^+ \to e^+\gamma$ decay through the diagrams in Fig.9. If the $SU(5)$ GUT relation for the down-type quark and lepton Yukawa coupling constants given by

$$y_e = y_d^T, \tag{83}$$

is used, V_R is given by the CKM matrix at the GUT scale as

$$(V_R)_{ij} = (V_{CKM}^{GUT})_{ji}, \tag{84}$$

where V_{CKM}^{GUT} can be obtained from the CKM matrix at the electroweak scale by taking into account the effects of running coupling constants from the electroweak to the GUT scales.

The prediction of the branching ratio of $\mu^+ \to e^+\gamma$ decay is presented in Fig.10 for typical SUSY parameters in $SU(5)$ SUSY GUT. The branching ratio reaches the order of 10^{-14} for a slepton mass of a few 100 GeV/c^2.

Some remarks on $SU(5)$ SUSY GUT are presented in the following.

- In the $SU(5)$ SUSY GUT model, LFV appears only in the right-handed slepton sector for small or moderate values of $\tan\beta$, which is defined by the ratio of two Higgs vacuum expectation values as $\tan\beta \equiv < H_2^0 > / < H_1^0 >$. This is because the renormalization effects contribute only to $\tilde{e}_R$, and not to $\tilde{l}_L$. As a result, the helicity of an electron (positron) in LFV processes becomes only right-handed (left-handed). For instance, only $\mu^+ \to e_L^+\gamma$ decay occurs, not $\mu^+ \to e_R^+\gamma$. These two processes can be distinguished when the angular distribution of the $\mu^+ \to e^+\gamma$ signal is measured by using polarized muons.

- There is partial cancellation among the Feynman diagrams which contribute to the $\mu^+ \to e^+\gamma$ amplitudes in the $SU(5)$ SUSY GUT (Hisano, *et al.*, 1997). This cancelation can be seen in Fig.10.

- In Eqs.(82) and (84), the off-diagonal elements of the right-handed slepton mass matrix are determined by the CKM matrix elements. When the favorable values of the CKM matrix elements are used, $|\lambda_\tau| \equiv |(V_R)_{13}(V_R)^*_{23}|$ of $(3-5)\times 10^{-4}$ is obtained. This results from the assumption that all of the Yukawa coupling constants are generated from the superpotential in Eq.(77). However, it is known that this assumption does not yield a realistic mass relation for the down-type quarks and charged leptons in the first and second generations. If higher dimensional terms or different $SU(5)$ representations of Higgs fields are included to remedy this problem, the simple relationship between the slepton mixing matrix and the CKM matrix in Eq.(84) would be lost, and λ_τ would become essentially a free parameter. As a consequence, the predicted branching ratios could be different from those in Fig.10. For example, if $|\lambda_\tau| \approx 10^{-2}$, the branching ratio is enhanced by three orders of magnitude from Fig.10. In addition, for a large $\tan\beta$, a further enhancement can be expected (Arkani-Hamed, *et al.*, 1996a). One example prediction of the $\mu^+ \to e^+\gamma$ branching ratio for a large $\tan\beta$ is shown in Fig.11 (Hisano, *et al.*, 1998b). When the higher dimensional terms are included, the mass

matrix for left-handed sleptons also has off-diagonal elements owing to the large bottom Yukawa coupling constant, and therefore the branching ratio of $\mu^+ \to e^+\gamma$ decay is enhanced by $(m_\tau/m_\mu)^2 \approx 10^2$, just as in the case of $SO(10)$ SUSY GUT discussed below. This enhancement can be seen in the non-minimal case in Fig.11. Furthermore, the destructive interference between the different diagrams in the minimal $SU(5)$ SUSY GUT discussed before may disappear.

- The $\mu^+ \to e^+e^+e^-$ decay and the $\mu^- - e^-$ conversion process receive contributions from the off-shell photon, Z-penguin and box diagrams, in addition to the photonic penguin diagram contributing to the $\mu^+ \to e^+\gamma$ decay. In $SU(5)$ SUSY GUT, the relative magnitudes between different contributions vary over the SUSY parameter space. This implies that the relations in Eqs.(69) and (70) may change for different SUSY input values. The predictions of the $\mu^+ \to e^+e^+e^-$ decay and the $\mu^- - e^-$ conversion in $SU(5)$ SUSY GUT are shown in Figs.12 and 13, respectively.

Large LFV effects are also expected in $SO(10)$ SUSY GUT. In the minimal $SO(10)$ SUSY GUT, the superpotential is given by

$$W_{SO(10)} = \frac{1}{2}(y_u)_{ij}\Psi_i \cdot \Phi_u \cdot \Psi_j + \frac{1}{2}(y_d)_{ij}\Psi_i \cdot \Phi_d \cdot \Psi_j, \tag{85}$$

where Ψ_i is the 16-dimensional representation of SO(10) and Φ_u and Φ_d are two 10-dimensional Higgs fields. In this model, both the left-handed and right-handed sleptons receive LFV effects. In particular, the diagrams shown in Fig.14 give a large contribution to the amplitude of $\mu^+ \to e^+\gamma$ decay because it is proportional to m_τ. Hence, the branching ratio is enhanced by $(m_\tau/m_\mu)^2$ compared to the minimal $SU(5)$ SUSY GUT. Owing to this enhancement, the branching ratios for muon LFV processes can become comparable to the present experimental upper bounds if the slepton mixing matrices are related to the observed CKM matrix elements. The predictions for the branching ratio of $\mu^+ \to e^+\gamma$ decay in $SO(10)$ SUSY GUT are shown in Fig.15. In $SO(10)$ SUSY GUT, since the photon-penguin diagrams dominate in the amplitudes of $\mu^+ \to e^+e^+e^-$ decay and $\mu^- - e^-$ conversion, their predicted branching ratios with respect to $\mu^+ \to e^+\gamma$ decay would follow Eqs.(69) and (70) over a wide SUSY parameter space (Barbieri, *et al.*, 1995a).

The rates of muon LFV processes depend on the structure on the Yukawa coupling constants at the GUT scale. The branching ratios for the muon LFV processes are calculated in various realistic $SO(10)$ SUSY GUT models (Arkani-Hamed, *et al.*, 1996a; Ciafaloni, *et al.*, 1996; Duong, *et al.*, 1996; Gómez and Goldberg, 1996). In the $SO(10)$ SUSY GUT models, the diagrams relevant to the $\mu^+ \to e^+\gamma$ amplitude would induce the electric dipole moments (EDM) of the electron and neutron (Dimopoulos and Hall, 1995). The branching ratios for muon LFV processes are compared with the prediction of EDMs, FCNC processes in the quark sector, and CP violations in B and K meson decays in both the $SU(5)$ and $SO(10)$ SUSY GUT models, and the leptonic signals are shown to be very sensitive to the interaction at the GUT scale (Barbieri, *et al.*, 1995b). The LFV process is also investigated in the breaking pattern of $SO(10) \to SU(3) \times SU_L(2) \times SU_R(2) \times U_{B-L}(1) \to SU(3) \times SU_L(2) \times U_Y(1)$(Deshpande, *et al.*, 1996) and in the $SU(4) \times SU_L(2) \times SU_R(2)$ model without GUT unification (King and Oliveira, 1999).

In some theoretical scenarios in which the mass matrices for squarks and sleptons at very high energy scale are not universal, but have some correlations or alignments with corresponding fermion matrices, it is possible to avoid the SUSY flavor problem and at the same time still have muon LFV branching ratios large enough to be detected. One such realization has been investigated concerning the dynamical alignment mechanism (Rattazzi and Sarid, 1996). An interesting possibility is a class of models based on $U(2)$ flavor symmetry where both the Yukawa coupling constants and the soft SUSY-breaking mass terms are controlled by the same approximate symmetry. In this case, the branching ratio for $\mu^+ \to e^+\gamma$ decay is expected to receive large SUSY contributions (Barbieri, *et al.*, 1996).

4. Supersymmetric models with a right-handed neutrino

A large LFV effect can be expected if the supermultiplets of right-handed Majorana neutrino are included in the SUSY Standard Model (Borzumati and Masiero, 1986). As explained in Section II A 3, the smallness of the neutrino masses can be explained by the see-saw mechanism. To include this see-saw mechanism, part of the lepton sector in the Lagrangian in Eq.(73) is replaced by

$$W_N = (y_e)_{ij} H_1 E_i^c L_j + (y_\nu)_{ij} H_2 N_i L_j + \frac{1}{2}(M_R)_{ij} N_i N_j, \tag{86}$$

where N_i is the right-handed neutrino supermultiplets and $(M_R)_{ij}$ is the Majorana mass matrix, and a new Yukawa coupling constant matrix, y_ν, is introduced. Since there are two Yukawa coupling matrices (y_e and y_ν) in the lepton sector, flavor mixing would arise and lepton flavor would no longer be conserved separately for each generation, just as in the quark sector. In SUSY models with universal soft SUSY-breaking at the Planck scale, the flavor mixing in left-handed sleptons would induce sizeable LFV effects in muon and tau decays through the renormalization effects from the Planck to the Majorana mass scales.

The expected magnitudes of the LFV effects depend on the Yukawa coupling constant and the flavor mixing in the lepton sector. In the basis where the Yukawa coupling constant matrix for charged leptons is diagonalized, the mass matrix of light neutrinos is given by

$$(m_\nu)_{ij} = (y_\nu)_{ki} (M_R^{-1})_{kl} (y_\nu)_{lj} \frac{v^2 \sin^2\beta}{2}, \tag{87}$$

where v is the Higgs vacuum expectation value, and β is the Higgs vacuum angle for the two Higgs doublet. On the other hand, the off-diagonal terms of the left-handed slepton mass matrix induced by the renormalization effect is

$$(m^2_{\tilde{l}_L})_{ij} \simeq -\frac{1}{8\pi^2}(y_\nu)^*_{ki}(y_\nu)_{kj} m_0^2 (3 + |A_0|^2) \ln(\frac{M_P}{M_R}). \tag{88}$$

In general, there is no direct relationship between the neutrino mixing in Eq.(87) and the slepton mixing relevant to $\mu \to e\gamma$, $\tau \to \mu\gamma$ and $\tau \to e\gamma$ in Eq.(88). If, however, we assume that the neutrino mixing mostly originates from the neutrino Yukawa coupling constants, $(y_\nu)_{ij}$, the information from the atmospheric and solar neutrinos can be related to the slepton mixing. Then, the branching ratios for $\mu^+ \to e^+\gamma$ and $\tau \to \mu\gamma$ decays can be evaluated by

using the neutrino mixing parameters (Hisano, *et al.*, 1995; Hisano, *et al.*, 1996; Hisano, *et al.*, 1998a; Hisano and Nomura, 1999a). Fig.16 shows the predicted branching ratio for the $\mu^+ \to e^+\gamma$ decay for different solutions of the solar neutrino mixing. As can be seen in Fig.16, it can reach the present experimental bound for the Majorana mass larger than $O(10^{14})$ GeV if the large-angle MSW solution for the solar-neutrino problem is chosen. It is noted that from Eq.(87), given a fixed value of the light neutrino mass (m_ν), the Yukawa coupling constant (y_ν) becomes larger for a larger value of the Majorana mass scale (M_R), resulting in that the LFV rate becomes larger in Eq.(88). The LFV rates increases approximately as the second power of M_R and, therefore, it could possibly probe the mass scale of the right-handed Majorana neutrino (M_R) in this scenario. Note that this prediction is in contrast to the see-saw mechanism without SUSY, in which the LFV rates for charged leptons are extremely suppressed, as discussed in Section III C.

5. Other supersymmetric models

Observable effects of muon LFV processes may arise through the renormalization effects in the slepton mass matrix. Because these effects may come from anywhere between the Planck and the electroweak scale, it is possible to consider some other interaction at a high energy scale as a new source of LFV.

Such an example is given in the context of the gauge-mediated SUSY breaking. If the mixing between the messenger fields of gauge mediation and the ordinary matter fields is allowed, a sizeable LFV effect can be generated through the renormalization of the slepton mass matrix (Dine, *et al.*, 1997; Dubovsky and Gorbunov, 1998). A similar effect appears in a supersymmetric E_6 type model, where the mixing between the ordinary leptons and the exotic leptons in the E_6 **27** representation could induce a large LFV effect via the slepton mixing (Kitano and Yamomoto, 1999).

6. LFV in slepton production and decay

If the charged sleptons are discovered in experiments at future colliders (like LHC and LC), LFV due to slepton mixing could be directly searched in their production and decay processes (Krasnikov, 1994; Krasnikov, 1996; Arkani-Hamed, *et al.*, 1996b). For example, a process like $e^+e^- \to \tilde{l}^+\tilde{l}^- \to e^\pm\tilde{\chi}_1^0\mu^\mp\tilde{\chi}_1^0$ breaks lepton flavor conservation, where the slepton $\tilde{l}^\pm$ is assumed to decay to a lepton and the neutralino $\tilde{\chi}_1^0$. Direct searches for the $e\mu$ final states in e^+e^- and e^-e^- collisions can probe the slepton-mixing angle between the selectron ($\tilde{e}$) and the smuon ($\tilde{\mu}$) of less than 0.1, which could be comparable to indirect searches such as the muon LFV processes (Arkani-Hamed, *et al.*, 1996b).

The production cross section for the slepton LFV processes depends on the masses and mixing of the sleptons. If two sleptons, like $\tilde{e}$ and $\tilde{\mu}$, are almost degenerate in their masses, a possible oscillation between them would occur in the decay process. Another interesting possibility is a CP violating signal in the slepton oscillation, which may arise due to a new complex phase in the slepton mixing matrices (Arkani-Hamed *et al.*, 1997; Bowser-Chao and Keung, 1997).

In $SU(5)$ SUSY GUT, LFV in the slepton pair production and decays, in particular with a tau in the final state, has been investigated, and it is found to be more sensitive than the searches for $\tau \to e(\mu)\gamma$ (Hirouchi and Tanaka, 1998). LFV signals in the production of left-handed sleptons at $\mu^+\mu^-$ and e^+e^- colliders are also considered in the framework of MSSM with right-handed neutrino motivated by the atmospheric-neutrino data. It is shown that the decay modes of either $\tau + \mu + 4$ *jets* + *missing energy* or $\tau + \mu + l + 2$ *jets* + *missing energy* could be useful to see the signals with suppressing any potential background (Hisano *et al.*, 1999b). Other possible LFV searches at a $e\mu$ collider (Choi *et al.*, 1998) and also a $e\gamma$ collider (Cao *et al.*, 1999) are also considered.

C. Other theoretical models

In the late 70's, especially in 1977, there were many theoretical papers on models with heavy neutrinos to discuss LFV (Cheng and Li, 1977a; Cheng and Li, 1977b; Bjorken, *et al.*, 1977; Lee, *et al.*, 1977a; Lee and Shrock, 1977b; Altarelli, *et al.*, 1977), after responding to the false rumor on $\mu^+ \to e^+\gamma$ signals at SIN (Schweizerisches Institut für Nuklearforschung). Since then, various theoretical models have appeared. In this section, we discuss LFV effects in theoretical models other than SUSY models. Although many possibilities to induce LFV effects might exist, we discuss only a few examples of different types of LFV. For other references, see, for instance, Vergados (1986), and Depommier and Leroy (1995).

1. Models with a massive neutrino

The simplest way to violate lepton flavor conservation is to introduce neutrino masses and mixing. However, it has been known that the branching ratio of $\mu^+ \to e^+\gamma$ decay from ordinary neutrino mixing is very suppressed if the neutrino mass and mixing suggested by the atmospheric and solar-neutrino experiments are used. For example, the predicted branching ratio from the Dirac neutrino masses and mixing is given by (Petcov, 1977; Bilenky, *et al.*, 1977)

$$B(\mu \to e\gamma) = \frac{3\alpha}{32\pi}\left|\sum_i (V_{MNS})^*_{\mu i}(V_{MNS})_{ei}\frac{m^2_{\nu_i}}{m^2_W}\right|^2, \tag{89}$$

where $(V_{MNS})_{ai}$ is the lepton flavor mixing matrix (MNS matrix) defined in Eq.(20). It is represented by

$$\nu_{La} = \sum_i (V_{MNS})_{ai}\nu_{Li}, \tag{90}$$

where ν_{La} is the neutrino field in the weak flavor basis, and ν_{Li} in the mass-diagonalized basis. Even if a 1 eV neutrino mass with maximal mixing is considered, Eq.(89) only gives a branching ratio on the order of 10^{-47}.

For the Majorana neutrino model of see-saw type (Cheng and Li, 1980), the suppression factor of $(m^2_{\nu_i}/m^2_W)$ in Eq.(89) is replaced by a factor of $O(m_{\nu_i}/M_R)$, where M_R is the mass of a heavy Majorana neutrino. Then, the branching ratio is still $O(10^{-40})$ or less for $m_\nu = 1$ eV and $M_R = 10^{10}$ GeV. It is, therefore, difficult to expect observable LFV effects from the ordinary neutrino masses and mixing indicated by the atmospheric and solar neutrinos.

2. Models with a doubly charged Higgs

There is a wide class of theoretical models which have an interesting enhancement for $\mu^+ \to e^+e^+e^-$ decay and $\mu^- - e^-$ conversion. If LFV is induced by a penguin diagram with a heavy boson and a light charged fermion, the photonic form factors $f_{E0}(q^2)$ and $f_{M0}(q^2)$ receive an enhancement factor of $\ln(m_{boson}/m_{fermion})$ from the loop diagrams in which a photon is attached to the internal light fermion line (Marciano and Sanda, 1977a; Marciano and Sanda, 1977b; Wilczek and Zee, 1977; Raidal and Santamaria, 1998). Since this factor is absent for $f_{E1}(q^2)$ and $f_{M1}(q^2)$, the branching ratio of $\mu^+ \to e^+\gamma$ decay has no enhancement. One of such models is a double charged Higgs boson which has the following interaction of

$$\mathcal{L} = h_{ij}\overline{e^c_{iR}}e_{jR}\phi^{++} + H.c., \tag{91}$$

where the loop diagrams with internal charged leptons and doubly charged scalar ϕ^{++} could induce a logarithmic enhancement (Raidal and Santamaria, 1998).

3. Supersymmetric models with R-parity violation

Another important class of models which might induce logarithmic enhancement is the SUSY models with R parity violation. In the MSSM, if we only require gauge invariance to write all possible superpotentials, the following interactions would also be allowed:

$$W = \lambda_{ijk}L_iL_jE^c_k + \lambda'_{ijk}L_iQ_jD^c_k + \lambda''_{ijk}U_iD^c_jD^c_k - \mu_iL_iH_2. \tag{92}$$

These interactions violate the baryon- or lepton-number conservations. To forbid proton decays that are too fast, a parity which distinguishes superparticles from ordinary particles is often required. This parity is called the R parity, and is defined as $R \equiv (-1)^{3B-L+2S}$, where B, L, and S are the baryon number, lepton number, and spin, respectively. We can, however, consider models with R-parity violation when combinations of the coupling constants which induce proton decays are highly suppressed, but the other coupling constants can be large.

Some combinations of the coupling constants are severely constrained by the LFV processes. It is known that the allowed values of $\lambda\lambda$ and $\lambda\lambda'$ and $\lambda'\lambda'$ still give large contributions at a tree level to the $\mu^+ \to e^+e^+e^-$ and $\mu^- - e^-$ conversion processes (Kim, *et al.*, 1982; Huitu, *et al.*, 1998; Faessler, *et al.*, 1999). Typical relevant tree diagrams are shown in Fig.17.

In SUSY models with R-parity violation, there also exist loop contributions for muon LFV processes, such as $\mu^+ \to e^+\gamma$ decay (Chaichian and Huitu, 1996), $\mu^+ \to e^+e^+e^-$ decay and $\mu^- - e^-$ conversion. The latter two processes would receive a logarithmic enhancement (Huitu, *et al.*, 1998). Fig.18 shows typical loop diagrams. From this one-loop diagram, the $\mu^- - e^-$ conversion process can also be induced from the $\lambda\lambda$ coupling constants. For example, from the loop diagrams with internal leptons, the following four form factors are given as

$$f_{E0}(q^2) = \pm f_{M0}(q^2) = -\frac{2(\lambda\lambda)}{3(4\pi)^2}\frac{-q^2}{m^2_{\tilde{\nu}}}\left(\ln\frac{-q^2}{m^2_{\tilde{\nu}}} + F(r)\right), \tag{93}$$

$$f_{M1}(0) = \mp f_{E1}(0) = -\frac{(\lambda\lambda)}{3(4\pi)^2}\frac{m^2_\mu}{m^2_{\tilde{\nu}}}, \tag{94}$$

where $r = m_{\tilde{\nu}}^2/(-q^2)$. $F(r)$ takes a value of the order of $O(1)$, except for $r \gg 1$, $F(r) = \ln r + \frac{4}{3}$. As a result, some of the $\lambda\lambda$ combinations are more severely constrained by the $\mu^- - e^-$ conversion than the tree-level process of $\mu^+ \to e^+e^+e^-$ decay.

The present constraints for the combinations of $\lambda\lambda$ and $\lambda^{'}\lambda^{'}$ couplings are summarized in Huitu, *et al.* (1998) and Faessler, *et al.* (1999).

4. Models with $Z^{'}$

There are many models where non-photonic LFV transitions occur at tree levels. Typical examples are a model with a Z' that has flavor off-diagonal couplings, or models with extra fermion families which mix with the three families at the tree level so that the Z boson has a LFV couplings (Bernabeu, *et al.*, 1993). In such cases, the $\mu^+ \to e^+e^+e^-$ and $\mu^- - e^-$ conversion processes are expected to be much more important than $\mu^+ \to e^+\gamma$ decay.

5. Models with Lorentz non-invariance

Recently, a possible violation of the Lorentz invariance has been suggested (Colemen and Glashow, 1999). In this context, the Lorentz transformation is not invariant, but only the translational and rotational symmetries are assumed to be exact in a preferred system. Thus, the maximum attainable velocity could be different for each species of particles, and this would cause many unique phenomena in particle physics and cosmic-ray physics.

One of the good tests of the violation of Lorentz invariance is the muon LFV processes (Colemen and Glashow, 1999). If a small Lorentz-non-invariant interaction exists in the SM Lagrangian, flavor mixing couplings can be generally allowed in the photon-fermion interaction. The current limit on the $\mu^+ \to e^+\gamma$ branching ratio puts a strong constraint on the relevant coupling constants. Another interesting effect is a change of the muon lifetime at a high energy. Since the $\mu \to e\gamma$ decay width due to the Lorentz non-invariant interaction would increase with γ^4, where γ is the Lorentz factor, it would dominate over the ordinary muon decay that increases with γ. Therefore, the muon lifetime might start decreasing as γ^{-3} at a sufficiently-high energy. The current limit on the energy dependence of the muon lifetime has been given by the experiment of the muon anomalous magnetic moment.

D. Lepton flavor violation with Polarized Muons

In this subsection, we discuss the usefulness of polarized muons in searches for $\mu^+ \to e^+\gamma$ and $\mu^+ \to e^+e^+e^-$ decays. As discussed later in Section IV, highly-polarized μ^+s (surface muons) are available experimentally. Therefore, it would be useful to examine what kind of new information can be obtained by measuring the angular distribution of decay products with respect the muon polarization.

When the initial muon is polarized in $\mu^+ \to e^+\gamma$ decay, the angular distribution of the positron is given by

$$\frac{dB(\mu^+ \to e^+\gamma)}{d\cos\theta_e} = 192\pi^2 \left(|A_R|^2 (1 - P_\mu \cos\theta_e) + |A_L|^2 (1 + P_\mu \cos\theta_e) \right), \tag{95}$$

where θ_e is the angle between the muon polarization and the positron momentum in the muon rest frame. A_R and A_L are given in Eqs.(59) and (60). P_μ is the magnitude of the muon polarization. A measurement of the e^+ polarization would give the relative amplitudes of A_R and A_L, which correspond to the emission of right-handed e^+ ($\mu^+ \to e^+_R\gamma$) and left-handed e^+ ($\mu^+ \to e^+_L\gamma$), respectively. This is shown schematically in Fig.19.

Since A_L and A_R are model-dependent, it would be useful to discriminate between different LFV mechanisms. For instance, the minimal $SU(5)$ SUSY GUT model predicts a vanishing A_R and a non-zero A_L, yielding a $(1 + P_\mu \cos\theta_e)$ distribution. On the other hand, the $SO(10)$ SUSY-GUT model predicts the helicity amplitudes for both right-handed and left-handed e^+s. For non-unified supersymmetric models with right-handed neutrino, A_R is non-zero but A_L is vanishing, giving a $(1 - P_\mu \cos\theta_e)$ distribution. Thus, a measurement of the angular distribution of e^+ with respect to the direction of muon polarization would provide a valuable means to clearly discriminate between these models.

The $\mu^+ \to e^+e^+e^-$ decay with polarized muons would provide us with an interesting possibility of measuring T violation (Treiman, *et al.*, 1977; Zee, 1985). A T-odd triple vector correlation, $\vec{\sigma}_\mu \cdot (\vec{p}_1 \times \vec{p}_2)$, can be defined, where $\vec{\sigma}_\mu$ is the muon spin, and $\vec{p}_1$ and $\vec{p}_2$ are two independent momenta of the e^+ in the final state. If CPT invariance holds, the information on CP violation in the LFV interaction may be obtained from this T-odd correlations of the decay products. The T-odd asymmetry would arise as an interference between the photon-penguin terms and the four-fermion terms. Details are discussed in Section V B 1. In particular, the T-odd asymmetry is evaluated in the $SU(5)$ SUSY GUT model based on supergravity (Okada, *et al.*, 1998). It is shown that an asymmetry up to 20% is possible if CP-violating phases are introduced in the soft SUSY-breaking mass terms. It would give independent information from the electric dipole moment (EDM) of the electron and neutron.

In the $\mu^+ \to e^+e^+e^-$ decay, parity-odd asymmetries can be also defined if the initial muons are polarized. These asymmetries are sensitive to the chiralities of the terms in the effective Lagrangian: both the photon-penguin terms (A_L and A_R) and the four fermion coupling terms (g_i). Measurements of the parity-odd asymmetries in $\mu^+ \to e^+e^+e^-$ decay, together with the branching ratios of $\mu^+ \to e^+\gamma$ and $\mu^+ \to e^+e^+e^-$ decays, are useful to distinguish different SUSY GUT models (Okada, *et al.*, 1999).

E. $|\Delta L_i| = 2$ processes

The LFV processes with $|\Delta L_i| = 2$ are like the muonium to anti-muonium conversion ($\mathrm{Mu} - \overline{\mathrm{Mu}}$ conversion), the wrong-flavor muon decay ($\mu^+ \to e^+\nu_\mu\overline{\nu}_e$), and others. The phenomenology of the $\mathrm{Mu} - \overline{\mathrm{Mu}}$ conversion can be described by an effective four fermion interaction. As an example, the interaction of $(V - A)(V - A)$ type was considered by Feinberg and Weinberg (Feinberg and Weinberg, 1961). It is given by

$$H_{\mathrm{Mu}\overline{\mathrm{Mu}}} = \Big(\frac{G_{\mathrm{Mu}\overline{\mathrm{Mu}}}}{\sqrt{2}}\Big)\overline{\mu}\gamma_\lambda(1-\gamma_5)e\overline{\mu}\gamma^\lambda(1-\gamma_5)e + H.c., \tag{96}$$

in which $G_{\mathrm{Mu}\overline{\mathrm{Mu}}}$ is a coupling constant characterizing the strength of the $\mathrm{Mu}-\overline{\mathrm{Mu}}$ conversion. As described in Section V E 3, the present experimental limit on $G_{\mathrm{Mu}\overline{\mathrm{Mu}}} \leq 3.0 \times 10^{-3} G_F$ is given (Willmann, *et al.*, 1999).

In general, there could be various combinations of different types of four fermion interactions. They are such as $(V+A)(V+A)$, $(V-A)(V+A)$, $(S-P)(S-P)$, $(S+P)(S+P)$, $(S-P)(S+P)$, SS and PP, where V, A, S and P are vector, axial vector, scalar, psuedoscalar effective interactions, respectively. The types of interactions are determined by assumed theoretical models. In Fig.20, example diagrams of speculative theoretical models responsible for the $\mathrm{Mu}-\overline{\mathrm{Mu}}$ conversion are shown. They are models of (a) the exchange of doubly charged Higgs bosons, (b) that of heavy Majorana neutrinos, (c) that of a neutral scalar particle (including a superparticle), and (d) that of a bilepton gauge boson. They are briefly described in the following.

A simple example which induces the $|\Delta L_i| = 2$ process is provided by a model with a doubly-charged singlet scalar boson (Chang and Keung, 1989). In this model, only the $(V+A)(V+A)$ interaction is generated and the $\mathrm{Mu}-\overline{\mathrm{Mu}}$ conversion rate can be as large as the present experimental limit within the constraints from the measurements of the anomalous muon magnetic moment and the high-energy Bhabha scattering. A more general case with the doubly charged scalar boson is also considered (Swartz, 1989).

In the left-right symmetric model with a triplet Higgs boson field, the $\mathrm{Mu}-\overline{\mathrm{Mu}}$ conversion could be induced by a doubly charged Higgs boson, $\triangle^{++}$ (Halprin, 1982). In this model, if the mass of the muon neutrino is greater than 35 keV/c^2 and less than the present direct experimental bound of 170 keV/c^2, there is an upper limit of the neutrino lifetime in order for the neutrino energy density in the universe not to exceed its present total energy density. From this requirement, a lower bound of $G_{\mathrm{Mu}\overline{\mathrm{Mu}}}$ is predicted as a function of the mass of the muon neutrino, m_{ν_μ} (Herczeg and Mohapatra, 1992). For the range 35 keV/$c^2 \leq m_{\nu_\mu} \leq$ 170 keV/c^2, a lower limit of $G_{\mathrm{Mu}\overline{\mathrm{Mu}}} \geq (1-40) \times 10^{-4} G_F$ is obtained.

Supposing that neutrinos are of Majorana nature, the $\mathrm{Mu}-\overline{\mathrm{Mu}}$ conversion could take place by an intermediate pair of neutrinos. This coupling is related to neutrinoless double β decays, yielding $G_{\mathrm{Mu}\overline{\mathrm{Mu}}} \leq 10^{-5} G_F$ (Halprin, 1982).

There is a class of models with a neutral scalar boson, which has a flavor-changing coupling to introduce the $|\Delta L_i| = 2$ processes (Hou and Wong, 1996). An important example of this kind of models is the supersymmetric model with $R-$parity violation, where a tau sneutrino exchange induces the $\mathrm{Mu}-\overline{\mathrm{Mu}}$ conversion (Mohapatra, 1992; Halprin and Masiero, 1993). In this case, the four fermion coupling is of the $(S-P)(S+P)$ type. The present experimental limit of the $\mathrm{Mu}-\overline{\mathrm{Mu}}$ conversion gives a constraint on the relevant coupling constant, $|\lambda_{132}\lambda^*_{231}| \leq 3 \times 10^{-4}$, for a superpartner mass of order 100 GeV/c^2. Also, the four fermion coupling constant for the $\mu^+ \to e^+ \nu_\mu \overline{\nu}_e$ decay is predicted to be similar in magnitude as that for the $\mathrm{Mu}-\overline{\mathrm{Mu}}$ conversion.

In some extensions of the SM gauge groups, there appear doubly charged gauge bosons (called bileptons), X^{--}, which couple only to leptons. They occur, for instance, in SU(15) GUT models (Frampton and Lee, 1990), or in a gauge model with $SU(3)_C \times SU(3)_L \times U(1)_Y$ (311 model) (Frampton, 1992). In these models, singly-charged and doubly-charged bilepton gauge bosons appear from breaking of the $SU(3)_L$ gauge symmetry to $SU(2)_L$ of the SM gauge groups. The mass bound of the bilepton gauge bosons is obtained from a precise determination of the Michel parameters of the normal muon decay (Carlson and Frampton, 1992), the muoniun hyperfine splitting, and the $\mu^+ \to e^+ \nu_\mu \overline{\nu}_e$ decay (Fujii, *et al.*, 1994). They give a lower bound of roughly 200 GeV/c^2. In these models, the $\mathrm{Mu}-\overline{\mathrm{Mu}}$ conversion could occur by the exchange of a doubly charged bilepton (Horikawa and

Sasaki, 1996; Fujii, *et al.*, 1993). The effective interaction is of the form $(V-A)(V+A)$, which is in contrast to either the traditional $(V-A)(V-A)$ interaction by Feinberg and Weinberg. The bilepton interaction is given by

$$\mathcal{L} = -\frac{g_{3l}}{2\sqrt{2}} X_{\mu}^{--} \bar{l} \gamma^{\mu} \gamma_5 C \bar{l}^T + H.c., \tag{97}$$

where $l = e, \mu, \tau$, and C is the charge-conjugation matrix. The gauge coupling constant, g_{3l}, is on the order of $O(1)$, and is determined from theoretical models. The $\mathrm{Mu} - \overline{\mathrm{Mu}}$ conversion rate ($P_{\mathrm{Mu}\overline{\mathrm{Mu}}}$) is given by

$$P_{\mathrm{Mu}\overline{\mathrm{Mu}}} = 4.5 \times 10^3 \times \left(\frac{g_{3l}}{m_X}\right)^4, \tag{98}$$

where m_X is the mass of the bilepton gauge boson. From the current experimental bound of the $\mathrm{Mu} - \overline{\mathrm{Mu}}$ conversion, a constraint of $m_X/g_{3l} \geq 2.6$ TeV/c^2 is obtained (Willmann, *et al.*, 1999).

To study the $|\Delta L_i| = 2$ processes, the reaction $e^- e^- \to \mu^- \mu^-$ has been known to be useful for a long time (Glashow, 1961). Such an experiments were carried out to place a constraint on $G_{\mathrm{Mu}\overline{\mathrm{Mu}}}$ (Barber, *et al.*, 1969). Recently, similar scattering processes at a high energy, such as at a ee linear collider or a $\mu\mu$ collider, have been discussed, based on mostly bilepton models (Frampton, 1992b; Hou, 1996b; Raidal, 1998b).

IV. NORMAL MUON DECAY

Normal muon decay remains the only purely leptonic process of weak interaction accessible to precise measurements with high statistics. The studies are free from the complications of the strong interaction and hadronic structure. For this reason, precise studies of normal muon decay would provide information unambiguously interpreted.

The experimental progress has benefited from the high-intensity muon beams available at the three meson factories, such as the Paul Scherrer Institute (PSI) in Switzerland, TRIUMF in Canada, LAMPF in U.S.A. (which was unfortunately shut down), and also lately the Rutherford Appleton Laboratory (RAL) in England. In particular, useful is a surface μ^+ beam, which arises from the decay of pions stopped at the surface of a pion production target. It has a monochromatic kinetic energy of 4.1 MeV (29.8 MeV/c in momentum) and 100% muon polarization antiparallel to its momentum direction. This high polarization of the surface muons is useful for various measurements requiring muon polarization.

In the past, studies of the normal muon decay have greatly contributed to develop the SM. It is now playing a role to probe for possible deviations from the SM. For example, see reviews by Fetscher and Gerber (1995) and Herczeg (1995). In the following, the current status of the studies of normal muon decay, in particular those which are being prepared or planned for the future, is discussed. They are such as measurements of the muon lifetime, the Michel spectrum, and the longitudinal polarization of e^+s in polarized $\mu^+ \to e^+\nu_e\overline{\nu}_\mu$ decay. The other important muon experiments, such as the muon anomalous magnetic moment and the muon electric dipole moment, are not discussed.

A. Muon lifetime

1. Phenomenology

The Fermi coupling constant, G_F, is one of the three precisely measured inputs of the SM, along with the fine structure constant (α) and the Z bosom mass (m_Z). Their updated values are given in Table VII. Note that the m_Z value in the Particle Data Group (Particle Data Group, 1998) is $m_Z = 91.187 \pm 0.007$ (77 ppm). However, after a recent improvement of m_Z (LEP and SLD Electroweak Working Group, 1999), the uncertainties of G_F and m_Z become comparable in the order, as can be seen in Table VII. G_F is determined from the muon lifetime (τ_μ) from Eq.(23). The complete two-loop QED corrections to an estimation of the muon lifetime was calculated (Van Ritbergen and Stuart, 1999). The theoretical errors to derive G_F from the muon lifetime are now reduced to be negligible, compared with the experimental uncertainty in the measurement of the muon lifetime. It would be necessary to improve the accuracy of G_F, if experimentally possible. To test the SM, it is required to compare G_F from the muon lifetime with those determined from other measurements, such as tau leptonic decays, or the M_W and other observables at the M_Z pole with similar accuracies (Marciano, 1999).

TABLE VII. Three fundamental values in the Standard Model.

Parameter	Experimental value	Uncertainty
$1/\alpha$	$137.0359895 \pm 0.0000061$	0.045 ppm
G_F	$(1.16639 \pm 0.00001) \times 10^{-5}$ GeV^{-2}	9 ppm
m_Z	91.1867 ± 0.0021 GeV/c^2	23 ppm

2. Experimental status

Experimentally, measurements of the muon lifetime were carried out at TRIUMF (Giovanetti, *et al.*, 1984) and at Saclay (Bardin, *et al.*, 1984). Since then, for more than a decade, no experimental efforts to improve the situation have been made. The present value of τ_μ is $\tau_\mu = 2.19703(4) \times 10^{-6}$ (± 18 ppm) (Particle Data Group, 1998). Recently, however, an experimental proposal at Rutherford Appleton Laboratory (RAL) to reduce the uncertainty of G_F by an order of magnitude has been undertaken (Nakamura, *et al.*, 1998), and two experimental proposals to PSI (Cavallo, *et al.*, 1999; Carey, *et al.*, 1999b) have been submitted.

An on-going experiment at the RIKEN-RAL muon facility, R77, uses a pulsed muon beam. In previous experiments with a continuous muon beam, only one incident muon within the time window of measurement was allowed in order to avoid any possible confusion in the decay of other muons occuring in the same time window. It, otherwise, would introduce distortion of the time spectrum of muon decay. This requirement, however, would lead to a limitation on muon beam intensity, and the sensitivity would be statistically limited. To overcome this problem, R77 at RIKEN-RAL has adopted a pulsed beam, whose pulse interval of 20 msec is much longer than the measurement window. Since all muons come at the same time, multiple muon decays within the measurement time window are allowed. There are several sources of systematic errors. One of them is from counting losses due to pile-up e^+ events and the dead time of detection, since the instantaneous beam intensity is strong. To avoid this effect, segmentation of the detectors is required. In R77, multiwire proportional chambers are used. Another systematic error might come from a precession of muon spin under an earth field. A special magnetic material will be adopted for the muon stopping target to depolarize the muon spin polarization. It aims, by accumulating 10^{11} muon decays, to achieve statistical and systematic errors of about 3 ppm (a total of 4 ppm) in the τ_μ measurement. Its initial phase, planning to accumulate 10^{10} muon decays, have already started in 1999.

There are two new planned experiments at PSI: R-99-06 (Cavallo, *et al.*, 1999) and R-99-07 (Carey, *et al.*, 1999b), where R-99-07 has just been approved. The both experiments are aiming at a factor 20 improvement over the current world average of τ_μ.

The approved experiment, R-99-07, is to use a chopped surface-muon beam at PSI. The muons are stopped in a sulfur target to reduce the residual muon polarization, and a transverse magnetic field of 75 G is applied to further de-phase it. The e^+ detector (μLan detector) consists of 180 triangular scintillating tiles distributed within the 20 super-triangles of an icosahedral geometry centered on the target. Each scintillating tile is viewed by a photo-multiplier, and the signal is recorded by a waveform digitizer developed in the $g-2$

experiment at BNL. This 4π geometry of the μLan detector, especially a sum of the point-like symmetric tile pairs with respect to the center, would reduce further any asymmetries due to spin rotation. The experiment has just been approved and a physics run is expected in three years.

The experiment, R-99-06, uses a fiber-active-scintillator target (FAST), which comprises plastic scintillating fibers of 0.5-mm diameter in an overall active volume of $20 \times 20 \times 20$ cm^3. A π^+ beam is stopped in the FAST target, and a $\pi^+ \to \mu^+ \to e^+$ decay chain is observed in the target. Owing to a high granularity and fast response of the FAST detector, many individual muon decays can be recorded in parallel in a high event rate such as 1 MHz. Since the μ^+s produced from π^+ decays at rest have an isotropic distribution, possible errors from the muon polarization can be eliminated. In its first stage, a DC π^+ beam is planned to use, and in the second stage, a pulsed π^+ beam will be used.

B. Michel decay spectrum

1. Phenomenology

The $e^\pm$ spectrum of the normal muon decay is given in Eq.(30) with the four Michel parameters of ρ, ξ, δ, and η. It includes all possible Lorentz-invariant interactions. A precise determination of the Michel parameters would serve stringent testing of the $(V-A)$ structure of electroweak interactions in the SM, and obtain a hint of new physics beyond the SM.

2. Experimental status

In the past, each of the Michel parameters in the normal muon decay was determined by several different experiments: for instance, the ρ parameter (Derenzo, 1969), the η parameter (Burkard, *et al.*, 1985b), the δ parameter (Balke, *et al.*, 1988), $P_\mu\xi$ (Beltrami, *et al.*, 1987), and $P_\mu\xi(\delta/\rho)$ (Jodidio, *et al.*, 1986).

A new experiment, E614 at TRIUMF, to measure the entire differential spectrum of positrons from the decay of polarized muons is being prepared (Abegg, *et al.*, 1996). By accumulating 10^9 muon decays, the goal of the E614 experiment is to measure the Michel parameters (ρ, ξ, δ and η) to precisions of $\Delta\rho < 1 \times 10^{-4}$, $\Delta\delta < 3 \times 10^{-4}$ and $\Delta(P_\mu\xi) < 2 \times 10^{-4}$. The aimed precisions are 3 to 10 times better than those previously achieved. Note that only the product $P_\mu\xi$ can be experimentally determined. For example, the expected constraint on the left-right symmetric model from E614 is presented in Fig.3.

A schematic view of the E614 detector is shown in Fig.21. The E614 spectrometer consists of a superconducting solenoid magnet with tracking chambers. In E614, a surface muon beam from the M13 beam channel at TRIUMF will be brought into the detector, and stopped in a muon-stopping target made of aluminum located at the center of the apparatus. An array of planar chambers, mounted symmetrically upstream and downstream from the target, will track the trajectories of e^+s from muon decays under a magnetic field of 2 T with a homogeneity of better than 10^{-4}. The positron spectrum will be measured over a wide range of $0.4 \le x \le 1.0$ for the positron energy, and $10^\circ \le \theta_e \le 70^\circ$ and $110^\circ \le \theta_e \le 170^\circ$ for

the angle between the muon spin direction and the positron momentum vector (θ_e), where x is defined in Section II C 1.

Experimentally, it is important to keep the muon polarization fully aligned with the magnetic field direction at the stopping target. Any reduction of P_μ^z, the projection of P_μ on the field direction, must be minimized at a level of 10^{-4}. Possible sources of reduction are a misalignment between the muon-beam axis and the magnetic field at the spectrometer, a fringing field of the spectrometer, a contamination of non-surface muons (such as cloud muons), multiple scattering of muons in the production target, and possible depolarization of the muon spin in the aluminum muon-stopping target. At the same time, as spectrometer requirements, low-mass tracking chambers to minimize multiple scattering of positrons and position accuracy of the detector assembly are crucial. Detector construction has been started, and physics data-taking is expected from 2001.

C. Polarization of e^+ in $\mu^+ \to e^+\nu_e\overline{\nu}_\mu$ decay

1. Phenomenology

The longitudinal polarization of e^+ (P_L) in $\mu^+ \to e^+\nu_e\overline{\nu}_\mu$ decay is already given in Eq.(38). When the muon is not polarized ($P_\mu = 0$) and the SM values of $\rho = \delta = 3/4$ are taken, P_L leads to

$$P_L(x, \cos\theta_e) = \xi^{'}. \tag{99}$$

It is independent of the values of x and $\cos\theta_e$. Therefore, a measurement of the longitudinal polarization of e^+s emitted by unpolarized muons would provide good a direct determination of the parameter $\xi^{'}$.

If the muon is polarized with the SM values of the ρ and δ parameters, P_L is given by

$$P_L(x, \cos\theta_e) = \xi^{'} + \frac{\xi P_\mu \cos\theta_e (2x-1)}{(3-2x) + \xi P_\mu \cos\theta_e (2x-1)} \cdot \frac{(\xi^{''} - \xi\xi^{'})}{\xi}. \tag{100}$$

From this, the measurement of P_L as a function of energy (x) and angle (θ_e) would give other information about the combination of parameters, $(\xi^{''} - \xi\xi^{'})/\xi$. In particular, for $x \approx 1$ and $\cos\theta_e \approx -1$, it leads to

$$P_L(x = 1, \cos\theta_e = -1) \approx \xi^{'} + \frac{-\xi P_\mu}{1 - \xi P_\mu} \cdot \frac{(\xi^{''} - \xi\xi^{'})}{\xi}. \tag{101}$$

The combination $(\xi^{''} - \xi\xi^{'})/\xi$ is multiplied by an enhancement factor of $\xi P_\mu/(1-\xi P_\mu)$, which could be large when P_μ is close to unity.

The two transverse polarization components (P_{T1} and P_{T2}) of the e^+ in $\mu^+ \to e^+\nu_e\overline{\nu}_\mu$ decay are given in Eqs.(36) and (37). If the time-reversal invariance holds, P_{T2}, which is the transverse e^+ polarization normal to the decay plane determined by P_μ and the e^+ momentum direction, should be vanishing. A non-zero P_{T2} would signal a violation of the time-reversal invariance. The electromagnetic final-state interaction, which mimics a T-odd effect, is known to be small. On the other hand, P_{T1}, which is not forbidden by the fundamental symmetries, is sensitive to the Michel parameter, η. It would be advantageous, since the determination of η from the isotropic part of the $e^\pm$ energy spectrum is difficult owing to the small x_0 factor ($\sim 10^{-2}$) multiplied by η.

2. Experimental status

The latest measurement of P_L of e^+ in $\mu^+ \to e^+\nu_e\overline{\nu}_\mu$ decay was carried out at SIN (Burkard, *et al.*, 1985a). A magnetized-iron foil was adopted as a polarimeter for the e^+ polarization, and was tilted by 45° with respect to the e^+ momentum direction. Either Bhabha scattering of e^+ off e^-s ($e^+e^- \to e^+e^-$) or annihilation in flight ($e^+e^- \to \gamma\gamma$) in the magnetized iron foil was utilized, where the cross sections of those processes have a particular dependence on the relative angle between the $e^\pm$ polarization directions. Since the magnitude and direction of e^- polarization in the magnetized-iron foil is known, the polarization of e^+ from $\mu^+ \to e^+\nu_e\overline{\nu}_\mu$ decay can be determined. Either e^+e^- or $\gamma\gamma$ pairs from the polarimeter were detected by four NaI(Tl) crystal detectors located behind. Both unpolarized and polarized muons were studied. From the case of unpolarized muons, $P_L(=\xi') = 0.998 \pm 0.042$ was obtained, whereas the current average value in the Particle Data Group is $P_L = 1.00 \pm 0.04$ (Particle Data Group, 1998), showing no strong evidence of the right-handed current. For the case of polarized muons, they obtained $(\xi'' - \xi \cdot \xi')/\xi = -0.35 \pm 0.33$ which, however, did not make better constraints of the coupling constants at this moment.

The transverse polarization components, P_{T1} and P_{T2}, of e^+ in $\mu^+ \to e^+\nu_e\overline{\nu}_\mu$ decay were measured by the same group (Burkard, *et al.*, 1985b). A magnetized-iron foil was used again as a polarimeter, but was placed perpendicular to the e^+ momentum direction. The measurement was based on the fact that two photons from the annihilation of transversely-polarized e^+ with e^-s in a magnetized-iron foil are preferentially emitted in the plane determined by the bisector of the e^+ polarization vector ($\vec{P}_T$) and the e^- polarization vector in a magnetized foil. Their results were $< P_{T1} >= 0.016 \pm 0.023$ and $< P_{T2} >= 0.007 \pm 0.023$. From the measured value of P_{T1}, $\eta = -0.007 \pm 0.013$ was obtained.

A new experiment, R-94-10 at PSI (Barnett, *et al.*, 1994), is in preparation to measure the transverse polarization, both P_{T_1} and P_{T_2}, of the positrons from polarized $\mu^+ \to e^+\nu_e\overline{\nu}_\mu$ decay, with a precision of 3×10^{-3}. The experimental principle is the same as the previous one, mentioned before. Major improvements are expected to be from a higher muon-stopping rate due to a higher proton current at the PSI cyclotron, installation of two analyzing foils with additional wire chamber in between, and replacement of four NaI(Tl) crystals by 127 hexagonal BGO crystal. An engineering run will start in 1999.

Another new experiment, R-97-06 at PSI (Van Hove, *et al.*, 1997), is under development to measure the longitudinal polarization, P_L, of the positrons emitted antiparallel to the muon spin from polarized $\mu^+ \to e^+\nu_e\overline{\nu}_\mu$ decay. As explained in Eq.(101), P_L at $x \approx 1$ and $\cos\theta_e \approx -1$ is sensitive to the combination of $(\xi'' - \xi\xi')/\xi$ with the enhancement factor. R-97-06 aims to measure this observable with an improvement of more than one order of magnitude over the previous experiments at SIN. It will use three solenoidal magnets to track e^+s from $\mu^+ \to e^+\nu_e\overline{\nu}_\mu$ decay with double-sided Si strip detectors. Two magnetized iron foils with opposite sign of the analyzing power are used as a polarimeter, followed by 127 BGO crystals to detect $e^\pm$s and also photons. The asymmetry for two different analyzing foils are compared for the two cases of polarized and unpolarized muons, giving a relative measurement to reduce systematic errors. The goal is to measure $(\xi'' - \xi\xi')/\xi$ to about 0.5 %. An engineer run with the complete setup is planed for late 1999.

V. LEPTON FLAVOR VIOLATING MUON DECAYS

The muon system is one of the best places to search for LFV, compared with the others. In Table VIII, the upper limits of various lepton flavor violating decays are listed. The sensitivity to LFV is superb in the muon system. It is mostly because of a large number of muons (of about $10^{14}-10^{15}$/year) available for experimental searches today. The theoretical frameworks for LFV were already presented in Section III. In this section, phenomenology and experimental results, including the prospect for future improvements for each of the forbidden muon LFV processes, are reviewed. They are such as $\mu^+ \to e^+\gamma$ decay, $\mu^+ \to e^+e^+e^-$ decay, $\mu^- - e^-$ conversion in a muonic atom, $\mu^- - e^+$ conversion, and muonium to anti-muonium conversion. In the first three processes, lepton flavors change by one unit ($|\Delta\ L_i| = 1$).

TABLE VIII. Limits of the lepton-flavor violating decays of muon, tau, pion, kaon and Z boson.

Reaction	Present limit	Reference
$\mu^+ \to e^+\gamma$	$< 1.2 \times 10^{-11}$	Brooks, *et al.* (1999)
$\mu^+ \to e^+e^+e^-$	$< 1.0 \times 10^{-12}$	Bellgardt, *et al.* (1988)
$\mu^- Ti \to e^- Ti$	$< 6.1 \times 10^{-13}$	Wintz (1998)
$\mu^+e^- \to \mu^-e^+$	$< 8.3 \times 10^{-11}$	Willmann, *et al.* (1999)
$\tau \to e\gamma$	$< 2.7 \times 10^{-6}$	Edwards, *et al.* (1997)
$\tau \to \mu\gamma$	$< 3.0 \times 10^{-6}$	Edwards, *et al.* (1997)
$\tau \to \mu\mu\mu$	$< 1.9 \times 10^{-6}$	Bliss, *et al.* (1998)
$\tau \to eee$	$< 2.9 \times 10^{-6}$	Bliss, *et al.* (1998)
$\pi^0 \to \mu e$	$< 8.6 \times 10^{-9}$	Krolak, *et al.* (1994)
$K_L^0 \to \mu e$	$< 4.7 \times 10^{-12}$	Ambrose, *et al.* (1998)
$K^+ \to \pi^+\mu^+e^-$	$< 2.1 \times 10^{-10}$	Lee, *et al.* (1990)
$K_L^0 \to \pi^0\mu^+e^-$	$< 3.1 \times 10^{-9}$	Arisaka, *et al.* (1998)
$Z^0 \to \mu e$	$< 1.7 \times 10^{-6}$	Akers, *et al.* (1995)
$Z^0 \to \tau e$	$< 9.8 \times 10^{-6}$	Akers, *et al.* (1995)
$Z^0 \to \tau\mu$	$< 1.2 \times 10^{-5}$	Abreu, *et al.* (1997)

A. $\mu^+ \to e^+\gamma$ decay

1. *Phenomenology of* $\mu^+ \to e^+\gamma$ *decay*

The most popular process of lepton-flavor-violating muon decay is $\mu^+ \to e^+\gamma$. The Lagrangian for the $\mu^+ \to e^+\gamma$ amplitude is given by, as shown in Eq.(57),

$$\mathcal{L}_{\mu\to e\gamma} = -\frac{4G_F}{\sqrt{2}}\left[m_\mu A_R \overline{\mu_R}\sigma^{\mu\nu} e_L F_{\mu\nu} + m_\mu A_L \overline{\mu_L}\sigma^{\mu\nu} e_R F_{\mu\nu} + H.c.\right]. \tag{102}$$

The differential angular distribution of $\mu^+ \to e^+\gamma$ decay is already given, as in Eq.(95), by

$$\frac{dB(\mu^+ \to e^+\gamma)}{d(\cos\theta_e)} = 192\pi^2\left[|A_R|^2\,(1 - P_\mu\cos\theta_e) + |A_L|^2\,(1 + P_\mu\cos\theta_e)\right], \tag{103}$$

where θ_e is the angle between the muon polarization and the e^+ momentum vectors. P_μ is the magnitude of the muon spin polarization. The branching ratio is presented by

$$B(\mu^+ \to e^+\gamma) = \frac{\Gamma(\mu^+ \to e^+\gamma)}{\Gamma(\mu^+ \to e^+\nu\overline{\nu})} = 384\pi^2(|A_R|^2 + |A_L|^2). \tag{104}$$

2. Event signature and backgrounds

The event signature of $\mu^+ \to e^+\gamma$ decay at rest is an e^+ and a photon in coincidence, moving collinearly back-to-back with their energies equal to half of the muon mass ($m_\mu/2 =$ 52.8 MeV). The searches in the past were carried out by using positive muon decay at rest to fully utilize its kinematics. A negative muon cannot be used, since it is captured by a nucleus when it is stopped in a material. There are two major backgrounds to a search for $\mu^+ \to e^+\gamma$. One is a physics (prompt) background from radiative muon decay, $\mu^+ \to e^+\nu_e\overline{\nu}_\mu\gamma$, when e^+ and photon are emitted back-to-back with the two neutrinos carrying off little energy. The other background is an accidental coincidence of an e^+ in a normal muon decay, $\mu^+ \to e^+\nu_e\overline{\nu}_\mu$, accompanied by a high energy photon. The sources of the latter might be either $\mu^+ \to e^+\nu_e\overline{\nu}_\mu\gamma$ decay, or annihilation-in-flight or external bremsstrahlung of e^+s from normal muon decay. These backgrounds are described in more detail in the following.

3. Physics background

One of the major physics backgrounds to the search for $\mu^+ \to e^+\gamma$ decay is radiative muon decay, $\mu^+ \to e^+\nu_e\overline{\nu}_\mu\gamma$ (branching ratio = 1.4 % for $E_\gamma > 10$ MeV), when the e^+ and photon are emitted back-to-back with two neutrinos carrying off little energy. The differential decay width of this radiative muon decay was calculated as a function of the e^+ energy (E_e) and the photon energy (E_γ) normalized to their maximum energies, namely $x = 2E_e/m_\mu$ and $y = 2E_\gamma/m_\mu$ (Fronsdal and Überall, 1959; Eckstein and Pratt, 1959). The ranges of x and y are already shown in Eq.(53). As a background to $\mu^+ \to e^+\gamma$, the kinematic case when $x \approx 1$ and $y \approx 1$ is important. In an approximation of the limit of $x \approx 1$ and $y \approx 1$ with an angle between e^+ and photon ($\theta_{e\gamma}$) of almost 180°, the differential decay width of $\mu^+ \to e^+\nu_e\overline{\nu}_\mu\gamma$ decay is given by (Kuno and Okada, 1996)

$$d\Gamma(\mu^+ \to e^+\nu\overline{\nu}\gamma) \cong \frac{G_F^2 m_\mu^5\alpha}{3\times 2^8\pi^4}\times$$
$$\left[(1-x)^2(1 - P_\mu\cos\theta_e) + \left(4(1-x)(1-y) - \frac{1}{2}z^2\right)(1 + P_\mu\cos\theta_e)\right]dxdyzdzd(\cos\theta_e), \tag{105}$$

where θ_e is the angle between the muon spin and the e^+ momentum direction. G_F is the Fermi coupling constant, α is the fine-structure constant, $z = \pi - \theta_{e\gamma}$, and $\cos z$ is expanded in a polynomial of z, since z is small. In Eq.(105), only the terms of up to the second

order of a combination of $(1-x)$, $(1-y)$ and z are kept. At $x \approx 1$ and $y \approx 1$, the effect of the positron mass is found to be very small, on the order of $(m_e/m_\mu)^2$, and is therefore neglected in Eq.(105). The first term in Eq.(105) represents the e^+ being emitted preferentially opposite to the muon spin direction, whereas in the second term the e^+ is emitted along the muon-spin direction. When $x = 1$ and $y = 1$ exactly, this differential decay width vanishes. However, in a real experiment, finite detector resolutions introduce background events which would ultimately limit the sensitivity of a search for $\mu^+ \to e^+\gamma$.

Given the detector resolution, the sensitivity limitation from this physics background can be estimated by integrating the differential decay width over the kinematic signal box. It is given by

$$\begin{aligned} dB(\mu^+ \to e^+\nu\overline{\nu}\gamma) &= \frac{1}{\Gamma(\mu^+ \to e^+\nu\overline{\nu})} \int_{1-\delta x}^{1} dx \int_{1-\delta y}^{1} dy \int_{0}^{\min(\delta z, 2\sqrt{(1-x)(1-y)})} dz \quad \frac{d\Gamma(\mu^+ \to e^+\nu\overline{\nu}\gamma)}{dxdydz}, \\ &= \frac{\alpha}{16\pi}\Big[J_1(1 - P_\mu \cos\theta_e) + J_2(1 + P_\mu \cos\theta_e)\Big] d(\cos\theta_e), \end{aligned} \tag{106}$$

where δx, δy and δz are a half width of the $\mu^+ \to e^+\gamma$ signal region for x, y and z, respectively. $\Gamma(\mu^+ \to e^+\nu\overline{\nu})$ is the total muon decay width. J_1 and J_2 are given as the sixth power of a combination of δx and δy. For the case of $\delta z > 2\sqrt{\delta x \delta y}$, they are presented by

$$J_1 = (\delta x)^4(\delta y)^2 \quad \text{and} \quad J_2 = \frac{8}{3}(\delta x)^3(\delta y)^3. \tag{107}$$

When the angular resolution meets $\delta z \leq 2\sqrt{\delta x \delta y}$, they are given by

$$J_1 = \frac{8}{3}(\delta x)^3(\delta y)(\frac{\delta z}{2})^2 - 2(\delta x)^2(\frac{\delta z}{2})^4 + \frac{1}{3}\frac{1}{(\delta y)^2}(\frac{\delta z}{2})^8, \tag{108}$$

$$J_2 = 8(\delta x)^2(\delta y)^2(\frac{\delta z}{2})^2 - 8(\delta x)(\delta y)(\frac{\delta z}{2})^4 + \frac{8}{3}(\frac{\delta z}{2})^6. \tag{109}$$

Experimentally, the resolution of the e^+ energy is better than that of the photon energy, *i.e.* $\delta x < \delta y$. Also, the angular resolution, δz, has been poor in past experiments. Thereby, J_2 is much larger than J_1 for most cases.

Fig.22 shows a fraction of the $\mu^+ \to e^+\nu_e\overline{\nu}_\mu\gamma$ decay for the given δx and δy values with unpolarized muons in the case of $\delta z \geq 2\sqrt{\delta x \delta y}$. From Fig.22, it can be seen that both δx and δy on the order of 0.01 are needed to achieve a sensitivity limit at the level of 10^{-15}.

Radiative corrections to the radiative muon decay for the case of the physics background to $\mu^+ \to e^+\gamma$ decay have been calculated to be on the order of several %, depending on the detector resolution (Arbuzov, *et al.*, 1998).

4. Accidental background

With a very high rate of incident muons, the accidental background becomes more important than the physics background. This is usually the case for the present and future experiments. The event rate of the accidental background normalized to the total decay rate ($B_{\rm acc}$) can be estimated by

$$B_{\rm acc} = R_\mu \cdot f_e^0 \cdot f_\gamma^0 \cdot (\Delta t_{e\gamma}) \cdot (\frac{\Delta\omega_{e\gamma}}{4\pi}), \tag{110}$$

where R_μ is the instantaneous muon intensity. f_e^0 and f_γ^0 are the integrated fractions of the spectrum of e^+ in the normal muon decay and that of photon (such as from $\mu^+ \to e^+\nu_e\overline{\nu}_\mu\gamma$ decay) within the signal region, respectively. They include their corresponding branching ratios. $\Delta t_{e\gamma}$ and $\Delta\omega_{e\gamma}$ are, respectively, the full widths of the signal regions for timing coincidence and angular constraint of the back-to-back kinematics.

Given the sizes of the signal region, B_{acc} can be evaluated. Let us take δx, δy, $\delta\theta_{e\gamma}$, and $\delta t_{e\gamma}$ to be the half width of the signal region for e^+, photon energies, angle $\theta_{e\gamma}$, and relative timing between e^+ and photon, respectively. f_e^0 can be estimated by integrating the Michel spectrum of the normal muon decay over $1-\delta x \le x \le 1$, yielding $f_e^0 \approx 2(\delta x)$. Given the angular resolution, $\delta\theta_{e\gamma}$, the back-to-back resolution $(\Delta\omega_{e\gamma}/4\pi)$ is presented by $(\Delta\omega_{e\gamma}/4\pi) = (\delta\theta_{e\gamma})^2/4$. As for f_γ^0, if the radiative muon decay $\mu^+ \to e^+\nu_e\overline{\nu}_\mu\gamma$ is considered as a source of the 52.8 MeV photon, it can be given by integrating Eq.(54) over 2π for θ_γ, and then over the photon energy within the width of the signal region $(1-\delta y \le y \le 1)$. For unpolarized muons, it is given by

$$f_\gamma^0 = \int_{1-\delta y}^{1} dy \int d(cos\theta_\gamma)\frac{dB(\mu^+ \to e^+\nu\overline{\nu}\gamma)}{dyd(cos\theta_\gamma)} \approx \Big(\frac{\alpha}{2\pi}\Big)(\delta y)^2\Big[\ln(\delta y) + 7.33\Big]. \tag{111}$$

From Eq.(111), it is shown that f_γ^0 for $\mu^+ \to e^+\nu_e\overline{\nu}_\mu\gamma$ decay is roughly proportional to $(\delta y)^2$.

The other sources of high-energy photons are annihilation in flight of e^+s in the normal muon decay and external bremsstrahlung. The contribution from annihilation of e^+ in flight depends on the materials along the e^+'s track path. Fig.23 shows, for instance, the contribution of annihilation in flight for that case of e^+s passing through a muon-stopping target of 50 mg in thickness. It indicates that its contribution from the target is smaller than the radiative muon decay, and only becomes important if the photon energy resolution becomes extremely good. However, it is dependent on the total amount of materials in an experimental setup.

From the above, the effective branching ratio of accidental background is given by

$$B_{acc} = R_\mu \cdot (2\delta x) \cdot \Big[\frac{\alpha}{2\pi}(\delta y)^2(\ln(\delta y) + 7.33)\Big] \times \Big(\frac{\delta\theta^2}{4}\Big) \cdot (2\delta t). \tag{112}$$

For instance, take some reference numbers such as the e^+ energy resolution of 1% (FWHM), the photon energy resolution of 6% (FWHM), $\Delta\omega_{e\gamma} = 3 \times 10^{-4}$ steradian, $\Delta t_{e\gamma} = 1$ nsec, and $R_\mu = 3 \times 10^8$ μ^+/sec, $B_{\rm acc}$ is 3×10^{-13}. The accidental background becomes severe. Therefore, it is critical to make significant improvements in the detector resolution in order to reduce the accidental background.

5. Muon polarization

The use of polarized muons has been found to be useful to suppress backgrounds for $\mu^+ \to e^+\gamma$ search (Kuno and Okada, 1996; Kuno, *et al.*, 1997a). For the physical (prompt) background, as already discussed in Subsection V A 3, the coefficient of J_2 is

much larger than J_1, since the resolution of the photon energy is much worse than that of the e^+ energy detection. Therefore, the angular distribution of the physics background follows approximately $(1+P_\mu \cos\theta)$ as long as $\delta y > \delta x$. Fig.24 shows the angular distribution of $\mu^+ \to e^+\nu_e\overline{\nu}_\mu\gamma$ with, for instance, $\delta y/\delta x = 4$. If we selectively measure the e^+s in $\mu^+ \to e^+\gamma$ going opposite to the muon-polarization direction, the background from $\mu^+ \to e^+\nu_e\overline{\nu}_\mu\gamma$ would be significantly reduced for the $\mu^+ \to e^+_R\gamma$ search. Furthermore, by varying δx and δy, the angular distribution of the $\mu^+ \to e^+\nu_e\overline{\nu}_\mu\gamma$ background can change according to Eq.(106), thus providing another means to discriminate the signal from the backgrounds.

Regarding the accidental background, the use of polarized muons has also provided a means for its suppression (Kuno, *et al.*, 1997a). It happens that the sources of accidental backgrounds have a specific angular distribution when a muon is polarized. For instance, the e^+s in the normal Michel μ^+ decay are emitted preferentially along the muon spin direction, following a $(1+P_\mu \cos\theta_e)$ distribution, as in Eq.(33), whereas the inclusive angular distribution of a high-energy photon (*e.g.* ≥ 50 MeV) from $\mu^+ \to e^+\nu_e\overline{\nu}_\mu\gamma$ decay follows a $(1 + P_\mu \cos\theta_\gamma)$ distribution, as in Eq.(54), where θ_γ is the angle of the photon direction with respect to the muon spin direction. It should be noted that this inclusive angular distribution was obtained after integrating the energy and direction of the e^+s, which is in contrast to the case of the physics background, where only the extreme kinematics of the e^+ and photon being back-to-back in $\mu^+ \to e^+\nu_e\overline{\nu}_\mu\gamma$ decay is relevant. It is further noted that the other sources of high-energy photons, such as external bremsstrahlung and annihilation in flight of e^+s from the normal muon decay, also follow a $(1 + P_\mu \cos\theta_\gamma)$ distribution.

This inclusive angular distribution of a high-energy photon in $\mu^+ \to e^+\nu_e\overline{\nu}_\mu\gamma$ implies that the accidental background could be suppressed for $\mu^+ \to e^+_L\gamma$, where high-energy photons must be detected at the opposite direction to the muon polarization. A similar suppression mechanism of accidental background can be seen for $\mu^+ \to e^+_R\gamma$ when high-energy positrons are detected at the opposite direction to the muon polarization. As a result, the selective measurements of either e^+s or photons antiparallel to the muon spin direction would give the same accidental background suppression for $\mu^+ \to e^+_R\gamma$ and $\mu^+ \to e^+_L\gamma$ decays, respectively. This favorable situation comes from the fact that the inclusive distributions of both high-energy e^+s and photons, respectively, in the normal and radiative muon decays, follow a $(1 + P_\mu \cos\theta)$ distribution, where θ is either θ_e or θ_γ. The suppression factor, η, is calculated for polarized muons by

$$\begin{aligned}\eta &\equiv \int_{\cos\theta_D}^{1} d(\cos\theta)(1 + P_\mu \cos\theta)(1 - P_\mu \cos\theta) \Big/ \int_{\cos\theta_D}^{1} d(cos\theta) \\ &= (1 - P_\mu^2) + \frac{1}{3}P_\mu^2(1 - \cos\theta_D)(2 + \cos\theta_D), \end{aligned} \tag{113}$$

where θ_D is a half opening angle of detection with respect to the muon polarization direction. η is shown in Fig.25 as a function of θ_D. For instance, for $\theta_D = 300$ mrad, an accidental background can be suppressed down to about 1/20 (1/10) when P_μ is 100 (97)%.

TABLE IX. Historical Progress of search for $\mu^+ \to e^+\gamma$ since the era of meson factories with 90 % C.L. upper limits. The resolutions quoted are given as a full width at half maximum (FWHM).

Place	Year	ΔE_e	ΔE_γ	$\Delta t_{e\gamma}$	$\Delta\theta_{e\gamma}$	Upper limit	References
TRIUMF	1977	10%	8.7%	6.7ns	–	$< 3.6 \times 10^{-9}$	Depommier, *et al.* (1977)
SIN	1980	8.7%	9.3%	1.4ns	–	$< 1.0 \times 10^{-9}$	Van der Schaaf, *et al.* (1980)
LANL	1982	8.8%	8%	1.9ns	37mrad	$< 1.7 \times 10^{-10}$	Kinnison, *et al.* (1982)
LANL	1988	8%	8%	1.8ns	87mrad	$< 4.9 \times 10^{-11}$	Bolton, *et al.* (1988)
LANL	1999	1.2%*	4.5%*	1.6ns	15mrad	$< 1.2 \times 10^{-11}$	Brooks, *et al.* (1999)

* shows an average of the numbers given in Brooks, *et al.* (1999).

6. Experimental status of $\mu^+ \to e^+\gamma$ decay

Experimental searches for $\mu^+ \to e^+\gamma$ have a long history of more than 50 years. These searches have been actively promoted by intense muon beams available at the meson factories. Experimental efforts have been devoted to improving the detection resolutions of four variables, namely the positron energy (E_e), the photon energy (E_γ), the timing between the positron and photon ($\Delta t_{e\gamma}$), and the angle between the positron and photon ($\Delta\theta_{e\gamma}$). Various kinds of apparatus have been tried in the past. In Table IX, several experimental results of 90% C.L. upper limit of $\mu^+ \to e^+\gamma$ decay in the past experiments are listed along with their achieved detection resolutions.

The upper limit quoted in the Particle Data Group (Particle Data Group, 1998) is $B(\mu^+ \to e^+\gamma) < 4.9 \times 10^{-11}$, which was obtained by an experiment with the "Crystal Box" detector (Bolton, *et al.*, 1988) at Los Alamos National Laboratory (LANL). Its apparatus consisted of 396 NaI(Tl) crystals, cylindrical drift chambers surrounding a muon-stopping target in a zero magnetic field.

Since then, a new experimental search for $\mu^+ \to e^+\gamma$ has been carried out by the MEGA collaboration at LANL. A schematic view of the MEGA spectrometer is shown in Fig.26. The MEGA detector consisted of a magnetic spectrometer for the positron and three concentric pair-spectrometers for the photon. They were placed inside a superconducting solenoid magnet of a 1.5 T field. The positron spectrometer comprised eight cylindrical wire chambers and scintillators for timing. The positron energy resolution (FWHM) was from 0.5 MeV (0.95%) to 0.85 MeV (1.6%) for a 52.8-MeV e^+, depending on the number of helical loops of e^+ tracks. For the pair-spectrometer, each layer had lead converters, MWPCs, drift chambers and scintillators. The photon energy resolutions (FWHM) were 1.7 MeV (3.3%) and 3.0 MeV (5.7%) for the outer and inner Pb conversion layers, respectively. A surface μ^+ beam of 29.8 MeV/c was introduced along the detector axis, and was stopped in the muon-stopping target made of a thin tilted Mylar foil. All of the charged particles from muon decays are confined within the positron spectrometer. The intensity of the muon beam was 2.5×10^8/sec with a macroscopic duty factor of 6%. The total number of muons stopped was 1.2×10^{14}. By using the likelihood method, a new limit of 1.2×10^{-11} with 90% C.L. has been reported (Brooks, *et al.*, 1999).

Recently, a new experimental proposal, R-99-05, aiming at a sensitivity of 10^{-14} in the $\mu^+ \to e^+\gamma$ branching ratio has been approved at PSI (Barkov, *et al.*, 1999). The improvement will be expected by utilizing a continuous muon beam of 100% duty factor at PSI. With keeping the same instantaneous beam intensity as MEGA, the total number of muons available can be increased by a factor of 16. Further improvement is a novel liquid xenon scintillation detector of the "Mini-Kamiokande" type, which is a 0.8-m^3 volume of liquid xenon viewed by an array of a total of 800 photomultipliers from all the sides. The expected resolutions (FWHM) of the photon energy and position are about 1.4% and 4 mm, respectively. As the e^+ detection, a solenoidal magnetic spectrometer with a graded magnetic field is adopted, in which the magnetic field is arranged so that e^+ from the $\mu^+ \to e^+\gamma$ decay follows a trajectory with a constant radius, independently of its emission angle. It allows easier identification of the e^+ in the $\mu^+ \to e^+\gamma$ decay. Physics data taking is expected to start in year 2003.

A search for $\mu^+ \to e^+\gamma\gamma$ was also undertaken simultaneously with the $\mu^+ \to e^+\gamma$ search. The present 90% C.L. upper limit of $B(\mu^+ \to e^+\gamma\gamma) < 7.2 \times 10^{-11}$ was obtained (Bolton, *et al.*, 1988).

B. $\mu^+ \to e^+e^+e^-$ decay

1. Phenomenology of $\mu^+ \to e^+e^+e^-$ decay

The decay width of $\mu^+ \to e^+e^-e^-$ is determined from the effective Lagrangian (at the m_μ scale) described in Eqs.(57) and (61) in Section III. The relevant interactions are

$$\begin{aligned}\mathcal{L}_{\mu\to eee} = -\frac{4G_F}{\sqrt{2}}\Big[& m_\mu A_R \overline{\mu_R}\sigma^{\mu\nu} e_L F_{\mu\nu} + m_\mu A_L \overline{\mu_L}\sigma^{\mu\nu} e_R F_{\mu\nu} \\ & + g_1(\overline{\mu_R}e_L)(\overline{e_R}e_L) + g_2(\overline{\mu_L}e_R)(\overline{e_L}e_R) \\ & + g_3(\overline{\mu_R}\gamma^\mu e_R)(\overline{e_R}\gamma_\mu e_R) + g_4(\overline{\mu_L}\gamma^\mu e_L)(\overline{e_L}\gamma_\mu e_L) \\ & + g_5(\overline{\mu_R}\gamma^\mu e_R)(\overline{e_L}\gamma_\mu e_L) + g_6(\overline{\mu_L}\gamma^\mu e_L)(\overline{e_R}\gamma_\mu e_R) + H.c.\Big], \end{aligned} \tag{114}$$

where the f_{E0} and f_{M0} photonic contributions in Eq.(58) are included in the four fermion coupling constants.

When muons are polarized, the kinematics of the $\mu^+ \to e^+e^+e^-$ decay is determined by two energy variables and two angle variables of the decay positrons (Okada, *et al.*, 1998; Okada, *et al.*, 1999). The energy variables are $x_1 = 2E_1/m_\mu$ and $x_2 = 2E_2/m_\mu$, where E_1 (E_2) is the higher (lower) energy of the decay positrons. The allowed regions of x_1 and x_2 are $\frac{1}{2} \le x_1 \le 1$ and $1 - x_1 \le x_2 \le x_1$, if m_e is neglected compared to m_μ. Let us take the coordinate as shown in Fig.27, where the z-axis is in the direction of the decay electron momentum ($\vec{p_3}$), and the $z-x$ plane is the decay plane. The positive direction of the x-axis is chosen to be in the hemisphere of higher-energy positron. The two angles (θ, φ) determine the direction of the muon polarization ($\vec{P}_\mu$) with respect to the decay plane.

In this coordinate, the differential branching ratio of the $\mu^+ \to e^+e^+e^-$ decay is given by

$$
\begin{aligned}
\frac{dB(\mu^+ \to e^+e^+e^-)}{dx_1dx_2d(\cos\theta)d\varphi} = \frac{3}{2\pi}\Big[& C_1\alpha_1(x_1,x_2)(1+P_\mu\cos\theta) + C_2\alpha_1(x_1,x_2)(1-P_\mu\cos\theta) \\
& + C_3\{\alpha_2(x_1,x_2) + P_\mu\beta_1(x_1,x_2)\cos\theta + P_\mu\gamma_1(x_1,x_2)\sin\theta\cos\varphi\} \\
& + C_4\{\alpha_2(x_1,x_2) - P_\mu\beta_1(x_1,x_2)\cos\theta - P_\mu\gamma_1(x_1,x_2)\sin\theta\cos\varphi\} \\
& + C_5\{\alpha_3(x_1,x_2) + P_\mu\beta_2(x_1,x_2)\cos\theta + P_\mu\gamma_2(x_1,x_2)\sin\theta\cos\varphi\} \\
& + C_6\{\alpha_3(x_1,x_2) - P_\mu\beta_2(x_1,x_2)\cos\theta - P_\mu\gamma_2(x_1,x_2)\sin\theta\cos\varphi\} \\
& + C_7\{\alpha_4(x_1,x_2)(1-P_\mu\cos\theta) + P_\mu\gamma_3(x_1,x_2)\sin\theta\cos\varphi\} \\
& + C_8\{\alpha_4(x_1,x_2)(1+P_\mu\cos\theta) - P_\mu\gamma_3(x_1,x_2)\sin\theta\cos\varphi\} \\
& + C_9\{\alpha_5(x_1,x_2)(1+P_\mu\cos\theta) - P_\mu\gamma_4(x_1,x_2)\sin\theta\cos\varphi\} \\
& + C_{10}\{\alpha_5(x_1,x_2)(1-P_\mu\cos\theta) + P_\mu\gamma_4(x_1,x_2)\sin\theta\cos\varphi\} \\
& + C_{11}P_\mu\gamma_3(x_1,x_2)\sin\theta\sin\varphi - C_{12}P_\mu\gamma_4(x_1,x_2)\sin\theta\sin\varphi + H.c.\Big], \quad (115)
\end{aligned}
$$

where P_μ is the magnitude of the polarization vector. Functions of α_i, β_i and γ_i are presented in the Appendix C. The coefficients of C_i are expressed by g_i $(i = 1-6)$, A_L and A_R. They are given by

$$
\begin{aligned}
& C_1 = \frac{|g_1|^2}{16} + |g_3|^2,\ C_2 = \frac{|g_2|^2}{16} + |g_4|^2, \\
& C_3 = |g_5|^2,\ C_4 = |g_6|^2, C_5 = |eA_R|^2,\ C_6 = |eA_L|^2, \\
& C_7 = \mathrm{Re}(eA_Rg_4^*),\ C_8 = \mathrm{Re}(eA_Lg_3^*),\ C_9 = \mathrm{Re}(eA_Rg_6^*),\ C_{10} = \mathrm{Re}(eA_Lg_5^*), \\
& C_{11} = \mathrm{Im}(eA_Rg_4^* + eA_Lg_3^*),\ C_{12} = \mathrm{Im}(eA_Rg_6^* + eA_Lg_5^*). \quad (116)
\end{aligned}
$$

In Eq.(115), there are four types of contributions which have different angular dependences with respect to the muon polarization. They are the contributions with an isotropic angular distribution, which are the even parity (P) and time-reversal (T), those proportional to either $\cos\theta$ or $\sin\theta\cos\varphi$, which are P-odd and T-even, and finally, those proportional to $\sin\theta\sin\varphi$, which are P-even and T-odd.

The integrated branching ratio and the T-odd asymmetry for $\mu^+ \to e^+e^+e^-$ decay are given by (Okada, *et al.*, 1999)

$$
\begin{aligned}
B(\mu^+ \to e^+e^+e^-) &= \int_{\frac{1}{2}}^1 dx_1 \int_{1-x_1}^{x_1} dx_2 \int_{-1}^1 d(\cos\theta) \int_0^\pi d\phi \frac{dB(\mu^+ \to e^+e^+e^-)}{dx_1dx_2d(\cos\theta)d\phi}, \\
&= 2(C_1+C_2) + (C_3+C_4) + 32\{\ln(\frac{m_\mu^2}{m_e^2}) - \frac{11}{4}\}(C_5+C_6) \\
&\quad +16(C_7+C_8) + 8(C_9+C_{10}), \quad (117) \\
A_T(\mu^+ \to e^+e^+e^-) &= \frac{1}{P_\mu B(\mu^+ \to e^+e^+e^-)}\Bigg[\int_{\frac{1}{2}}^1 dx_1 \int_{1-x_1}^{x_1} dx_2 \int_{-1}^1 d(\cos\theta) \int_0^\pi d\phi \frac{dB(\mu^+ \to e^+e^+e^-)}{dx_1dx_2d(\cos\theta)d\phi} \\
&\quad - \int_{\frac{1}{2}}^1 dx_1 \int_{1-x_1}^{x_1} dx_2 \int_{-1}^1 d\cos\theta \int_\pi^{2\pi} d\phi \frac{dB(\mu^+ \to e^+e^+e^-)}{dx_1dx_2d(\cos\theta)d\phi}\Bigg] \\
&= \frac{64}{35}\frac{1}{B(\mu^+ \to e^+e^+e^-)}\{3C_{11} - 2C_{12}\}. \quad (118)
\end{aligned}
$$

The T-odd asymmetry turns out to be proportional to $\mathrm{Im}(eA_Rg_4^* + eA_Lg_3^*)$ $(= C_{11})$ and $\mathrm{Im}(eA_Rg_6^* + eA_Lg_5^*)$ $(= C_{12})$. It arises from interference between the on-shell photon-penguin terms and the four-fermion terms.

If only the photon-penguin diagrams contribute to $\mu^+ \to e^+e^+e^-$ decay (namely in the case of $C_5 \neq 0$, $C_6 \neq 0$, and the others =0), a model-independent relation between the two branching ratios can be derived, as follows:

$$\frac{B(\mu^+ \to e^+e^+e^-)}{B(\mu^+ \to e^+\gamma)} \simeq \frac{\alpha}{3\pi}(\ln(\frac{m_\mu^2}{m_e^2}) - \frac{11}{4}) = 0.006. \tag{119}$$

2. Event signature and backgrounds

The event signature of the $\mu^+ \to e^+e^+e^-$ decay is kinematically well constrained, since all particles in the final state are detectable. Muon decay at rest has been used in all past experiments. In this case, the conservation of momentum ($|\sum_i \vec{p}_i| = 0$) and energy ($\sum_i E_i = m_\mu$) could be effectively used together with the timing coincidence between two e^+s and one e^-, where $\vec{p}_i$ and E_i ($i = 1, 3$) are the momentum and energy of each of the three e's, respectively.

One of the physics background processes is an allowed muon decay, $\mu^+ \to e^+e^+e^-\nu_e\overline{\nu}_\mu$, which becomes a serious background when ν_e and $\overline{\nu}_\mu$ have very small energies. Its branching ratio is $B(\mu^+ \to e^+e^+e^-\nu_e\overline{\nu}_\mu) = (3.4 \pm 0.4) \times 10^{-5}$. The other background is an accidental coincidence of an e^+ from normal muon decay with an uncorrelated e^+e^- pair, where a e^+e^- pair could be produced either from Bhabha scattering of e^+, or from the external conversion of the photon in $\mu^+ \to e^+\nu_e\overline{\nu}_\mu\gamma$ decay. Since the e^+e^- pair from photon conversion has a small invariant mass, it could be removed by eliminating events with a small opening angle between e^+ and e^-. This, however, causes a loss of the signal sensitivity, in particular for theoretical models in which $\mu^+ \to e^+e^+e^-$ decay occurs mostly through photonic diagrams.

The other background, which comes especially at the trigger level, comprises fake events with an e^+ curling back to the target, which mimics an e^+e^- pair. For this background, an e^+e^- pair forms its relative angle of 180°, and can therefore be rejected.

3. Experimental status of $\mu^+ \to e^+e^+e^-$ decay

TABLE X. Historical progress and summary of searches for $\mu^+ \to e^+e^+e^-$ decay.

Place	Year	90%C.L. upper limit	Reference
JINR	1976	$< 1.9 \times 10^{-9}$	Korenchenko, *et al.* (1976)
LANL	1984	$< 1.3 \times 10^{-10}$	Bolton, *et al.* (1984)
PSI	1984	$< 1.6 \times 10^{-10}$	Bertl, *et al.* (1984)
PSI	1985	$< 2.4 \times 10^{-12}$	Bertl, *et al.* (1985)
LANL	1988	$< 3.5 \times 10^{-11}$	Bolton, *et al.* (1988)
PSI	1988	$< 1.0 \times 10^{-12}$	Bellgardt, *et al.* (1988)
JINR	1991	$< 3.6 \times 10^{-11}$	Baranov, *et al.* (1991)

After the pioneering measurement in 1976 using a cylindrical spectrometer, which gave an upper limit of $B(\mu^+ \to e^+e^+e^-) < 1.9 \times 10^{-9}$ (Korenchenko, *et al.*, 1976), various experiments to search for $\mu^+ \to e^+e^+e^-$ decay have been carried out, as shown in Table X. In particular, a series of experimental measurements with the SINDRUM magnetic spectrometer at SIN (Bertl, *et al.*, 1984; Bertl, *et al.*, 1985; Bellgardt, *et al.*, 1988) were carried out. A surface μ^+ beam with $5 \times 10^6 \mu^+$/sec was used, and the muons were stopped in a hollow double-cone target. The e^+s and e^-s were tracked by the SINDRUM spectrometer, which consisted of five concentric multiwire proportional chambers (MWPC) and a cylindrical array of 64 plastic scintillation counters under a solenoid magnetic field of 0.33 T. The momentum resolution was $\Delta p/p = (12.0 \pm 0.3)$ % (FWHM) at p =50 MeV/c. This experiment gave a 90% C.L. upper limit of $B(\mu^+ \to e^+e^+e^-) < 1.0 \times 10^{-12}$, assuming a constant matrix element for the $\mu^+ \to e^+e^+e^-$ decay (Bellgardt, *et al.*, 1988). They also observed 9070 ± 10 events of $\mu^+ \to e^+e^+e^-\nu_e\overline{\nu}_\mu$ decay. A detailed analysis of the differential decay rate of $\mu^+ \to e^+e^+e^-\nu_e\overline{\nu}_\mu$ decay was studied, and was found to be consistent with the $V-A$ interaction (Kersch, *et al.*, 1988).

Another recent experiment to search for $\mu^+ \to e^+e^+e^-$ was performed at Joint Institute for Nuclear Research (JINR), Dubna, Russia (Baranov, *et al.*, 1991). A magnetic 4π spectrometer with cylindrical proportional chambers was used. They obtained an upper limit of 90% CL of $B(\mu^+ \to e^+e^+e^-) < 3.6 \times 10^{-11}$, where the matrix element of $\mu^+ \to e^+e^+e^-$ was assumed to be constant.

C. $\mu^- - e^-$ coherent conversion in a muonic atom

1. Phenomenology of $\mu^- - e^-$ conversion

Another prominent process concerning lepton flavor violation is $\mu^- - e^-$ conversion in a muonic atom. When a negative muon is stopped in some material, it is trapped by an atom, and forms a muonic atom. After it cascades down in energy levels in the muonic atom, a muon is bound in its $1s$ ground state. The fate of the muon is then either decay in an orbit ($\mu^- \to e^-\nu_\mu\overline{\nu}_e$) or capture by a nucleus of mass number A and atomic number Z, namely

$$\mu^- + (A, Z) \to \nu_\mu + (A, Z-1). \tag{120}$$

However, in the context of physics beyond the Standard Model, the exotic process of neutrinoless muon capture, such as

$$\mu^- + (A, Z) \to e^- + (A, Z), \tag{121}$$

is also expected. This process is called $\mu^- - e^-$ conversion in a muonic atom. It violates the conservation of the lepton flavor numbers, L_e and L_μ, by one unit, but conserves the total lepton number, L.

The branching ratio of $\mu^- - e^-$ conversion can be given by

$$B(\mu^- + (A, Z) \to e^- + (A, Z)) \equiv \frac{\Gamma(\mu^- + (A, Z) \to e^- + (A, Z))}{\Gamma(\mu^- + (A, Z) \to capture)}, \tag{122}$$

where Γ is the corresponding decay width.

The final state of the nucleus (A, Z) could be either the ground state or excited states. In general, the transition process to the ground state, which is called coherent capture, is dominant. The rate of the coherent capture process over non-coherent ones is enhanced by a factor approximately equal to the number of nucleons in the nucleus, since all of the nucleons participate in the process.

The possible contributions to $\mu^- - e^-$ conversion in a muonic atom can be grouped into two parts, which are the photonic contribution and the non-photonic contribution. Therefore, in principle, this process is theoretically interesting, since it does occur by mechanisms which do not contribute to the $\mu^+ \to e^+\gamma$ process. The study of the photonic contribution was initiated by Weinberg and Feinberg (Weinberg and Feinberg, 1959). The non-photonic contribution was studied later, for instance by Marciano and Sanda (1977b).

Let us first discuss the photonic transition. The effective Lagrangian for the photonic transition is written as

$$\mathcal{L}_{photo} = -eJ^{\mu}_{photo}A_{\mu}. \tag{123}$$

The matrix element of the $\mu^-(p_\mu) \to e^-(p_e)\gamma^*(q)$ transition, where p_μ, p_e and $q = p_\mu - p_e$ are the muon, electron and virtual photon four-momenta respectively, is given by

$$\begin{aligned} M_{photonic} &= -eA^*_{\mu}(q) < e^-(p_e)|J^{\mu}_{photo}(0)|\mu^-(p_\mu) >, \\ &= -eA^*_{\mu}(q)\overline{u}_e(p_e)\Big[(f_{E0}(q^2) + \gamma_5 f_{M0}(q^2))\gamma_\nu(g^{\mu\nu} - \frac{q^\mu q^\nu}{q^2}) \\ &\quad +(f_{M1}(q^2) + \gamma_5 f_{E1}(q^2))\frac{i\sigma_{\mu\nu}q^\nu}{m_\mu}\Big]u_\mu(p_\mu). \end{aligned} \tag{124}$$

Based on Eq.(124), the branching ratio of the coherent $\mu^- - e^-$ conversion through the photonic contribution is given by (Weinberg and Feinberg, 1959)

$$B(\mu^- N \to e^- N) = (8\alpha^5 m_\mu Z^4_{eff} Z F_p^2 \xi^2) \cdot \frac{1}{\Gamma_{capt}}, \tag{125}$$

where Γ_{cap} is the total muon capture rate. ξ^2 is given by

$$\xi^2 = |f_{E0}(-m_\mu^2) + f_{M1}(-m_\mu^2)|^2 + |f_{E1}(-m_\mu^2) + f_{M0}(-m_\mu^2)|^2. \tag{126}$$

It is noted that in photonic diagrams, in contrast to $\mu^+ \to e^+\gamma$, not only f_{E1} and f_{M1}, but also f_{E0} and f_{M0}, can contribute to the $\mu^- - e^-$ conversion. Z_{eff} is an effective atomic charge obtained by averaging the muon wave function over the nuclear density (Chiang, *et al.*, 1993). This is defined as

$$\frac{\alpha^3 m_\mu^3}{\pi}\frac{Z^4_{eff}}{Z} = \int d^3x |\Phi_\mu(x)|^2 \rho_p(x) \equiv < \Phi_{1s} >^2, \tag{127}$$

where $\Phi_\mu(x)$ is the non-relativistic muon wave function for the *1s* state of the muonic atom and $\rho_p(x)$ is the proton density in the nucleus normalized as

$$\int d^3x \rho_p(x) = 1. \tag{128}$$

F_p^2 is the nuclear matrix element squared, given by

$$F_p = \int d^3x e^{-ip_e x} \rho_p(x) = 4\pi \int \rho_p(r) \frac{\sin m_\mu r}{m_\mu r} r^2 dr. \tag{129}$$

In Eq.(125), the $\mu^- - e^-$ conversion process is roughly proportional to $(Z_{eff})^4 Z$, whereas the normal muon capture, Γ_{capt}, is proportional to $(Z_{eff})^4$. The enhancement by a factor of Z in the $\mu^- - e^-$ coherent conversion is evident.

Let us next discuss the non-photonic contribution. The general four fermion interaction of the $\mu^- - e^-$ conversion at the quark level is given by

$$\begin{aligned}
\mathcal{L}_{non-photo} = -\frac{G_F}{\sqrt{2}} \sum_{q=u,d,s\ldots} \Big[& (g_{LS(q)} \overline{e_L} \mu_R + g_{RS(q)} \overline{e_R} \mu_L) \overline{q} q \\
& + (g_{LP(q)} \overline{e_L} \mu_R + g_{RP(q)} \overline{e_R} \mu_L) \overline{q} \gamma_5 q \\
& + (g_{LV(q)} \overline{e_L} \gamma^\mu \mu_L + g_{RV(q)} \overline{e_R} \gamma^\mu \mu_R) \overline{q} \gamma_\mu q \\
& + (g_{LA(q)} \overline{e_L} \gamma^\mu \mu_L + g_{RA(q)} \overline{e_R} \gamma^\mu \mu_R) \overline{q} \gamma_\mu \gamma_5 q \\
& + \frac{1}{2} (g_{LT(q)} \overline{e_L} \sigma^{\mu\nu} \mu_R + g_{RT(q)} \overline{e_R} \sigma^{\mu\nu} \mu_L) \overline{q} \sigma_{\mu\nu} q + H.c. \Big].
\end{aligned} \tag{130}$$

At first, this effective Lagrangian at the quark level is converted into that at the nucleon level by using the nucleon form factors (Vergados, 1986; Bernabeu, *et al.*, 1993; Faessler, *et al.*, 1999). Since the momentum transfer in the $\mu^- - e^-$ conversion process is smaller than the size of the nucleon structure, the momentum dependence of the nucleon form factors can be neglected. In such a case, the matrix element of the quark currents can be replaced by the corresponding nucleon current by using

$$\begin{aligned}
< p|\overline{q} \Gamma_K q|p > &= G_K^{(q,p)} \overline{p} \Gamma_K p, \\
< n|\overline{q} \Gamma_K q|n > &= G_K^{(q,n)} \overline{n} \Gamma_K n,
\end{aligned} \tag{131}$$

with $\Gamma_K = (1, \gamma_5, \gamma_\mu, \gamma_\mu\gamma_5, \sigma_{\mu\nu})$ for $K = (S, P, V, A, T)$. For the vector current, $G_V^{(u,p)} = G_V^{(d,n)} = 2$ and $G_V^{(d,p)} = G_V^{(u,n)} = 1$. In general, the isospin invariance requires the relations $G_K^{(u,p)} = G_K^{(d,n)}$, $G_K^{(u,p)} = G_K^{(d,n)}$ and $G_K^{(s,p)} = G_K^{(s,n)}$. The effective Lagrangian at the nucleon level is given by

$$\begin{aligned}
\mathcal{L}_{non-photo} = -\frac{G_F}{\sqrt{2}} \Big[& \overline{e_L} \mu_R \overline{\Psi} \{ (g_{LS}^{(0)} + g_{LS}^{(1)} \tau_3) + (g_{LP}^{(0)} + g_{LP}^{(1)} \tau_3) \gamma_5 \} \Psi \\
& + \overline{e_R} \mu_L \overline{\Psi} \{ (g_{RS}^{(0)} + g_{RS}^{(1)} \tau_3) + (g_{RP}^{(0)} + g_{RP}^{(1)} \tau_3) \gamma_5 \} \Psi \\
& + \overline{e_L} \gamma^\mu \mu_L \overline{\Psi} \gamma_\mu \{ (g_{LV}^{(0)} + g_{LV}^{(1)} \tau_3) + (g_{LA}^{(0)} + g_{LA}^{(1)} \tau_3) \gamma_5 \} \Psi \\
& + \overline{e_R} \gamma^\mu \mu_R \overline{\Psi} \gamma_\mu \{ (g_{RV}^{(0)} + g_{RV}^{(1)} \tau_3) + (g_{RA}^{(0)} + g_{RA}^{(1)} \tau_3) \gamma_5 \} \Psi \\
& + \frac{1}{2} \overline{e_L} \sigma^{\mu\nu} \mu_R \overline{\Psi} \sigma_{\mu\nu} \{ (g_{LT}^{(0)} + g_{LT}^{(1)} \tau_3) \} \Psi + \frac{1}{2} \overline{e_R} \sigma^{\mu\nu} \mu_L \overline{\Psi} \sigma_{\mu\nu} \{ (g_{RT}^{(0)} + g_{RT}^{(1)} \tau_3) \} \Psi + H.c. \Big],
\end{aligned} \tag{132}$$

where $\Psi = (p, n)^T$ and the isoscalar and isovector coupling constants $g_{XK}^{(0)}$ and $g_{XK}^{(1)}$ ($X = L, R$, and $K = S, P, V, A, T$) are respectively given by

$$g^{(0)}_{XK} = \frac{1}{2}\sum_{q=u,d,s}(g_{XK(q)}G^{(q,p)}_K + g_{XK(q)}G^{(q,n)}_K), \tag{133}$$

$$g^{(1)}_{XK} = \frac{1}{2}\sum_{q=u,d,s}(g_{XK(q)}G^{(q,p)}_K - g_{XK(q)}G^{(q,n)}_K). \tag{134}$$

For coherent $\mu^- - e^-$ conversion, only the scalar and vector coupling constants can be kept. By using a non-relativistic approximation for the muon wave function, the transition rate is given by

$$B(\mu^- N \to e^- N) = \frac{p_e E_e G_F^2}{8\pi}(|X_L(p_e)|^2 + |X_R(p_e)|^2)\frac{1}{\Gamma_{capt}}, \tag{135}$$

where

$$X_L(p_e) = (g^{(0)}_{LS} + g^{(1)}_{LS} + g^{(0)}_{LV} + g^{(1)}_{LV})ZM_p(p_e) + (g^{(0)}_{LS} - g^{(1)}_{LS} + g^{(0)}_{LV} - g^{(1)}_{LV})NM_n(p_e), \tag{136}$$

$$X_R(p_e) = (g^{(0)}_{RS} + g^{(1)}_{RS} + g^{(0)}_{RV} + g^{(1)}_{RV})ZM_p(p_e) + (g^{(0)}_{RS} - g^{(1)}_{RS} + g^{(0)}_{RV} - g^{(1)}_{RV})NM_n(p_e), \tag{137}$$

and $N \equiv A - Z$ is the number of neutrons in the nuclei. $M_p(p)$ and$M_n(p)$ are given by

$$M_p(p) = \int d^3x e^{-ipx}\rho_p(x)\Phi_\mu(x), \quad M_n(p) = \int d^3x e^{-ipx}\rho_n(x)\Phi_\mu(x), \tag{138}$$

with the proton and neutron densities, $\rho_p(x)$ and $\rho_n(x)$, normalized to unity. If it is assumed that the proton and neutron densities are equal and that the muon wave function does not change very much in the nucleus, by using Eq.(127), Eq.(135) can be deduced into

$$B(\mu^- N \to e^- N) = \frac{p_e E_e m_\mu^3 G_F^2 \alpha^3 Z_{eff}^4 F_p^2}{8\pi^2 Z}\Big\{|\ (Z+N)(g^{(0)}_{LS} + g^{(0)}_{LV}) + (Z-N)(g^{(1)}_{LS} + g^{(1)}_{LV})\ |^2$$
$$+|\ (Z+N)(g^{(0)}_{RS} + g^{(0)}_{RV}) + (Z-N)(g^{(1)}_{RS} + g^{(1)}_{RV})\ |^2\Big\} \cdot \frac{1}{\Gamma_{capt}}. \tag{139}$$

This equation corresponds to Eq.(125) for the photonic case, which was derived in a similar approximation. In Eq.(139), the coherent process is enhanced by a factor of the number of nucleons, as can be seen in Eq.(125).

In general, both photonic and non-photonic contributions might exist. If the non-relativistic approximation for the muon wave function is used and the momentum transfer of q^2 is replaced by $-m_\mu^2$, the photonic contribution can be regarded as additional terms to the vector-coupling constants. They are given by

$$\Delta g^{(0)}_{LV} = \Delta g^{(1)}_{LV} = \frac{2\sqrt{2}\alpha\pi}{G_F m_\mu^2}(f_{E0}(-m_\mu^2) + f_{M1}(-m_\mu^2) + f_{M0}(-m_\mu^2) + f_{E1}(-m_\mu^2)), \tag{140}$$

$$\Delta g^{(0)}_{RV} = \Delta g^{(1)}_{RV} = \frac{2\sqrt{2}\alpha\pi}{G_F m_\mu^2}(f_{E0}(-m_\mu^2) + f_{M1}(-m_\mu^2) - f_{M0}(-m_\mu^2) - f_{E1}(-m_\mu^2)). \tag{141}$$

These contributions are added to the corresponding vector coupling constants in Eq.(139). In such a case, the interference terms should be taken into account as well.

So far, the non-relativistic approximation for the muon wave function and a plane wave for the emitted electron have been used to derive the $\mu^- - e^-$ conversion rates. Possible corrections for this approximation turn out to be important for heavy nuclei. A relativistic treatment based on the Dirac equation was considered and the corrections to the Weinberg-Feinberg formulas were calculated (Shanker, 1979). Recently, the photonic transitions due to f_{M1} and f_{E1} were further examined by properly treating the electric potential in the muonic atom (Czarnecki, *et al.*, 1997).

In the case that the photonic contributions of $f_{E1}(q^2)$ and $f_{M1}(q^2)$ dominate over the other contributions, the rate of $\mu^- - e^-$ conversion can be parameterized by (Czarnecki, *et al.*, 1997)

$$B(\mu^- N \to e^- N) = 3 \cdot 10^{12}(|f_{E1}|^2 + |f_{M1}|^2)B(A,Z), \tag{142}$$

where $B(A,Z)$ represents the rate dependence on the mass number (A) and the atomic number (Z) of the target nucleus. This particular case becomes important, for instance, in $SO(10)$ SUSY GUT. The values of $B(A,Z)$, based on different approximations, are tabulated in Table XI, where $B_{WF}(A,Z)$ is from the Weinberg-Feinberg approximation (Weinberg and Feinberg, 1959), $B_S(A,Z)$ is from Shanker (1979), and $B_{CMK}(A,Z)$ is from Czarnecki, *et al.* (1997). From Eq.(142), the ratio of $B(\mu^+ \to e^+\gamma)/B(\mu^- N \to e^- N)$ is given by

$$\frac{B(\mu^+ \to e^+\gamma)}{B(\mu^- N \to e^- N)} = \frac{96\pi^3\alpha}{G_F^2 m_\mu^4} \cdot \frac{1}{3 \cdot 10^{12} B(A,Z)} \sim \frac{428}{B(A,Z)}. \tag{143}$$

By using the values in Table XI, the ratio $B(\mu^+ \to e^+\gamma)/B(\mu^- N \to e^- N)$ for different target nuclei can be calculated. It varies from 389 for ^{27}Al, 238 for ^{48}Ti, and 342 for ^{208}Pb. This result indicates that the rate of $\mu^- - e^-$ conversion has a maximum around the medium nuclei ($A \approx 60$), and flattens out or slightly decreases for heavy nuclei. However, the calculations, which took into account the nuclear effect, show a different Z dependence (Chiang, *et al.*, 1993; Kosmas and Vergados, 1996; Kosmas, *et al.*, 1998).

TABLE XI. Z dependence of the photonic contribution in the $\mu^- - e^-$ conversion estimated by various theoretical models (after Czarnecki, *et al.*, (1997)).

Models	Al	Ti	Pb	Reference
$B_{WF}(A,Z)$	1.2	2.0	1.6	Weinberg and Feinberg (1959)
$B_S(A,Z)$	1.3	2.2	2.2	Shanker (1979)
$B_{CMK}(A,Z)$	1.1	1.8	1.25	Czarnecki, *et al.* (1997)

The $\mu^- - e^-$ conversion rates to the ground state and all excited states have been calculated by either the shell-model closure approximation (Kosmas, *et al.*, 1990) or the quasi-particle random-phase-approximation (QRPA) (Kosmas, *et al.*, 1994). The fraction of the coherent transition to the ground state is dominant. It was calculated specifically for ^{48}Ti to be (95-99)% in the QRPA approximation, which is even larger than in the shell-model closure approximation. It is also experimentally advantageous, since the background from excited states induced by the reaction can be minimized. It was also found that among the transitions to excited states, the dipole 1^- state is large both in the photonic and non-photonic contributions (Kosmas, *et al.*, 1994).

2. Event signature and backgrounds

The event signature of the coherent $\mu^- - e^-$ conversion in a muonic atom is a mono-energetic single electron emitted from muon capture with an energy of

$$\begin{aligned} E_{\mu e} &= m_\mu - B_\mu - E^0_{rec} \\ &\approx m_\mu - B_\mu, \end{aligned} \tag{144}$$

where m_μ is the muon mass, and B_μ and E^0_{rec} are the binding energy of the $1s$ muonic atom and the nuclear-recoil energy, respectively. The nuclear-recoil energy is approximately $E^0_{rec} \approx (m_\mu - B_\mu)^2/(2M_A)$, where M_A is the mass of the recoiling nucleus, which is small. Since B_μ is different for various nuclei, the peak energy of the $\mu^- - e^-$ conversion signal changes. For instance, it varies from $E_{\mu e} = 104.3$ MeV for titanium to $E_{\mu e} = 94.9$ MeV for lead.

From an experimental point of view, $\mu^- - e^-$ conversion is very attractive. First, the e^- energy of about 105 MeV is far above the end-point energy of the muon decay spectrum ($\sim$ 52.8 MeV). Second, since the event signature is a mono-energetic electron, no coincidence measurement is required. The search for this process has a potential to improve the sensitivity by using a high muon rate without suffering from accidental background, which would be serious background for other processes, such as $\mu^+ \to e^+\gamma$ and $\mu^+ \to e^+e^+e^-$ decays.

One of the major backgrounds is muon decay in orbit from a muonic atom (also called a bound muon decay), in which the e^- endpoint energy is the same as the energy of the signal. It is discussed in more detail below. The other background sources are (i) radiative pion capture ($\pi^- + (A, Z) \to (A, Z-1) + \gamma$) or radiative muon captures ($\mu^- + (A, Z) \to \nu_\mu + (A, Z-1) + \gamma$) followed by internal and external asymmetric e^+e^- conversion of the photon ($\gamma \to e^+e^-$) with e^+ undetected, (ii) electrons in the beam scattering off the target, (iii) muon decay in flight, and (iv) cosmic rays. Note that the maximum e^- energy (E^{max}_{bg}) from the background of radiative muon capture is given by

$$\begin{aligned} E^{max}_{bg} &= m_\mu - B_\mu - E_{rec} - \Delta_{Z-1} \\ &\approx m_\mu - B_\mu - \Delta_{Z-1}, \end{aligned} \tag{145}$$

where Δ_{Z-1} is the difference in the nuclear binding energy of the initial and final nucleus involved in radiative muon capture. Therefore, an appropriate target with a large Δ_{Z-1} can be selected so as to keep a wide background-free region for the coherent signal. The typical values of E^{max}_{bg} are 89.7 MeV and 91.4 MeV for ^{48}Ti and ^{46}Ti, respectively, whereas $E_{\mu e}$ is 104.3 MeV. In general, to eliminate these backgrounds, the purity of the beam (with no contamination of pions and electrons) is crucial, together with a highly efficient veto for cosmic rays.

When the muon is polarized, the angular distribution of e^- in the coherent $\mu^- - e^-$ conversion process is given by

$$\frac{dB(\mu^- N \to e^- N)}{d(\cos\theta_e)} = \frac{p_e E_e G_F^2}{16\pi}\left[|X_L(p_e)|^2(1 - P_\mu \cos\theta_e) + |X_R(p_e)|^2(1 + P_\mu \cos\theta_e)\right] \cdot \frac{1}{\Gamma_{capt}}, \tag{146}$$

where θ_e is the angle between the e^- direction and the muon spin direction. Since the nucleus does not change for the coherent process, the conversion electron carries the original muon spin. X_L and X_R are given in Eqs.(136) and (137), and correspond to the emission of left-handed electrons (e^-_L) and right-handed electrons (e^-_R), respectively. As in polarized $\mu^+ \to e^+\gamma$ decay, in principle, the angular distribution would be useful to discriminate between theoretical models. However, even if negative muons in the beam are 100% spin polarized, they are depolarized during their atomic cascades down to the *1s* ground state. For a nucleus with zero nuclear spin, the residual polarization is about 16% (Evseev, 1975). For a nucleus with non-zero nuclear spin, it becomes much smaller. It would make a measurement of the angular distribution difficult unless high statistics is accumulated. If the μ^- polarization is restored, however, it might provide useful information. One possible way to repolarize a negative muon in a muonic atom is to use a polarized nuclear target (Nagamine and Yamazaki, 1974; Kuno, *et al.*, 1986).

3. Muon decay in orbit

Muon decay in orbit (Porter and Primakoff, 1951) is one of the important background sources in the search for $\mu^- - e^-$ conversion in a muonic atom, since the end point of the electron spectrum comes close to the signal region of $\mu^- - e^-$ conversion. Only the high-energy end of the electron energy spectrum is of interest for $\mu^- - e^-$ conversion experiments. At the high-energy end, the effect of the nuclear-recoil energy plays an important role (on its phase space). There have been several studies on its electron energy spectrum with nuclear-recoil energy taken into account (Hänggi, *et al.*, 1974; Herzog, *et al.*, 1980; Shanker, 1982). With the approximation of a constant nuclear-recoil energy, the electron spectrum with an expansion in powers of the electron energy (E_e) at the end-point energy is given by (Shanker, 1982)

$$N(E_e)dE_e = \Big(\frac{E_e}{m_\mu}\Big)^2 \Big(\frac{\delta_1}{m_\mu}\Big)^5 \Big[D + E\cdot(\frac{\delta_1}{m_\mu}) + F\cdot(\frac{\delta}{m_\mu})\Big] dE_e, \tag{147}$$

where $\delta = E_{\mu e} - E_e$ and $\delta_1 = (m_\mu - B_\mu) - E_{rec} - E_e$. $E_{\mu e}$ is the e^- energy of the $\mu^- - e^-$ conversion signal defined in Eq.(144). E_{rec} is the nuclear-recoil energy given by $E_{rec} \approx E_e^2/(2M_A)$. It should be stressed that the spectrum falls off sharply as the fifth power of δ_1 towards its end point. The coefficients D, E and F as well as the end-point energy are given in a numerical table (Shanker, 1982). The contributions of the E and F terms to the total rate are about 4% and 8% respectively for $Z = 29$ and $E_e = 100$ MeV. Eq.(147) agrees with those in Hänggi, *et al.* (1974) and Herzog, *et al.* (1980). In the evaluation of the leading term D, important are (1) the use of a correct electron wave function incorporating the finite nuclear charge distribution, (2) the use of the Dirac muon wave function, and (3) the use of the small component of the muon relativistic wave function. In particular, the effect of (1) is large (Shanker and Roy, 1997).

Experimentally, to avoid any background from muon decay in orbit, the momentum resolution of e^- detection must be improved. Fig.28 shows the effective branching ratio of the muon decay in orbit as a function of E_e for the case of a titanium target, where $E_{\mu e} = 104.3$ MeV. It was calculated using Eq.(147). For a resolution better than 2%, the contribution from muon decay in orbit occurs at a level below 10^{-14}.

What is the asymmetric angular distribution of electrons in muon decay in orbit, if muons are polarized ? Numerical calculations can be made by taking into account the angular distribution of electrons from polarized muon decay in orbit (Watanabe, *et al.*, 1987). It is given by

$$N(E_e, \theta_e) dE_e (\frac{d\Omega_e}{4\pi}) = N_0(E_e)\Big(1 + \alpha(E_e) P_\mu \cos\theta_e\Big)(\frac{d\Omega_e}{4\pi}), \tag{148}$$

where $\alpha(E_e)$ is the asymmetry parameter, which becomes $\alpha(E_e) = -1$ at the end-point, giving a distinct $(1 - P_\mu \cos\theta_e)$ distribution; namely, electrons are likely to be emitted opposite to the muon polarization direction. At low energy, $\alpha(E_e)$ becomes positive and electrons are emitted along the muon polarization. The Coulomb effect is significant for heavy nuclei, like ^{208}Pb, but very small for light nuclei, like ^{16}O. The calculated results of the decay rate, emitted electron energy spectrum, and asymmetry parameters for muon decay in orbit are given in numerical tables for some nuclei (Watanabe, *et al.*, 1993).

4. Experimental status of $\mu^- - e^-$ conversion

The SINDRUM II collaboration at PSI is carrying out experiments to search for $\mu^- - e^-$ conversion in various nuclei. A schematic view of the SINDRUM II spectrometer is shown in Fig.29. It consists of a set of concentric cylindrical drift chambers inside a superconducting solenoid magnet of 1.2 T. Negative muons with a momentum of about 90 MeV/c were stopped in a target located at the center of the apparatus, after passing a CH_2 moderator and a beam counter made of plastic scintillator. Charged particles with transverse momentum (with respect to the magnetic field direction) above 100 MeV/c, originating from the target, hit two layers of plastic scintillation arrays and then two layers of drift chambers, and eventually hit plexiglass Cherenkov hodoscopes placed at both ends. Charged particles having transverse momentum below about 100 MeV/c were contained inside, and could not reach the tracking region under a magnetic field of 1.2 T. A momentum resolution of about 2.8% (FWHM) for the energy region of conversion electrons was achieved. For the background rejection, the e^- energy (E_e), a time delay between the times of charged particle tracks in the spectrometer and the beam-counter signal (Δt), the position of the origin of the reconstructed trajectory (Δz), the polar track angle, are used in an off-line analysis. Events with small Δt were removed so as to reject prompt backgrounds, such as electron scattering and radiative pion capture.

In a 1993 run with a titanium target, a total of 3×10^{13} stopped μ^-s were accumulated at a rate of 1.2×10^7 μ^-/sec from the $\mu E1$ beam line at PSI. The overall efficiency was about 13 %. The e^- momentum spectrum for the Ti target in the 1993 data is shown in Fig.30, where the successive background rejections by prompt veto (*i.e.* Δt cut) and cosmic-ray suppression are shown. Since no events were found in the signal region, a 90% C.L. upper limit of 6.1×10^{-13} was obtained (Wintz, 1998). Also, for a lead target, it gave $B(\mu^- Pb \to e^- Pb) < 4.6 \times 10^{-11}$ (Honecker, *et al.*, 1996).

A next round of the SINDRUM II experiment is under preparation at the $\pi E5$ beam line at PSI. The key element of the next stage is a pion-muon converter (PMC) to eliminate contamination of pions and electrons in the muon beam. It is needed since a veto of secondary pions and electrons by a beam counter will no longer be working with a high rate, such as

TABLE XII. History and summary of $\mu^- - e^-$ conversion in various nuclei.

Process	90% C.L. upper limit	place	year	reference
$\mu^- + Cu \to e^- + Cu$	$< 1.6 \times 10^{-8}$	SREL	1972	Bryman, *et al.* (1972)
$\mu^- + {}^{32}S \to e^- + {}^{32}S$	$< 7 \times 10^{-11}$	SIN	1982	Badertscher, *et al.* (1982)
$\mu^- + Ti \to e^- + Ti$	$< 1.6 \times 10^{-11}$	TRIUMF	1985	Bryman, *et al.* (1985)
$\mu^- + Ti \to e^- + Ti$	$< 4.6 \times 10^{-12}$	TRIUMF	1988	Ahmad, *et al.* (1988)
$\mu^- + Pb \to e^- + Pb$	$< 4.9 \times 10^{-10}$	TRIUMF	1988	Ahmad, *et al.* (1988)
$\mu^- + Ti \to e^- + Ti$	$< 4.3 \times 10^{-12}$	PSI	1993	Dohmen, *et al.* (1993)
$\mu^- + Pb \to e^- + Pb$	$< 4.6 \times 10^{-11}$	PSI	1996	Honecker, *et al.* (1996)
$\mu^- + Ti \to e^- + Ti$	$< 6.1 \times 10^{-13}$	PSI	1998	Wintz (1998)

10^8 μ^-s/sec, at the $\pi E5$ beam line. The PMC consists of a long-straight superconducting solenoid magnet with length of 8.5 m and an inner diameter of 0.4 m. It is located between the pion target and the SINDRUM II spectrometer, and produces the same magnetic field as in the SINDRUM II spectrometer, 2 T. Low-energy negative muons (called cloud muons) from the production target are injected into the PMC. After the 8.5-m flight length, most of the pions in a beam would decay out, resulting in a negligible pion contamination. Unfortunately, the original PMC magnet did not fulfill the specification at the initial installation stage, and thus caused a severe delay. After its new assembly, the magnet finally met the goal. With a lower magnetic field of the PMC magnet, data with a gold target were taken in 1998. A new run for a Ti target is expected to start in spring, 1999, with aimed sensitivity of $B(\mu^- Ti \to e^- Ti) <$ a few $\times\ 10^{-14}$.

A new experiment, E940, at Brookhaven National Laboratory (BNL) AGS, the MECO (Muon Electron COnversion) experiment, was prepared (Bachman, *et al.*, 1997). MECO aims to search for $\mu^- + Al \to e^- + Al$ at a sensitivity below 10^{-16}. It will use a new high-intensity pulsed muon beam, which could yield about 10^{11} μ^-s/sec stopped in a target. A schematic layout of the MECO detector is shown in Fig.31. The MECO apparatus consists of a superconducting (SC) solenoid magnet to capture pions from the production target (production solenoid), a curved transport SC solenoid magnet system (transport solenoid), and a SC solenoid spectrometer, which observes only the 105-MeV signal electrons (detector solenoid). Based on the solenoid capture scheme originally proposed by MELC (Dzhilkibaev and Lobashev, 1989), it has an axially graded magnetic field (from 3.5 T to 2.0 T) to efficiently capture pions from a tungsten target located on the axis of the solenoid magnet. The curved transport solenoid will capture muons from pion decays, and select the momentum and sign of charged particles by using collimators at three positions. Layers of thin aluminum targets where μ^-s are stopped are placed in the detector solenoid with an axially graded magnetic field. The conversion electron of 105 MeV is momentum analyzed with a resolution of 300 keV (RMS) and an acceptance of 25% in a straw tracking chamber. A pulsed proton beam of about 1 MHz repetition with a pulse length of 30 nsec can be extracted at the AGS. A high extinction between the beam pulses (the ratio of a number of protons between pulses to that in the beam pulse) of 10^{-9} is needed to eliminate severe beam background at a high rate. They expect to observe 6 signal events for $B(\mu^- Al \to e^- Al) \approx 10^{-16}$ during a one-year run, with an expected background of 0.4 events.

D. $\mu^- - e^+$ conversion in a muonic atom

1. Phenomenology of $\mu^- - e^+$ conversion

The other neutrinoless muon-capture process is a charge-changing reaction, such as

$$\mu^- + (A, Z) \rightarrow e^+ + (A, Z-2)^*, \tag{149}$$

which violates the conservation of the total lepton number as well as the lepton flavor numbers, L_e and L_μ. This process is closely related to neutrinoless double $\beta-$decay ($\beta\beta_{0\nu}$), since both processes require a mechanism involving two nucleons. The final state of the nucleus $(A, Z-2)^*$ could be either the ground state (gs) or excited states (ex). Since the final nucleus is not the same as the initial nucleus, no coherent enhancement, even for the transition to the ground state, is expected. The branching ratio of the $\mu^- - e^+$ conversion is defined by

$$B(\mu^- + (A, Z) \rightarrow e^+ + (A, Z-2)^*) \equiv \frac{\Gamma(\mu^- + (A, Z) \rightarrow e^+ + (A, Z-2)^*)}{\Gamma(\mu^- + (A, Z) \rightarrow capture)}. \tag{150}$$

Various theoretical models predict the rates accessible experimentally. One is the minimum supersymmetric models (MSSM) with R-parity breaking, which allows the predicted branching ratio of the $\mu^- - e^+$ conversion on the level of 10^{-12}, since the λ and λ' parameters involved are not constrained (Babu and Mohapatra, 1995). The left-right symmetric models with a low-mass W_R also predict the $\mu^- - e^+$ conversion branching ratio of 10^{-14}, estimated by the same authors.

2. Event signature and backgrounds

The energy of the positron from the $\mu^- - e^+$ conversion is given by

$$\begin{aligned} E_{\mu e^+} &= m_\mu - B_\mu - E_{rec} - \Delta_{Z-2} \\ &\approx m_\mu - B_\mu - \Delta_{Z-2}, \end{aligned} \tag{151}$$

where Δ_{Z-2} is the difference in the nuclear binding energy between the (A, Z) and $(A, Z-2)$ nuclei, with the excitation energy in the final nucleus taken into account. In $\mu^- - e^+$ conversion, because of the absence of coherent enhancement, the final nucleus could be either in the ground state or in excited states. Usually, it is assumed that a large fraction of the final nucleus could be in the giant dipole resonance state, which has a mean energy of 20 MeV and a width of 20 MeV. Therefore, the e^+ from $\mu^- - e^+$ conversion will have a broad momentum distribution corresponding to the width of giant dipole resonance excitation.

The major background is radiative muon capture (RMC) or radiative pion capture (RPC), followed by asymmetric e^+e^- conversion of the photon. For some nuclei, the endpoint of the RMC background in Eq.(145) can be selected to be much lower than the signal. For instance, for a titanium target, the maximum endpoint of RMC (of about 90 MeV) is about 10 MeV lower than the signal energy of about $E_{\mu e^+} \approx 100$ MeV. The background from RPC must be reduced from the rejection of pions in the beam.

3. Experimental status of $\mu^- - e^+$ conversion

TABLE XIII. Historical progress and summary of $\mu^- - e^+$ conversion in various nuclei. gs and ex denote the transitions to the ground state and excited states (mostly giant dipole-resonance states) respectively.

Process	90% C.L. upper limit	place	year	reference
$\mu^- + Cu \to e^+ + Co$	2.6×10^{-8}	SREL	1972	Bryman, *et al.* (1972)
$\mu^- + S \to e^+ + Si$	9×10^{-10}	SIN	1982	Badertscher, *et al.* (1982)
$\mu^- + Ti \to e^+ + Ca(gs)$	9×10^{-12}	TRIUMF	1988	Ahmad, *et al.* (1988)
$\mu^- + Ti \to e^+ + Ca(ex)$	1.7×10^{-10}	TRIUMF	1988	Ahmad, *et al.* (1988)
$\mu^- + Ti \to e^+ + Ca(gs)$	4.3×10^{-12}	PSI	1993	Dohmen, *et al.* (1993)
$\mu^- + Ti \to e^+ + Ca(ex)$	8.9×10^{-11}	PSI	1993	Dohmen, *et al.* (1993)
$\mu^- + Ti \to e^+ + Ca(gs)$	1.7×10^{-12}	PSI	1998	Kaulard, *et al.* (1998)
$\mu^- + Ti \to e^+ + Ca(ex)$	3.6×10^{-11}	PSI	1998	Kaulard, *et al.* (1998)

The SINDRUM II Collaboration at PSI has reported on a search for the charge-changing $\mu^- + Ti \to e^+ + Ca$ in muonic atoms (Kaulard, *et al.*, 1998). It was carried out simultaneously with a measurement of $\mu^- + Ti \to e^- + Ti$. The e^+ momentum spectrum is shown in Fig.32. The results are given separately for the transition to the ground state and that to the giant dipole resonance. They are summarized in Table XIII, together with the previous results.

E. Muonium to anti-muonium conversion

A muonium atom is a hydrogen-like bound state of μ^+ and e^-. The spontaneous conversion (or oscillation) of a muonium atom (μ^+e^- or Mu) to its anti-atom, anti-muonium atom (μ^-e^+ or $\overline{\mathrm{Mu}}$) is another interesting class of muon LFV process. In this $\mathrm{Mu} - \overline{\mathrm{Mu}}$ conversion, the lepton flavors change by two units ($\Delta L_{e/\mu} = \pm 2$) in the ordinary law of separate additive muon and electron numbers, whereas it would be consistent with multiplicative muon or electron number conservation (Feinberg and Weinberg, 1961). The possibility was suggested by Pontecorvo in 1957 (Pontecorvo, 1957), even before the muonium atom was observed for the first time at the Nevis cyclotron of Columbia University (Hughes, *et al.*, 1960).

1. Phenomenology of $\mathrm{Mu} - \overline{\mathrm{Mu}}$ conversion

Various interactions could induce the $|\Delta L_i| = 2$ processes, such as $\mathrm{Mu} - \overline{\mathrm{Mu}}$ conversion, as discussed in Section III E. To discuss the phenomenology of the $\mathrm{Mu} - \overline{\mathrm{Mu}}$ conversion, as an example, the effective four fermion interaction of the $(V-A)(V-A)$ type (Feinberg and Weinberg, 1961) is taken. It is given by

$$H_{\mathrm{Mu}\overline{\mathrm{Mu}}} = \Big(\frac{G_{\mathrm{Mu}\overline{\mathrm{Mu}}}}{\sqrt{2}}\Big)\overline{\mu}\gamma_\lambda(1-\gamma_5)e\overline{\mu}\gamma^\lambda(1-\gamma_5)e + H.c. \tag{152}$$

in which $G_{\mathrm{Mu}\overline{\mathrm{Mu}}}$ is a coupling constant characterizing the strength of the interaction.

In the absence of an external magnetic field, the muonium and the anti-muonium have the same ground-state energy levels. The possible new interaction in Eq.(152) would cause a splitting of their energy levels of

$$\delta \equiv 2 < \overline{M}|H_{\mathrm{Mu}\overline{\mathrm{Mu}}}|M >= \frac{8G_F}{\sqrt{2}n^2\pi a_0^3}\Big(\frac{G_{\mathrm{Mu}\overline{\mathrm{Mu}}}}{G_F}\Big), \tag{153}$$

where n is the principal quantum number of the muonium atom, and a_0 is the Bohr radius of the muonium atom. For the ground state of the muonium atom ($n = 1$),

$$\delta = 1.5 \times 10^{-12} \cdot \Big(\frac{G_{\mathrm{Mu}\overline{\mathrm{Mu}}}}{G_F}\Big) \quad (\mathrm{eV}). \tag{154}$$

The $\mathrm{Mu} - \overline{\mathrm{Mu}}$ conversion is analogous to $K^0 - \overline{K^0}$ mixing. If a muonium atom is formed at $t = 0$ in a vacuum under no external electromagnetic field, it could oscillate into an anti-muonium atom with time. For a small δ value, the probability ($\wp_{\mathrm{Mu}\overline{\mathrm{Mu}}}$) is approximately given by (Willmann and Jungmann, 1998)

$$\wp_{\mathrm{Mu}\overline{\mathrm{Mu}}}(t) = \sin^2\Big(\frac{\delta t}{2}\Big) \cdot \lambda_\mu e^{-\lambda_\mu t} \approx \Big(\frac{\delta t}{2}\Big)^2 \cdot \lambda_\mu e^{-\lambda_\mu t}, \tag{155}$$

where $\lambda_\mu = 1/\tau_\mu (= 2.996 \times 10^{-10}$ eV) is the muon decay width. The maximum probability of anti-muonium decay is $t_{max} = 2\tau_\mu$. Fig.33 shows the oscillation pattern as a function of time. The total conversion probability after integration over time ($P^0_{\mathrm{Mu}\overline{\mathrm{Mu}}}$) in a zero magnetic field is

$$P^0_{\mathrm{Mu}\overline{\mathrm{Mu}}} = \int_0^\infty \wp_{\mathrm{Mu}\overline{\mathrm{Mu}}}(t)dt = \frac{|\delta|^2}{2(|\delta|^2 + |\lambda_\mu|^2)} = 2.56 \times 10^{-5} \cdot \Big(\frac{G_{\mathrm{Mu}\overline{\mathrm{Mu}}}}{G_F}\Big)^2. \tag{156}$$

The experimental limit constrains the upper limit of magnitude of $G_{\mathrm{Mu}\overline{\mathrm{Mu}}}$. The limit of $G_{\mathrm{Mu}\overline{\mathrm{Mu}}}$ is improved by the square root of the conversion probability.

The presence of an external electromagnetic field would remove the degeneracy between the muonium and the anti-muonium atoms. It would reduce the probability of the muonium to anti-muonium conversion. The splitting of different muonium energy levels in the presence of a magnetic field is calculated by using the Breit-Rabi formula for the states of their total spin, F, and its z-component, m_F. In a magnetic field, the $(F, m_F) = (1, \pm 1) \rightarrow (1, \pm 1)$ transitions become rapidly suppressed, even at a weak field, because of the Zeeman splitting of energy levels. The transitions between different F states are also highly suppressed, even in a zero magnetic field, owing to the muonium *1s* hyperfine splitting (of 1.846×10^{-5} eV). By taking into account the magnetic-field dependences of different energy levels of muonium and anti-muonium and their transition rates, Eq.(156) can be modified for unpolarized muons by

$$P_{\mathrm{Mu}\overline{\mathrm{Mu}}}(B) = \frac{1}{4}\sum_{F,m_F} \frac{|\delta|^2}{2(|\delta|^2 + |\triangle|^2 + |\lambda_\mu|^2)} \equiv P^0_{\mathrm{Mu}\overline{\mathrm{Mu}}} \cdot S_B(B), \tag{157}$$

where $\Delta \equiv E_{Mu}(F, m_F) - E_{\overline{Mu}}(F, m_F)$, and δ and Δ are functions of the magnitude of the magnetic field (B). The reduction factor, $S_B(B)$, has been calculated for possible interactions of different types (Hou and Wong, 1995; Horikawa and Sasaki, 1996). Fig.34 shows

the dependence of the Mu $-$ $\overline{\text{Mu}}$ conversion probability on the external magnetic field and different coupling types. For example, for the traditional $(V-A)(V-A)$ interaction, the conversion rate becomes one half at a magnetic field of about 10 mG and is further strongly suppressed for a magnetic field greater than 10^3 G.

2. Event signature and backgrounds

In experiments of the Mu $-$ $\overline{\text{Mu}}$ conversion, an anti-muonium converted from a muonium initially produced is searched. The experimental signature of an anti-muonium decay is the emission of an energetic e^- from $\mu^- \to e^- \overline{\nu}_\mu \nu_e$ decay with a dissociated e^+ left behind with an average kinetic energy of 13.5 eV. This corresponds to the binding energy of the *1s* state of a muonium atom.

The sensitivity to Mu $-$ $\overline{\text{Mu}}$ conversion is known to be suppressed when the muonium atom is in matter. This occurs since a negative muon in anti-muonium is easily captured by surrounding atoms. Therefore, recent experiments have been performed by using muonium atoms in a vacuum.

There are two major sources of potential backgrounds. One is accidental coincidences of energetic e^- produced by Bhabha scattering of e^+ from μ^+ decay in a muonium and the scattered e^+. The second is the physics (prompt) background from the $\mu^+ \to e^+ \nu_e \overline{\nu}_\mu e^+ e^-$ decay (whose branching ratio is 3.4×10^{-5}), when the e^- becomes energetic and only one of the two e^+s is detected.

3. Experimental status of Mu $-$ $\overline{\text{Mu}}$ *conversion*

TABLE XIV. Historical progress and summary of Mu $-$ $\overline{\text{Mu}}$ conversion.

Place	Year	$G_{\text{Mu}\overline{\text{Mu}}}/G_F$	Reference
TRIUMF	1982	< 42	Marshall, *et al.* (1982)
TRIUMF	1986	< 20	Beer, *et al.* (1986)
TRIUMF	1990	< 0.29	Huber, *et al.* (1990)
LANL	1991	< 0.16	Matthias, *et al.* (1991)
LANL	1993	< 6.9	Ni, *et al.* (1993)
PSI	1996	< 0.018	Abela, *et al.* (1996)
JINR	1997	< 0.14	Gordeev, *et al.* (1997)
PSI	1999	< 0.003	Willmann, *et al.* (1999)

The historical progress in the searches for Mu $-$ $\overline{\text{Mu}}$ conversion is listed in Table XIV. A recent experiment was carried out at PSI (Willmann, *et al.*, 1999). The experiment fully utilized the powerful techniques developed at the previous experiment at LANL (Matthias, *et al.*, 1991), which requires the coincidence identification of both particles in the anti-muonium decay. Its experimental setup is shown in Fig.35. Muonium atoms were produced by stopping surface muons in a SiO_2 powder target, where some fraction diffused out through the target surface with thermal energy in a vacuum. To detect e^- from μ^- decay, a magnetic

spectrometer was used. It consisted of five concentric multiwire proportional chambers with 64 segmented hodoscopes at a 0.1 T magnetic field. The e^+ with an average kinetic energy of 13.5 eV was detected by micro-channel plate detectors after electrostatic acceleration to 8 keV. With the production of about 5.7×10^{10} muonium atoms, their analysis yielded one event satisfying all of the required criteria with the expected background events of 1.7 ± 0.2 due to accidental coincidence. The Monte-Carlo data and real data are given in Fig.36. The 90% C.L. upper limit on the conversion probability at zero magnetic filed is

$$P^0_{\mathrm{Mu}\overline{\mathrm{Mu}}} \leq 8.3 \times 10^{-11}/S_B(B), \tag{158}$$

where the factor $S_B(B)$ describes the suppression of the $\mathrm{Mu} - \overline{\mathrm{Mu}}$ conversion in an external magnetic field, B. It could be translated into the upper limit on the effective coupling constant, $G_{\mathrm{Mu}\overline{\mathrm{Mu}}}$, which is given by

$$G_{\mathrm{Mu}\overline{\mathrm{Mu}}} \leq 3.0 \times 10^{-3} G_F \tag{159}$$

at 90% C.L. upper limit under a 0.1 T magnetic field.

VI. FUTURE PROSPECTS

The field of muon decay physics is presently very productive, even after its long history of over 60 years. Currently, there are several new experiments which are being either prepared or planned. Some of them, which were mentioned in this article, are R77 at RIKEN-RAL and R-99-07 at PSI for the muon lifetime measurement (in Section IV A 2), E614 at TRIUMF to measure the Michel spectrum and its asymmetry (in Section IV B 2), R-94-10 and R-97-07 at PSI to measure the e^+ polarization in polarized $\mu^+ \to e^+\nu_e\overline{\nu}_\mu$ decay (in Section IV C 2), R-99-05 at PSI for $\mu^+ \to e^+\gamma$ decay (in Section V A 6), the new phase of SINDRUM-II at PSI, and E940 (MECO) at BNL for $\mu^- - e^-$ conversion (in Section V C 4). Each of them is aiming at an improvement of about an order of magnitude or more over the previous experiments. The potential progress expected by each of such experiments is based not only on innovative ideas on detection methods, but also on muon beams of high intensity and good quality. In particular, the planned searches for muon LFV processes strongly rely on the beam, such as the PMC in SINDRUM-II and the superconducting solenoid capture and transport systems for the MECO experiment. More muon fluxes with less contamination are critical for further improvements.

Currently, two out of the three meson factories are operational. One of the two operational machines, the PSI cyclotron, has increased its proton current, achieving 1.5 mA, the highest proton current in the world. The muon beam intensities for various existing laboratories are listed in Table XV. In addition, the use of higher energy proton machines, such as the BNL AGS for negative muons, is being considered for the MECO experiment, where a pulsed-beam capability at the AGS and a larger cross section of negative pions at a few 10 GeV proton energy are to be utilized. In the long-term future, there are several new projects to construct high-intensity proton accelerators: the JAERI/KEK Joint Project (previously JHF) (JAERI/KEK Joint Project, 1999), which consists of a 50-GeV proton synchrotron (50-GeV PS) with a 15 μA beam intensity, and a 3-GeV proton synchrotron with a 330 μA beam intensity; the SNS (Spallation Neutron Source) at Oak Ridge; a possible European Spallation Neutron Source (ESS). Probably, a proton driver for a $\mu^+\mu^-$ collider (Muon Collider Collaboration, 1996; Ankenbrandt *et al.*, 1999) can be included in the long-term future. Note that among the above, only the 50-GeV PS is planned to have a continuous proton beam by slow beam extraction, whereas the others may have only fast beam extraction of a low repetition rate.

Regarding LFV, besides the study of muon decays, a unique possibility of lepton flavor changing Rutherford scattering, where the conversion of incident electrons into muons of the same energy by scattering in the external electric field of a massive nucleus, is also discussed (Abraham and Lampe, 1996). However, the expected cross section is very small to compete with rare muon decay processes, and technical details have not yet been discussed.

A. Towards new high-intensity muon sources

Significant improvements in low-energy muon physics could be expected if a high-intensity muon source, having a beam intensity of $10^{12} - 10^{13}$ $\mu^\pm$s/sec with a narrow energy-spread and less contamination, can be realized. The muon beam intensity envisaged would

TABLE XV. Intensities of existing muon beams available.

Facility	Protons	Time structure	Muon Intensity	
PSI	1.5 mA	continuous	3×10^8 μ^+s/sec	at 28 MeV/c (surface muons)
	590 MeV	(50 MHz)	1×10^8 μ^-s/sec	at 100 MeV/c
TRIUMF	150 μA	continuous	2×10^7 μ^+s/sec	at 28 MeV/c (surface muons)
	500 MeV	(50 MHz)	3×10^6 μ^-s/sec	at 100 MeV/c
RAL	200 μA	pulsed	1×10^6 μ^+s/sec [1)]	at 28 MeV/c (surface muons)
	800 MeV	(50 Hz)	1×10^5 μ^-s/sec	at 50 MeV/c
MSL [2)]	6 μA	pulsed	1×10^5 μ^+s/sec	at 28 MeV/c (surface muons)
	500 MeV	(20 Hz)	1×10^4 μ^-s/sec	at 55 MeV/c
JINR [3)]	4 μA	continuous	3×10^4 μ^+s/sec	at 28 MeV/c (surface muons)
	660 MeV		1×10^3 μ^-s/sec	at 100 MeV/c

[1)] The highest instantaneous intensity of $2 \times 10^4 \mu^+$s/200 nsec.
[2)] Meson Science Laboratory at KEK, using the existing 500 MeV Booster ring.
[3)] Phasotron, Joint Institute for Nuclear Research, Dubna, Russia.

be four or five orders of magnitude higher than that available today. Ideas of such a high-intensity muon source are based on (i) solenoid pion capture, (ii) phase rotation, and (iii) muon cooling. A schematic view of the basic concept is shown in Fig.37.

In solenoid pion capture, low-energy pions and muons are trapped in a high solenoidal magnetic field (such as 10 T or more). From Monte Carlo simulations with appropriate pion production cross sections, about 0.3 to 0.1 captured pions (of less than 0.5 GeV/c) per proton are estimated for proton beam energies of 50 GeV to 10 GeV, respectively. For a proton intensity of the existing and planned proton machines of about $10^{13} - 10^{14}$ protons/sec, a large number of captured pions sufficient for the aimed intensity are expected.

The phase rotation is to accelerate slow muons and to decelerate fast muons by a strong radio-frequency (RF) electric field, yielding a narrow longitudinal momentum spread. To identify fast and slow muons by their time of flight from the production time, a very narrow pulsed proton beam must be used. An intensity enhancement of a factor of about ten in the longitudinal energy distribution is estimated from Monte Carlo simulations (Kuno, 1997b).

The muon cooling, which is based on ionization cooling (Skrinskii and Parkhomuchuk, 1981), is to reduce muon beam emittance. The longitudinal cooling is based on the repetition of energy loss by ionization and subsequent acceleration to restore the longitudinal momentum. The ionization cooling works only for muons.

These ideas have emerged in studies of a $\mu^+\mu^-$ collider at the high-energy frontier (Muon Collider Collaboration, 1996; Ankenbrandt *et al.*, 1999). The physics potential with low energy muons available from the front-end of the $\mu^+\mu^-$ collider complex has been discussed. Although there are many common R&D items between a low-energy muon source and a $\mu^+\mu^-$ collider, there are discussions on whether the front-end muon collider (FMC) could be directly used in experiments with muons. The FMC will run with a pulsed beam of slow repetition (at typically 15 Hz). However, most experiments with muons require a beam with a high duty factor, or a nearly continuous beam, because of the reduction of the instantaneous

rate (Molzon, 1997). The precise requirement on the beam time structure depends on the type of experiments. For instance, searches for $\mu^+ \to e^+\gamma$ and $\mu^+ \to e^+e^+e^-$ must use a continuous beam to reduce the instantaneous rate, whereas searches for $\mu^- - e^-$ (or $\mu^- - e^+$) conversion, Mu $-$ $\overline{\text{Mu}}$ conversion and a measurement of the muon lifetime need a pulsed beam with a pulse separation of an order of the muon lifetime ($\sim$ μsec). Thus, independent R&D items, in particular concerning phase rotation and the muon cooling system, exist in a low-energy muon source. These technical issues must be pursued separately.

There are several dedicated R&D programs on low-energy muon sources with high intensity. One of those is the PRISM project at KEK in Japan (Kuno, 1998). The PRISM project, which is an acronym of Phase-Rotation Intense Secondary Meson beam, would combine solenoid capture, phase rotation and possibly modest muon cooling to produce a cooled muon beam. The requirements on muon cooling as a secondary beam is not as strict as that in the $\mu^+\mu^-$ collider. Its R&D program starts from a relatively low repetition rate ($\sim$ kHz), and aims at a higher repetition in the future. The others are the MUONS project at TRIUMF (Blackmore, *et al.*, 1997), and the Super-Super Muon Channel project at the RIKEN-RAL muon facility (Ishida and Nagamine, 1998). For the last project, a new scheme of the production of cooled μ^+s by laser ionization of thermal muonium is also proposed (Nagamine, 1996).

Once a highly intense muon source with a narrow energy spread and less contamination is available, physics programs with stopped muons, in particular searches for rare muon LFV processes, would be significantly improved. First of all, the potential sensitivity achievable in searches for rare processes is ultimately limited by the number of muons available. Therefore, a high-intensity beam is essential. Small beam contamination is necessary to further reduce any background associated with it. A narrow energy spread of the beam will allow a thin muon stopping target to improve the detection resolution. For instance, if about $10^{19} - 10^{20}$ muons/year are available, a new experiment on $\mu^- - e^-$ conversion with a sensitivity of 10^{-18} could be possible (Blackmore, *et al.*, 1997).

The high-intensity muon sources could be used not only for experiments with low-energy muons, but also for experiments with energetic muons if the muons thus produced are injected into additional accelerators for further acceleration. Potential programs might include the measurements of the muon anomalous magnetic moment and the muon electric dipole moment, and also a muon accumulator ring for neutrino sources (Geer, 1998; CERN Report, 1999). In addition to particle-physics programs, a broad research field from materials science to biology would benefit from new highly intense muon sources, which would definitely open up a new era of muon science.

VII. CONCLUSIONS

We have described the current theoretical and experimental status in the field of muon decay to search for physics beyond the Standard Model. Among many interesting topics of physics related to muons, we have discussed the precise measurements of normal muon decay, and the searches for muon LFV processes. In particular, we have highly stressed the importance of muon LFV processes.

The physics motivation for LFV is extremely strong. LFV has recently attracted much attention from theorists and experimentalists, more than ever. This has happened because SUSY models predict large branching ratios for LFV processes. Their predictions are just as large as one or two orders of magnitude lower than the present experimental limits. They could be accessible and tested by future experiments. There are many scenarios of SUSY models which predict sizeable LFV effects. They are such as SUSY GUT, SUSY with right-handed (heavy) Majorana neutrinos, SUSY with R-parity violation and others. They would provide an opportunity to give a hint on physics at very high energy scales, like either the GUT scale or the mass scale of a heavy right-handed Majorana neutrino for the see-saw mechanism. Of course, there are many other classes of theoretical models which predict a large LFV effect besides SUSY. Therefore, LFV searches have robust potential to uncover new physics beyond the SM.

We have presented the phenomenology of muon LFV processes of $|\Delta L_i| = 1$, such as the $\mu^+ \to e^+\gamma$ and $\mu^+ \to e^+e^+e^-$ decays, the $\mu^- - e^-$ conversion in a muonic atom, and those of $|\Delta L_i| = 2$ such as the muonium to anti-muonium conversion. We discussed all of the above processes of $|\Delta L_i| = 1$ within the same framework of the effective Lagrangian to illustrate how various contributions (such as photonic and non-photonic) can be disentangled with measurements of the three muon LFV processes. Thereby, searches for these three processes are equally important. If the muon is polarized, additional information could be obtained by measuring the angular distributions in the $\mu^+ \to e^+\gamma$ decay and $\mu^- - e^-$ conversion, and T-odd and P-odd correlations in the $\mu^+ \to e^+e^+e^-$ decay. Furthermore, for the $\mu^+ \to e^+\gamma$ decay, the use of polarized muons would be useful to eliminate any background processes in the search. Experimentally, positive muons in a surface muon beam are known to be 100% polarized, and thereby the use of polarized muons will be feasible in the future. Then, we have briefly mentioned the most recent experimental results, such as MEGA for $\mu^+ \to e^+\gamma$ decay, SINDRUM-II for $\mu^- - e^-$ conversion, the recent search for $\mathrm{Mu} - \overline{\mathrm{Mu}}$ conversion at PSI, and others, together with future experimental prospects. In addition, precision measurements of the normal muon decay, $\mu^+ \to e^+\nu_e\overline{\nu}_\mu$, have attracted much interest. In the near future, new measurements of the muon lifetime, of the Michel spectrum and its asymmetry, and of the e^+ polarization in polarized $\mu^+ \to e^+\nu_e\overline{\nu}_\mu$ decay will be carried out while aiming at an order of magnitude improvement.

A new intense muon source with $10^{12} - 10^{13}$ $\mu^\pm$s/sec would be strongly required to make substantial improvements in low-energy muon physics. The aimed intensity is four or five orders of magnitude higher than that available now. The ideas for such a muon source are based on (i) solenoid pion capture, (ii) phase rotation, and (iii) muon cooling. These ideas came from a $\mu^+\mu^-$ collider. However, the beam time structure must be of high duty factor for low-energy muon physics, leading to new technical challenges which do not exist for the $\mu^+\mu^-$ collider R&D studies. To overcome these issues, several R&D programs dedicated to

low-energy muons are now being undertaken at KEK, RIKEN and TRIUMF. With increased muon fluxes, the searches for rare muon LFV processes, as well as precision measurements of muon decay, are expected to be significantly advanced.

Muon physics becomes important with strong physics motivations. There are extraordinary opportunities which will allow us to explore discovery potentials of physics beyond the SM, with low-energy muons.

ACKNOWLEDGMENTS

It is a great pleasure to thank the many people who helped us to write this review article; P. Depommier, J. Deutsch, D.R. Gill, J. Hisano, K.P. Jungmann, J.A. Macdonald, R. Mischke, W.R. Molzon, S.N. Nakamura, K. Okumura, Y. Shimizu, H.C. Walter, and P. Wintz. Especially, Pierre Depommier gave many useful comments on the whole manuscript. We also wish to thank many people for discussions, in particular, A. Czarnecki, T. Goto, P. Herczeg, R. Kitano, A. Maki, W.J. Marciano, Y. Mori, K. Nagamine, S. Nagamiya, S. Orito, S.T. Petcov, N. Sasao, A. van der Schaaf, J. Vergados, and T.K. Yokoi. One of us (Y.K.) acknowledges all the colleagues of the PRISM working group. The work of Y.K. was supported in part by the Grant-in-aid of the Ministry of Education, Science, Sports and Culture, Government of Japan (No. 10309009 and No. 11691134). The work of Y.O. was supported in part by the Grant-in-Aid of the Ministry of Education, Science, Sports and Culture, Government of Japan (No. 09640381), Priority area "Supersymmetry and Unified Theory of Elementary Particles" (No. 707), and "Physics of CP Violation" (No. 09246105).

APPENDIX A: RADIATIVE MUON DECAY

The differential branching ratio of the radiative muon decay, $\mu^+ \to e^+\nu_e\overline{\nu}_\mu\gamma$, is given in Eq.(52). The functions appearing in Eq.(52), $F(x,y,d)$, $G(x,y,d)$ and $H(x,y,d)$ in the SM, are given as follows:

$$\begin{aligned} F &= F^{(0)} + rF^{(1)} + r^2F^{(2)}, \\ G &= G^{(0)} + rG^{(1)} + r^2G^{(2)}, \\ H &= H^{(0)} + rH^{(1)} + r^2H^{(2)}, \end{aligned} \tag{A1}$$

where $r = (m_e/m_\mu)^2$. m_e and m_μ are the masses of an electron and a muon, respectively. Here, x and y are the normalized electron and photon energies, $x = 2E_e/m_\mu$ and $y = 2E_\gamma/m_\mu$; d is given by $d \equiv 1 - \beta\hat{p_e}\cdot\hat{p_\gamma}$. $\hat{p_e}$ and $\hat{p_\gamma}$ are unit momentum vectors of the electron and the photon respectively. β is defined as $\beta \equiv |\vec{p_e}|/E_e$.

$$\begin{aligned} F^{(0)}(x,y,d) = {} & \frac{8}{d}\{y^2(3-2y) + 6xy(1-y) + 2x^2(3-4y) - 4x^3\} \\ & +8\{-xy(3-y-y^2) - x^2(3-y-4y^2) + 2x^3(1+2y)\} \\ & +2d\{x^2y(6-5y-2y^2) - 2x^3y(4+3y)\} + 2d^2x^3y^2(2+y) \end{aligned} \tag{A2}$$

$$\begin{aligned} F^{(1)}(x,y,d) = {} & \frac{32}{d^2}\{-\frac{y(3-2y)}{x} - (3-4y) + 2x\} + \frac{8}{d}\{y(6-5y) - 2x(4+y) + 6x^2\} \\ & +8\{x(4-3y+y^2) - 3x^2(1+y)\} + 6dx^2y(2+y) \end{aligned} \tag{A3}$$

$$F^{(2)}(x,y,d) = \frac{32}{d^2}\{\frac{(4-3y)}{x} - 3\} + \frac{48y}{d} \tag{A4}$$

$$\begin{aligned} G^{(0)}(x,y,d) = {} & \frac{8}{d}\{xy(1-2y) + 2x^2(1-3y) - 4x^3\} + 4\{-x^2(2-3y-4y^2) + 2x^3(2+3y)\} \\ & -4dx^3y(2+y) \end{aligned} \tag{A5}$$

$$G^{(1)}(x,y,d) = \frac{32}{d^2}(-1+2y+2x) + \frac{8}{d}(-xy+6x^2) - 12x^2(2+y) \tag{A6}$$

$$G^{(2)}(x,y,d) = -\frac{96}{d^2} \tag{A7}$$

$$\begin{aligned} H^{(0)}(x,y,d) = {} & \frac{8}{d}\{y^2(1-2y) + xy(1-4y) - 2x^2y\} + 4\{2xy^2(1+y) - x^2y(1-4y) + 2x^3y\} \\ & +2d\{x^2y^2(1-2y) - 4x^3y^2\} + 2d^2x^3y^3 \end{aligned} \tag{A8}$$

$$H^{(1)}(x,y,d) = \frac{32}{d^2}\{-\frac{y(1-2y)}{x} + 2y\} + \frac{8}{d}\{y(2-5y) - xy\} + 4xy(2y-3x) + 6dx^2y^2 \tag{A9}$$

$$H^{(2)}(x,y,d) = -\frac{96y}{d^2x} + \frac{48y}{d} \tag{A10}$$

APPENDIX B: MSSM LAGRANGIAN

The Lagrangian for the minimal supersymmetric standard model (MSSM) is described. In SUSY theories, elementary fields are introduced as a pair of bosonic and fermionic fields. Such a pair is called a supermultiplet. There are two types of supermultiplets, a gauge

multiplet and a chiral multiplet. A gauge multiplet consists of a gauge field (A^a_μ) and its superpartner, a gauge fermion (or gaugino) field (λ^a), which is a Majorana fermion field in the adjoint representation of the gauge group. In the MSSM, we have to introduce gaugino fields for $SU(3)_C$, $SU(2)_L$ and $U(1)_Y$ gauge groups. A chiral multiplet is a set of a complex scalar field (ϕ) and a left-handed Weyl fermion field (ψ_L). Its complex conjugate is called an anti-chiral multiplet which consists of ϕ^* and ψ_R. In the MSSM, these chiral multiplets correspond to matter fields, namely quark, lepton and Higgs fields and its superpartners. The fields in the same chiral multiplet have the same quantum numbers for the gauge groups. Chiral multiplets necessary for the MSSM are listed with their quantum numbers in Table XVI. The right-handed squarks and sleptons are defined as follows: $(\tilde{u}^c_{iL})^* = \tilde{u}_{iR}$, $(\tilde{d}^c_{iL})^* = \tilde{d}_{iR}$, and $(\tilde{e}^c_{iL})^* = \tilde{e}_{iR}$. We sometimes use a notation $\tilde{\phi}$ and $\tilde{\psi}_L$ for superpartners of ϕ and ψ_L and Φ for a supermultiplet (ϕ, ψ_L).

TABLE XVI. Chiral multiplets in MSSM.

	$Q_i(\tilde{q}_{iL},q_{iL})$	$U^c_i(\tilde{u}^c_{iL},u^c_{iL})$	$D^c_i(\tilde{d}^c_{iL},d^c_{iL})$	$L_i(\tilde{l}_{iL},l_{iL})$	$E^c_i(\tilde{e}^c_{iL},e^c_{iL})$	$H_1(H_1,\tilde{H}_1)$	$H_2(H_2,\tilde{H}_2)$
$SU(3)_C$	**3**	$\bar{\mathbf{3}}$	$\bar{\mathbf{3}}$	**1**	**1**	**1**	**1**
$SU(2)_L$	**2**	**1**	**1**	**2**	**1**	**2**	**2**
$U(1)_Y$	$\frac{1}{6}$	$-\frac{2}{3}$	$\frac{1}{3}$	$-\frac{1}{2}$	1	$-\frac{1}{2}$	$\frac{1}{2}$

In phenomenological applications of SUSY model, the SUSY Lagrangian consists of two parts, namely the SUSY invariant Lagrangian and the soft SUSY breaking terms.

$$\mathcal{L} = \mathcal{L}_{SUSY\ inv} + \mathcal{L}_{SUSY\ breaking} \tag{B1}$$

The SUSY invariant part of the MSSM Lagrangian is given as follows. $\mathcal{L}_{SUSY\ inv}$ can be decomposed into two parts,

$$\mathcal{L}_{SUSY\ inv} = \mathcal{L}_{gauge} + \mathcal{L}_{superpotential}, \tag{B2}$$

$\mathcal{L}_{gauge}$ depends on the gauge coupling constants, and is given by

$$\begin{aligned}\mathcal{L}_{gauge} = & \sum_{gauge\ multiplet} F^{(a)}_{\mu\nu} F^{(a)\mu\nu} + \sum_{chiral\ multiplet} (i\overline{\psi_{iL}}\gamma\cdot\mathcal{D}\psi_{iL} + |\mathcal{D}_\mu\phi_i|^2) \\ & + \mathcal{L}_{gaugino-matter} + \mathcal{L}_{D\ term},\end{aligned} \tag{B3}$$

where for each gauge group the $\mathcal{L}_{gaugino-matter}$ and $\mathcal{L}_{D\ term}$ terms are given by

$$\mathcal{L}_{gaugino-matter} = -\sum_i \sqrt{2} g \phi_i^\dagger \overline{\lambda}^a T^a \psi_{iL} + H.c., \tag{B4}$$

$$\mathcal{L}_{D\ term} = -\sum_a \frac{g^2}{2} \sum_i (\phi_i^\dagger T^a \phi_i)^2. \tag{B5}$$

In addition to the normal gauge interactions defined in the covariant derivatives, these two types of interactions specified by the gauge coupling constants in Eqs.(B4) and (B5) are

necessary to keep the SUSY invariance of the Lagrangian. $\mathcal{L}_{superpotential}$ is determined from the superpotential $W(\phi_i)$, which is a function of scalar fields of the chiral multiplets,

$$\mathcal{L}_{superpotential} = -\sum_i |\frac{W(\phi)}{\partial\phi_i}|^2 - \frac{1}{2}\frac{\partial^2 W(\phi)}{\partial\phi_i\partial\phi_j}\overline{(\psi_{iL})^c}\psi_{jL} + H.c. \tag{B6}$$

The superpotential therefore generates a set of bosonic and fermionic interactions. From the gauge invariance, the superpotential ($W(\phi_i)$) for the MSSM is given by

$$W_{MSSM} = (y_e)_{ij}H_1E_i^cL_j + (y_d)_{ij}H_1D_i^cQ_j + (y_u)_{ij}H_2U_i^cQ_j - \mu H_1H_2, \tag{B7}$$

where the contraction of the $SU(2)$ indices is made by using the anti-symmetric tensor, $\varepsilon_{\alpha\beta}$. Also, the R-parity conservation is required (Section III C 3). By substituting these functions in Eq.(B6), this superpotential would induce the ordinary Yukawa couplings and the higgsino mass terms as well as the other interactions which are necessary to ensure the SUSY invariance.

The soft SUSY breaking mass terms are defined as terms which do not introduce quadratic divergence, and essentially serve as mass terms for superpartners. A general form of SUSY-breaking terms in the MSSM is given by

$$\begin{aligned}\mathcal{L}_{SUSY\ breaking} = & -(m_e^2)_{ij}\tilde{e}^*_{Ri}\tilde{e}_{Rj} - (m_l^2)_{ij}\tilde{l}^*_{Li}\tilde{l}_{Lj} - (m_d^2)_{ij}\tilde{d}^*_{Ri}\tilde{d}_{Rj} \\ & -(m_u^2)_{ij}\tilde{u}^*_{Ri}\tilde{u}_{Rj} - (m_q^2)_{ij}\tilde{q}^*_{Li}\tilde{q}_{Li} - m^2_{H_1}H_1^*H_1 - m^2_{H_2}H_2^*H_2 \\ & -[m_0(A_e)_{ij}H_1\tilde{e}^*_i\tilde{e}_j + m_0(A_d)_{ij}H_1\tilde{D}^*_i\tilde{Q}_j \\ & +m_0(A_u)_{ij}H_2\tilde{U}^*_i\tilde{Q}_j - \mu B H_1H_2 \\ & +\frac{1}{2}M_1\overline{\tilde{B}_R}\tilde{B}_L + \frac{1}{2}M_2\overline{\tilde{W}_R}\tilde{W}_L + \frac{1}{2}M_3\overline{\tilde{G}_R}\tilde{G}_L + h.c.].\end{aligned} \tag{B8}$$

These terms are quadratic terms for scalar quarks, leptons and Higgs fields, scalar trilinear terms (A terms) and gaugino Majorana mass terms. These terms are supposed to be generated from spontaneous symmetry breaking of SUSY, presumably at some high energy scale in some sector outside the MSSM dynamics, such as the supergravity or the dynamical SUSY breaking sector. For more details, see for example Nilles (1984) or Haber and Kane (1985).

APPENDIX C: DIFFERENTIAL BRANCHING RATIO OF THE $\mu^+ \to e^+e^+e^-$ DECAY

The differential branching ratio of the $\mu^+ \to e^+e^+e^-$ decay is given in Eq.(115). The kinematical functions appearing in Eq.(115), $\alpha_i(x_1, x_2)$, $\beta_i(x_1, x_2)$ and $\gamma_i(x_1, x_2)$, are given as follows ($x_i \equiv 2E_i/m_\mu$ $(i = 1, 2)$ are the normalized e^+ energies):

$$\begin{aligned}\alpha_1(x_1, x_2) &= 8(2 - x_1 - x_2)(x_1 + x_2 - 1), \\ \alpha_2(x_1, x_2) &= 2\{x_1(1 - x_1) + x_2(1 - x_2)\}, \\ \alpha_3(x_1, x_2) &= 8\{\frac{2x_2^2 - 2x_2 + 1}{1 - x_1} + \frac{2x_1^2 - 2x_1 + 1}{1 - x_2}\},\end{aligned}$$

$$
\begin{aligned}
\alpha_4(x_1,x_2) &= 32(x_1+x_2-1),\\
\alpha_5(x_1,x_2) &= 8(2-x_1-x_2),\\
\beta_1(x_1,x_2) &= 2\frac{(x_1+x_2)(x_1^2+x_2^2)-3(x_1+x_2)^2+6(x_1+x_2)-4}{(2-x_1-x_2)},\\
\beta_2(x_1,x_2) &= \frac{8}{(1-x_1)(1-x_2)(2-x_1-x_2)}\times\\
&\quad \{2(x_1+x_2)(x_1^3+x_2^3)-4(x_1+x_2)(2x_1^2+x_1x_2+2x_2^2)\\
&\quad +(19x_1^2+30x_1x_2+19x_2^2)-12(2x_1+2x_2-1)\},\\
\gamma_1(x_1,x_2) &= 4\frac{\sqrt{(1-x_1)(1-x_2)(x_1+x_2-1)}(x_1-x_2)}{(2-x_2-x_1)},\\
\gamma_2(x_1,x_2) &= 32\sqrt{\frac{(x_1+x_2-1)}{(1-x_1)(1-x_2)}}\frac{(x_1+x_2-1)(x_2-x_1)}{(2-x_1-x_2)},\\
\gamma_3(x_1,x_2) &= 16\sqrt{\frac{(x_1+x_2-1)}{(1-x_1)(1-x_2)}}(x_1+x_2-1)(x_2-x_1),\\
\gamma_4(x_1,x_2) &= 8\sqrt{\frac{(x_1+x_2-1)}{(1-x_1)(1-x_2)}}(2-x_1-x_2)(x_2-x_1).
\end{aligned}
\tag{C1}
$$

REFERENCES

Abachi, S. (D0 Collaboration), 1996, Phys. Rev. Lett. **76**, 3271.

Abdurashitov, J.N., *et al.* (SAGE Collaboration), 1996, Phys. Rev. Lett. **77**, 4708.

Abegg, R., *et al.* (TRIUMF E614 Collaboration), 1996, An experimental proposal to TRIUMF "Precision Measurement of the Michel Parameters of μ^+ Decay".

Abela, R., *et al.*, 1996, Phys. Rev. Lett. **77**, 1950.

Abraham, K.J., and B. Lampe, 1996, Phys. Lett. B **367**, 299.

Abreu, P., *et al.* (DELPHI Collaboration), 1997, Z. Phys. C **73**, 243.

Ahmad, S., *et al.*, 1988, Phy. Rev. D **38** 2102.

Akers, R., *et al.* (OPAL Collaboration), 1995, Z. Phys. C **67**, 555.

Altarelli, G., L. Baulieu, N. Cabibbo, L. Maiani, and R. Petronzio, 1977, Nucl. Phys. B **125**, 285.

Amaldi, U., W. de Boer, and H. Furstenau, 1991, Phys. Lett. D **25**, 3092.

Ambrose, D., *et al.* (BNL E871 Collaboration), 1998, Phys. Rev. Lett. **81** 5734.

Ankenbrandt, C.M., *et al.* (Muon Collider Collaboration), 1999, Phys. Rev. ST Accel. Bean 2, 081001.

Arbuzov, A.B., O. Krehl, E.A. Kuraev, E.N. Magar, B.G. Shaikhatdenov, 1998, Phys. Lett. B **432**, 421.

Arisaka, K., *et al.*, 1998, Phys. Lett. B **432**, 230.

Arkani-Hamed, N., H.-C. Cheng, and L.J. Hall, 1996a, Phys. Rev. D **53**, 413.

Arkani-Hamed, N., H.-C. Cheng, J.L. Feng, and L.J. Hall, 1996b, Phys. Rev. Lett. **77**, 1937.

Arkani-Hamed, J.L. Feng, L.J. Hall, and H.-C. Cheng, 1997, Nucl. Phys. B **505**, 3.

Athanassopoulos, C., *et al.* (LSND Collaboration), 1998, Phys. ReV. Lett. **81**, 1774.

Babu, K.S., and R.N. Mohapatra, 1995, Phys. Rev. Lett. **75**, 2276.

Bachman, M., *et al.* (MECO Collaboration), 1997, An experimental proposal E940 to Brookhaven National Laboratory AGS, "A Search for $\mu^- N \to e^- N$ with Sensitivity below 10^{-16}".

Badertscher, A., *et al.*, 1982, Nucl. Phys. A **377**, 406.

Balke, B., *et al.*, 1988, Phys. Rev. D **37**, 587.

Baranov, V.A., *et al.*, 1991, Sov. J. Nucl. Physics **53**, 802.

Barber, W.C., *et al.*, 1969, Phys. Rev. Lett. **22** 902.

Barbieri, R., and L.J. Hall, 1994, Phys. Lett. B **228** 212.

Barbieri, R., L.J. Hall, and A. Strumia, 1995a, Nucl. Phys. B **445**, 219.

Barbieri, R., L.J. Hall, and A. Strumia, 1995b, Nucl. Phys. B **449**, 437.

Barbieri, R., G. Dvali, and L.J. Hall, 1996, Phys. Lett. B **377**, 76.

Bardin, G., *et al.*, 1984, Phys. Lett. B **137**, 135.

Barkov, L.M., *et al.*, 1999, a research proposal to PSI "Search for $\mu^+ \to e^+\gamma$ down to 10^{-14} branching ratio".

Barnett, I., *et al.*, 1994, a proposal for an experiment at PSI, "Measurement of the transverse polarization of positrons from the decay of polarized muons".

Beer, G.A., *et al.*, 1986, Phys. Rev. Lett. **57**, 671.

Behrends, R.E., R.J. Finkelstein, and A. Sirlin, 1956, Phys. Rev. **101**, 866.

Bellgardt, U., *et al.*, 1988, Nucl. Phys. B **229**, 1.

Beltrami, I., *et al.*, 1987, Phys. Lett. B **194**, 326.

Bernabeu, J., E. Nardi, and D. Tommasini, 1993, Nucl. Phys. B **409**, 69.

Bertl, W., *et al.*, 1984, Phys. Lett. B **140**, 299.
Bertl, W., *et al.*, 1985, Nucl. Phys. B **260**, 1.
Bilenky, S.M., S.T. Petcov, B. Pontecorvo, 1977, Phys. Lett. B **67**, 309.
Bilenky, S.M., and S.T. Petcov, 1987, Rev. Mod. Phys. **59**, 671.
Bjorken, J.D., K. Lane, and S. Weinberg, 1977, Phys. Rev. D **16**, 1474.
Blackmore, E., *et al.*, 1997, "MUONS at TRIUMF", TRIUMF internal report, unpublished.
Bliss, D.W., *et al.*, 1998, Phys. Rev. D **57**, 5903.
Bolton, R.D., *et al.*, 1984, Phys. Rev. Lett. **53**, 1415.
Bolton, R.D., *et al.*, 1988, Phys. Rev. D **38**, 2077.
Borzumati, F., and A. Masiero, 1986, Phys. Rev. **57**, 961.
Bouchiat, C., and L. Michel, 1957, Phys. Rev. **106**, 170.
Bowser-Chao, D., and W.-K. Keung, 1997, Phy. Rev. D **56** 3924.
Brooks, M.L., *et al.* (MEGA Collaboration), 1999, hep-ex/9905013, submitted to Phys. Rev. Lett.
Bryman, D.A., M. Blecher, K. Gotow, and R.J. Powers, 1972, Phys. Rev. Lett. **28**, 1469.
Bryman, D.A., *et al.*, 1985, Phys. Rev. Lett. **55** 465.
Burkard, H., *et al.*, 1985a, Phys. Lett. B **150**, 242.
Burkard, H., *et al.*, 1985b, Phys. Lett. B **160**, 343.
Cao, J.-J., T. Han, X. Zhang, and G.-R. Lu, 1999, Phy. Rev. D **59** 09501.
Carena, M., G.F. Giudice, and C.E.M. Wagner, 1997, Phys. Lett. B **390**, 234.
Carey, R.M., *et al.*, 1999a, Phys. Rev. Lett. **82**, 1632.
Carey, R.M., *et al.*, 1999b, an experimental proposal to PSI, "A Precision Measurement of the Positive Muon Lifetime Using a Pulsed Muon Beam and the μLan Detector".
Carlson, E.D., and P.H. Frampton, 1992, Phys. Lett. B **283**, 123.
Cavallo, F.R. *et al.*, 1999, a letter of intent to PSI, "A Preceision Measurement of the μ^+ Lifetime (G_F) with the FAST detector".
CERN Report, 1999, CERN 99-02 and ECFA 99-197, "Prospective Study of Muon Storage Rings at CERN", edited by B. Autin, A. Blondel, and J. Ellis.
Chaichian, M., and K. Huitu, 1996, Phys. Lett. B **384**, 157.
Chang, D., and W.Y. Keung, 1989, Phys. Rev. Lett. **62**, 2583.
Chattopadhyay, U. and P. Nath, 1996, Phys. Rev. D **53**, 1648.
Cheng, T.P., and L.F. Li, 1977a, Phys. Rev. Lett. **38**, 381.
Cheng, T.P., and L.F. Li, 1977b, Phys. Rev. D **16**, 1425.
Cheng, T.P., and L.F. Li, 1980, Phys. Rev. Lett. **45**, 1908.
Chiang, H.C., E. Oset, T.S. Kosmas, A. Faessler, and J.D. Vergados, 1993, Nucl. Phys. A **559**, 526.
Choi, S.Y., C.S. Kim, Y.J. Kwon, and S.-H. Lee, 1998, Phy. Rev. D **57** 7023.
Ciafaloni, P., A. Romanino and A. Strumia, 1996, Nucl. Phys. **B458**, 3.
Cleveland, B.T. *et al.*, 1998, Astrophys. J. **496**, 505.
Cohen, E.R., and B.N. Taylor, 1987, Rev. Mod. Phys. **59**, 1121.
Cohen, A.G., D.B. Kaplan, and A.E. Nelson, 1996, Phys. Lett. B **388**, 588.
Coleman, S., and S.L. Glashow, 1999, Phy. Rev. D **59** 116008.
Conversi, M., E. Pancini, and O. Piccioni, 1947, Phys. Rev. **71**, 209.
Crittenden, R.R., W.D. Walker, and J. Ballam, 1961, Phys. Rev. **121**, 1823.
Czarnecki, A., W.J. Marciano, and K. Melnikov, 1997, in *Proceedings of Workshop on*

Physics at the First Muon Collider and at the Front End of the Muon Collider, edited by S.H. Geer and R. Raja, Fermilab, U.S.A., AIP Conference Proceedings 435, p.409.
Czarnecki, A., and W.J. Marciano, 1998, "Lepton anomalous magnetic moments – a theory update", preprint BNL-HET-98/43, hep-ph/9810512.
Danby, G., J.M. Gaillard, K. Goulianos, L.M. Lederman, N. Mistry, M. Schwartz, and J. Steinberger, 1962, Phys. Rev. Lett. **9**, 36.
Depommier, P. *et al.*, 1977, Phys. Rev. Lett. **39**, 1113.
Depommier, P., 1987, in *Neutrinos* edited by H.V. Klapdor, (Springer, Berlin), p.265.
Depommier, P., and C. Leroy, 1995, Reports on Progress in Phys. **58**, 61.
Derenzo, S.E., 1969, Phys. Rev. **181**, 1854.
Deshpande, N.G., B. Dutta and E. Keith, 1996, Phys. Rev. D **54**, 730.
Dimopoulos, S., and H. Georgi, 1981, Nucl. Phys. B **193**, 150.
Dimopoulos, S., and L. Hall, 1995, Phys. Lett. B **344**, 185.
Dine, M., and A.E. Nelson, 1993, Phys. Rev. D **48**, 1277.
Dine, M., A.E. Nelson, and Y. Shirman, 1995, Phys. Rev. D **51**, 1362.
Dine, M., A.E. Nelson, Y. Nir, and Y. Shirman, 1996, Phys. Rev. D **53**, 2658.
Dine, M., Y. Nir, and Y. Shirman, 1997, Phy. Rev. D **55** 1501.
Dohmen, C., *et al.* (SINDRUM II Collaboration), 1993, Phys. Lett. B **317**, 631.
Dubovsky, S.L., and D.S. Gorbunov, 1998, Phys. Lett. B **419**, 223.
Duong, T.V., B. Dutta, and E. Keith, 1996, Phys. Lett. B **378**, 128.
Dzhilkibaev, R.M., and V.M. Lobashev, 1989, Sov. J. Nucl. Phys. **49**, 384.
Eckstein, S.G., and R.H. Pratt, 1959, Ann. of Phys. **8**, 297 (1959).
Edwards, K.W., *et al.* (CLEO Collaboration), 1997, Phys. Rev. B **55**, R3919.
Eichenberger, W., R. Engfer, and A. van der Schaaf, 1984, Nucl. Phys. A **412**, 523.
Eitel, K., *et al.* (KARMEN Collaboration), 1999, Nucl. Phys. Proc. Suppl. **70**, 210.
Ellis, J., S. Kelly, and D. Nanopoulos, 1991, Phys. Lett. B **260**, 131.
Engfer R., and H.K. Walter, 1986, Ann. Rev. Nucl. Part. Sci. **36**, 327.
Evseev, V.S., 1975, in *Muon Physics Vol.III Chemistry and Solids*, edited by V.W. Hughes and C.S. Wu (Academic Press), p.236.
Faessler, A., T.S. Kosmas, S. Kovalemko, and J.D. Vergados, 1999, hep-ph/9904335, "Constraints on R-parity Violating Supersymmetry from $\mu^- - e^-$ Nuclear Conversion".
Feinberg, G., 1958, Phys. Rev. **116**, 1482.
Feinberg, G., and S. Weinberg, 1961, Phys. Rev. Lett. **123**, 1439.
Fetscher, W., H.J. Gerber, and K.F. Johnson, 1986, Phys. Lett. B **173**, 102.
Fetscher, W., and H.J. Gerber, 1995, in *Precision Tests of the Standard Electroweak Model* edited by P. Langacker (World Scientific), p.657.
Fetscher, W. and H.J. Gerber, 1998, in *Particle Data Group: Review of Particle Properties*, Euro. Phys. Journal **3**, p.282.
Feynman, R.P., and M. Gell-Mann, 1958, Phys. Rev. **109**, 193.
Fisher, P., B. Kayser, and K.S. McFarland, 1999, "Neutrino Mass and Oscillation", hep-ph/9906244, submitted to Ann. Rev. Nucl. Part. Sci.
Frampton, P.H., and B.H. Lee, 1990, Phys. Rev. Lett. **64**, 619.
Frampton, P.H., 1992, Phys. Rev. Lett. **69**, 2889.
Frampton, P.H., 1992b, Phys. Rev. D **45**, 4240.
Frankel, S., 1975, in *Muon Physics II: Weak Interaction*, edited by V.W. Hughes and C.S.

Wu (Academic, New York), p83.
Freedman, S.J., *et al.*, 1993, Phys. Rev. D **47**, 811.
Fronsdal, C., and H. Überall, 1959, Phys. Rev. **118**, 654.
Fujii, H., S. Nakamura, and K. Sasaki, 1993, Phys. Lett. B **299**, 342.
Fujii, H., Y. Mimura, K. Sasaki, and T. Sasaki, 1994, Phys. Rev. D **49**, 559.
Fukuda, Y., *et al.* (Kamiokande Collaboration), 1996, Phys. Rev. Lett. **77**, 1683.
Fukuda, Y., *et al.* (Super-Kamiokande Collaboration), 1998a, Phys. Rev. Lett. **81**, 1158, and Erratum: 1998, *ibid.* **81** 4279.
Fukuda, Y., *et al.* (Super-Kamiokande Collaboration), 1998b, Phys. Rev. Lett. **81**, 1562.
Fukugita, M. and T. Yanagida, 1994, in *Physics and Astrophysics of Neutrinos*, edited by M. Fukugita and A. Suzuki (Springer-Verlag), p.1.
Gabrielli, E., and U. Sarid, 1997, Phys. Rev. Lett. **79**, 4752.
Geer, S., 1998, Phys. Rev. D **57**, 6989, and Erratum: 1999, *ibid.* D **59**, 039903.
Gell-Mann, M., P. Ramond, and R. Slansky, 1979, in *Supergravity*, edited by D. Freedman and P. van Nieuwenhuizen, (North Holland, Amsterdam), p.315.
Giovanetti, K.L., *et al.*, 1984, Phys. Rev. D **29**, 343.
Giudice, G.F., and R. Rattazzi, 1998, "Theories with Gauge Mediated Supersymmetry Breaking", hep-ph/9801271, submitted to Phys. Rep.
Glashow, S.L., 1961, Phys. Rev. Lett. **6**, 196.
Glashow, S.L., and L.M. Krauss, 1987, Phys. Lett. B **190**, 199.
Glashow, S.L., P.J. Kerman, and L.M. Krauss, 1999, Phys. Lett. B **445**, 412.
Gomez, M.E. and H. Goldberg, 1996, Phys. Rev. D **53**, 5244.
Gordeev, V.A., *et al.*, 1997, Phys. Atom. Nucl. **60**, 1164: 1997, Yad. Fiz. **60**, 1291.
Haber, H.E., and G.L. Kane, 1985, Phys. Rep. **117**, 75.
Hall, L.J., V.A. Kostelecky and S. Raby, 1986, Nucl. Phys. B **267**, 415.
Halprin, A., 1982, Phys. Rev. Lett. **48**, 1313.
Halprin, A. and A. Masiero, 1993, Phys. Rev. D **48**, 2987.
Hampel, W., *et al.* (Gallex Collaboration), 1999, Phys. Lett. B **447**, 127.
Hänggi, P., R.D. Viollier, U. Raff, and K. Adler, 1974, Phys. Lett. B **51**, 119.
Herczeg, P., 1986, Phys. Rev. D **34**, 3449.
Herczeg, P., and R.N. Mohapatra, 1992, Phys. Rev. Lett. **69**, 2475.
Herczeg, P., 1995, in *Precision Tests of the Standard Electroweak Model* edited by P. Langacker (World Scientific), p.786.
Herzog, F., and K. Adler, 1980, Helv. Phys. Acta **53**, 53.
Hincks, E.P., and B. Pontecorvo, 1947, Phys. Rev. Lett. **73**, 246.
Hirouchi, M., and M. Tanaka, 1998, Phy. Rev. D **58** 032004.
Hisano, J., T. Moroi, K. Tobe, M. Yamaguchi, and T. Yanagida, 1995, Phys. Lett. B **357**, 576.
Hisano, J., T. Moroi, K. Tobe, and M. Yamaguchi, 1996, Phys. Rev. D **53**, 2442.
Hisano, J., T. Moroi, K. Tobe, and M. Yamaguchi, 1997, Phys. Lett. B **391**, 341, and Errata: 1997, *ibid.* B **397**, 357.
Hisano, J., D. Nomura, and T. Yanagida, 1998a, Phys. Lett. B **437**, 351.
Hisano, J., D. Nomura, Y. Okada, Y. Shimizu, and M. Tanaka, 1998b, Phys. Rev. D **58**, 116010.
Hisano, J., and D. Nomura, 1999a, Phys. Rev. D **59**, 116005.

Hisano, J., M.M. Nojiri, Y. Shimizu, and M .Tanaka, 1999b, Phy. Rev. D **60** 055008.
Honecker, W., *et al.* (SINDRUM II Collaboration), 1996, Phys. Rev. Lett. **76**, 200.
Horikawa, K., and K. Sasaki, 1996, Phys. Rev. D **53**, 560.
Hou, W.S., and G.G. Wong, 1995, Phys. Lett. B **357**, 145.
Hou, W.S., and G.G. Wong, 1996, Phys. Rev. D **53**, 1537.
Hou, W.S., 1996b, Nucl. Phys. B **51A**, 40.
Huber, T.M., *et al.*, 1990, Phys. Rev. D **41**, 2709.
Hughes, V.W., D.W. McColm, K. Ziock and R. Prepost, 1960, Phys. Rev. Lett. **5**, 63.
Hughes, V.W., and T. Kinoshita, 1999, Rev. Mod. Phys. **71**, S133.
Huitu, K., J. Maalampi, M. Raidal, and A. Santamaria, 1998, Phys. Lett. B **430**, 355.
Ishida, K., and K. Nagamine, 1998, in *Proceedings of International Workshop on JHF Science*, edited by J. Chiba, M. Furusaka, H. Miyatake and S. Sawada, Vol.II, p.12.
JAERI/KEK Joint Project Proposal, 1999, unpublished.
Jodidio, A., *et al.*, 1986, Phys. Rev. D **34**, 1967, and Erratum: 1988, *ibid.* **37**, 237.
Kaulard, J., *et al.*, 1998, Phys. Lett. B **422**, 334.
Kersch, A. N. Kraus, and R. Engfer, 1988, Nucl. Phys. A **485**, 606.
Kim, J.E., P. Ko, and D.G. Lee, 1997, Phys. Rev. D **56**, 100.
King, S.F., and M. Oliveira, 1999, Phys. Rev. D **60**, 035003.
Kinnison, W.W., *et al.*, 1982, Phys. Rev. D **25**, 2846.
Kinoshita, T., and A. Sirlin, 1957a, Phys. Rev. **107**, 593.
Kinoshita, T., and A. Sirlin, 1957b, Phys. Rev. **108**, 844.
Kinoshita, T., and A. Sirlin, 1959, Phys. Rev. **113**, 1652.
Kitano, R., and K. Yamamoto, 1999, KEK preprint KEK-TH-62, hep-ph/995459, "Lepton flavor violation in a supersymmetic E_6 type model".
Kobayashi, M., and T. Maskawa, 1973, Prog. Theor. Phys. **49**, 652.
Korenchenko, S.M., *et al.*, 1976, Sov. Phys. JETP **43**, 1.
Kosmas, T.S., and J.D. Vergados, 1990, Nucl. Phys. A **510**, 641.
Kosmas, T.S., J.D. Vergados, O. Civitarese, and A. Faessler, 1994, Nucl. Phys. A **570**, 637.
Kosmas, T.S., and J.D. Vergados, 1996, Phys. Rep. **264**, 251.
Kosmas, T.S., J.D. Vergados, and A. Faessler, 1998, Phys. Atom. Nucl. **61**, 1161: 1998, Yad. Fiz. **61**, 1261.
Krasnikov, N.V., 1994, Mod. Phys. Lett. A **9** 791.
Krasnikov, N.V., 1996, Phys. Lett. B **388**, 783.
Krolak, P., *et al.*, 1994, Phys. Lett. B **320**, 407.
Kuno, Y., K. Nagamine, and T. Yamazaki, 1986, Nucl. Phys. A **475**, 615.
Kuno, Y. and Y. Okada, 1996, Phys. Rev. Lett. **77**, 434.
Kuno, Y., A. Maki, and Y. Okada, 1997a, Phys. Rev. D **55**, 2517.
Kuno, Y., 1997b, in *Proceedings of Workshop on Physics at the First Muon Collider and at the Front End of the Muon Collider*, edited by S.H. Geer and R. Raja (AIP Conference Proceedings 435), p.261.
Kuno, Y., *et al.*, 1998, in *Proceedings of Workshop on High Intensity Secondary Beam with Phase Rotation*, edited by Y. Kuno and N. Sasao, p.71.
Lagarrigue, A., and C. Peyrou, 1952, Acad. Sci. Paris, **234**, 873.
Langacker, P., and S.U. Sankar, 1989, Phys. Rev. D **40**, 1569.
Langacker, P., and M. Luo, 1991, Phys. Rev. D **44**, 817.

Lee, B.W., S. Pakvasa, R.E. Shrock, and H. Sugawara, 1977a, Phys. Rev. Lett. **38**, 937.
Lee, B.W., and R.E. Shrock, 1977b, Phys. Rev. D **16**, 1444.
Lee, A.M., *et al.*, 1990, Phys. Rev. Lett. **64**, 165.
Lenard, A., 1953, Phys. Rev. **90**, 968.
LEP Electroweak Working Group and SLD Heavy Flavor and Electroweak Goups, 1999, CERN-EP/99-15 preprint "A Combination of Preliminary Electroweak Measurements and Constraints on the Standard Model".
Lobashev, V.M., 1998, in *Proceedings of 18th Workshop on Physics in Collisions"*, edited by S. Bianco, A. Calcaterra, P. de Simone, F.L. Fabbri (Frascati Physics series, 11), p.179.
Lokonathan, S. and J. Steinberger, 1955, Phys. Rev. **98**, 240.
Lopez, J.L., D.V. Nanopoulos, and X. Wang, 1994, Phys. Rev. D **49**, 366.
Maki, Z., M. Nakagawa, and S. Sakata, 1962, Prog. Theor. Phys. **28**, 870.
Marciano, W.J., and A.I. Sanda, 1977a, Phys. Lett. B **67**, 303.
Marciano, W.J., and A.I. Sanda, 1977b, Phys. Rev. Lett. **38**, 1512.
Marciano, W.J., and A. Sirlin, 1988, Phys. Rev. Lett. **61**, 1815.
Marciano, W.J., 1999, preprint hep-ph/9903451, "Fermi Constants and New Physics".
Marshall, G.M., *et al.*, 1982, Phys. Rev. D **25**, 1174.
Matthias, B., *et al.*, 1991, Phys. ReV. Lett. **66**, 2716.
Michel, L., 1950, Proc. Phys. Soc. A **63**, 514.
Mikheyev, S.P., and A.Yu. Smirnov, 1985, Yad. Fiz. **42**, 1441 [Sov. J. Nucl. Phys. **42**, 913.]
Mohapatra, R.N., 1992, Z. Phys. C **56**, 117.
Mohapatra, R.N., and P.B. Pal, 1998, *Massive Neutrinos in Physics and Astrophysics (Second Edition)*, (World Scientific).
Molzon, W.R., 1997, in *Proceedings of Workshop on Physics at the First Muon Collider and at the Front End of the Muon Collider*, edited by S.H. Geer and R. Raja (AIP Conference Proceedings 435), p.152.
Moroi, T., 1996, Phys. Rev. D **53**, 6565.
Muon Collider Collaboration, 1996, "$\mu^+\mu^-$ Collider – A Feasibility Study", preprint BNL-52503, Fermilab-Conf.-96/092, LBNL-38946.
Nagamine, K., and T. Yamazaki, 1974, Nucl. Phys. A **219**, 104.
Nagamine, K., 1996, Nucl. Phys. B (Proc. Suppl.) **51A**, 115.
Nakamura, S., *et al.*, 1998, A research proposal to RIKEN-RAL (R77), "Precise Measurement of the μ^+ Lifetime and Test of the Exponential Law".
Neddermeyer, S.H, and C.D.Anderson, 1937, Phys. Rev. **51**, 884.
Ni, B., *et al.*, 1993, Phys. Rev. D **48**, 1976.
Nilles, H.P., 1984, Phys. Rep. **110**, 1.
Nir, Y., and N. Seiberg, 1993, Phys. Lett. B **309**, 337.
Nishijima, K., 1957, Phys. Rev. **108**, 907.
Okada, Y., K. Okamura, and Y. Shimizu, 1998, Phys. Rev. D **58**, 051901.
Okada, Y., K. Okamura, and Y. Shimizu, 1999, KEK Preprint KEK-TH-623, "$\mu^+ \to e^+\gamma$ and $\mu^+ \to e^+e^+e^-$ Processes with Polarized Muons and Supersymmetric Grand Unified Theories", hep-ph/9906446.
Otten, E.W. and Ch. Weinheimer, 1998, in *Proceedings of the First International Symposium on Lepton and Baryon Number Violation*, edited by H.V. Klapdor-Kleingrothaus and I.V. Krivosheina (Institute of Physics Publishing, Bristol and Philadelphia), p.309.

Particle Data Group, 1998, Euro. Phys. Journal, **3**, 1.
Petcov, S.T., 1977, Yad. Fiz. **25**, 641 [1977, Sov. J. Nucl. Phys. **25**, 340].
Pich, A., and J.P. Silva, 1995, Phys. Rev. D **52**, 4006.
Pich, A., 1997, in *Proceedings of NATO Advanced Study Institute on Masses of Fundamental Particles*, edited by M. Levy, J. Iliopoulos, R. Gastmans, J.-M. Gerard (New York, Plenum, NATO ASI series B, Physics 363), p.173.
Pontecorvo, B., 1957, Zh. Eksp. Teor. Fiz. **33** 549 [1958, Sov. Phys. JETP, **6**, 429].
Porter, C.E., and H. Primakoff, 1951, Phys. Rev. **83**, 849.
Pratt, R., 1958, Phys. Rev. **111**, 646.
Raidal, M., and A. Santamaria, 1998, Phys. Lett. **B421**, 250.
Raidal, M., 1998b, Phys. Rev. D **57**, 2013.
Rattazzi, R., and U. Salid, 1996, Nucl. Phys. **B475**, 27.
Sakai, N., 1981, Z. Phys. **C11**, 153.
Scheck, F., 1978, Phys. Rep. **44**, 187.
Schwinger, J., 1957, Ann. Phys. **2**, 407.
Shanker, O., 1979, Phys. Rev. **D20**, 1608.
Shanker, O., 1982, Phys. Rev. **D25**, 1847.
Shanker, O., and R. Roy, 1997, Phys. Rev. **D55**, 7307.
Skrinskii, A.N., and V.V. Parkhomchuk, 1981, Fiz. Elem. Chastits At. Yadra, **12**, 557, [1981, Sov. J. Part. Nucl. **12** 223].
Steinberger, J., 1948, Phys. Rev. **74**, 500.
Steinberger, J., and H.B. Wolfe, 1955, Phys. Rev. **100**, 1490.
Swartz, M.L, 1989, Phys. Rev. D **40**, 1521.
Treiman, S.B., F. Wilczek, and A. Zee, 1977, Phys. Rev. D **16**, 152.
Van der Schaaf, A., *et al.*, 1980, Nucl. Phys. A **340**, 249.
Van der Schaaf, A., 1993, Progress in Particle and Nuclear Physics **31**, 1.
Van Hove, P., *et al.*, 1997, An experimental proposal R-97-06 to PSI, "A Precision Measurement of the Michel Parameter ξ'' in Polarized Muon Decay".
Van Ritbergen, T., and R.G. Stuart, 1999, Phys. Rev. Lett. **82**, 488.
Vergados, J.D., 1986, Phys. Rep. **133** 1.
Yanagida, T., 1979, in *Proceedings of Workshop on Unified Theory and Baryon Number in the Universe*, edited by O. Sawada and A. Sugamoto.
Yukawa, H., 1935, Prog. Phys. Math. Soc. Japan, **17**, 48.
Watanabe, R., M. Fukui, H. Ohtsubo, and M. Morita, 1987, Prog. Theor. Phys. **78**, 114.
Watanabe, R., K. Muto, T. Oda, T. Niwa, H. Ohtsubo, R. Morita, and M. Morita, 1993, Atomic Data and Nucl. Data Table, **54**, 165.
Weinberg, S., and G. Feinberg, 1959, Phys. Rev. Lett. **3**, 111, and Erratum: 1959, *ibid.*, 244.
Wilczek, F., and A. Zee, 1977, Phys. Rev. Lett. **38**, 531.
Willmann, L., and K.P. Jungmann, 1998, Physics **499**, 43.
Willmann, L., *et al.*, 1999, Phys. Rev. Lett. **82**, 49.
Wintz, P., 1998, in *Proceedings of the First International Symposium on Lepton and Baryon Number Violation*, edited by H.V. Klapdor-Kleingrothaus and I.V. Krivosheina (Institute of Physics Publishing, Bristol and Philadelphia), p.534.
Wolfenstein, L., 1978, Phys. Rev. D **17**, 2369.
Zee, A., 1985, Phys. Rev. Lett. **55**, 2382.

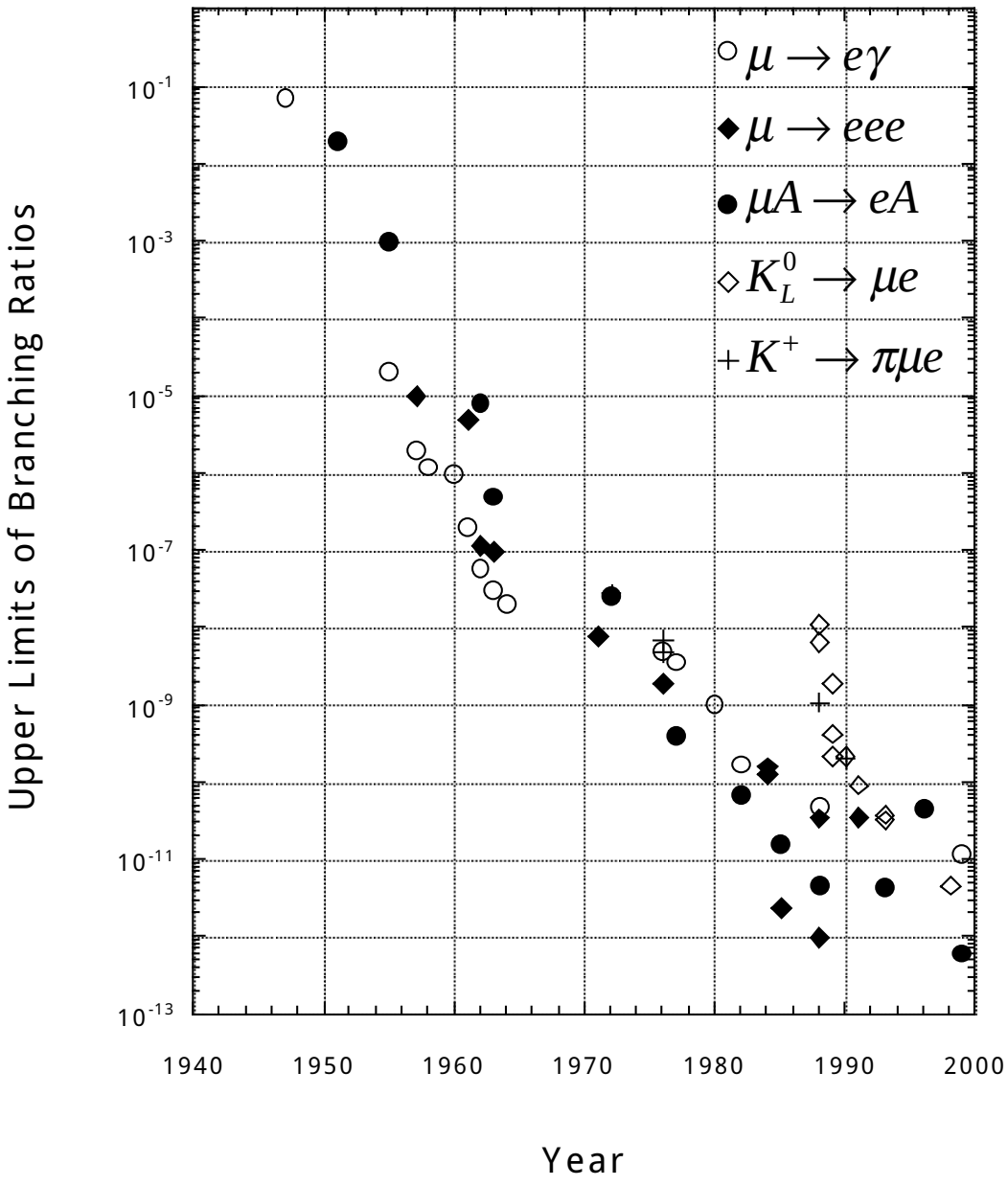

FIG. 1. Historical progress of LFV searches for various processes of muons and kaons.

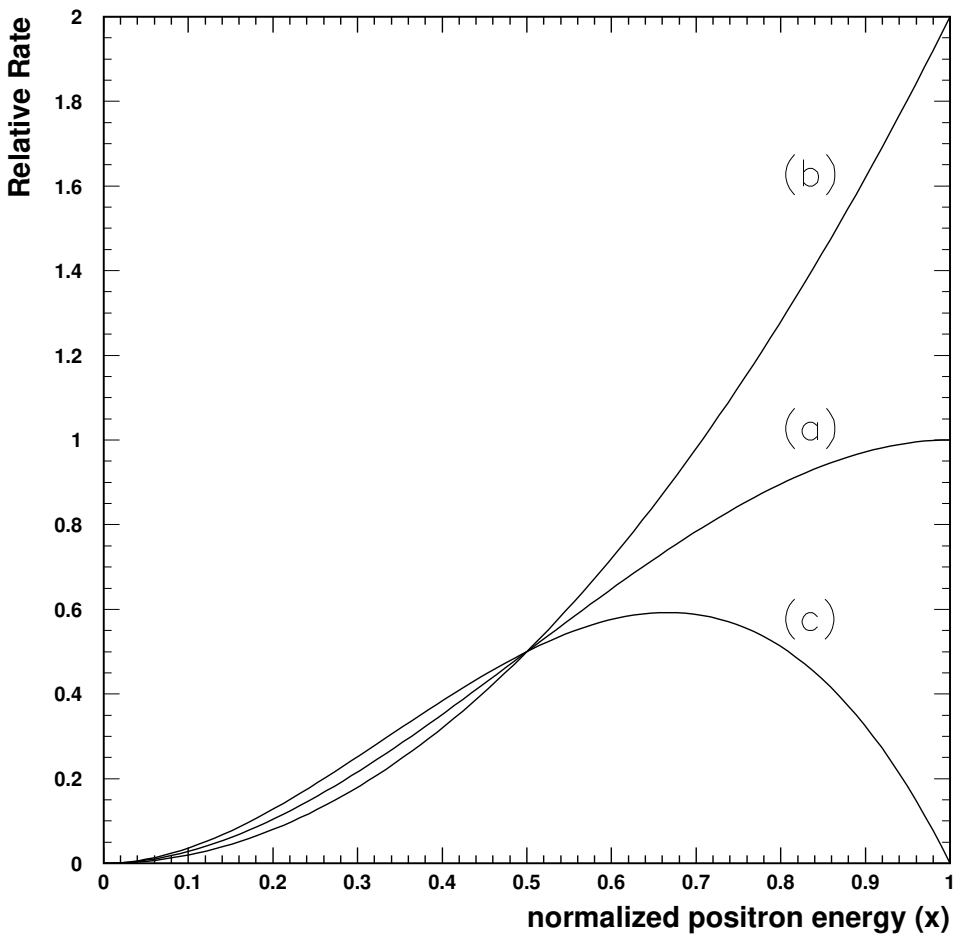

FIG. 2. Michel e^+ energy spectrum of polarized $\mu^+ \to e^+\nu_e\overline{\nu}_\mu$ decay with 100% muon polarization ($P_\mu = 1$). (a) $\cos\theta_e = 0$, (b) $\cos\theta_e = 1$, and (c) $\cos\theta_e = -1$.

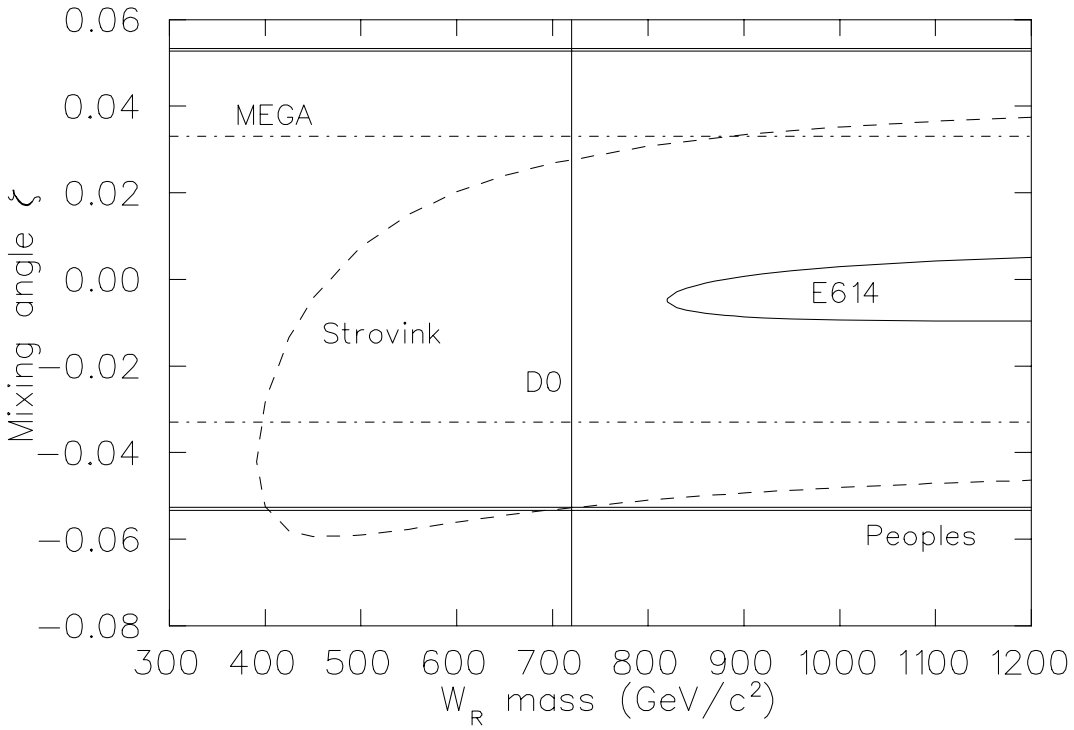

FIG. 3. Constraints on the mass of W_R vs. its mixing angle (ζ) in the manifest left-right symmetric model. The experimental constraints of "Strovink", "Peoples", "MEGA" and "D0" are from Jodidio, *et al.* (1986), Derenzo (1969), the MEGA experiment (unpublished), and Abachi, *et al.* (1996), respectively. The aimed goal for E614 is also shown (provided by D.R.Gill).

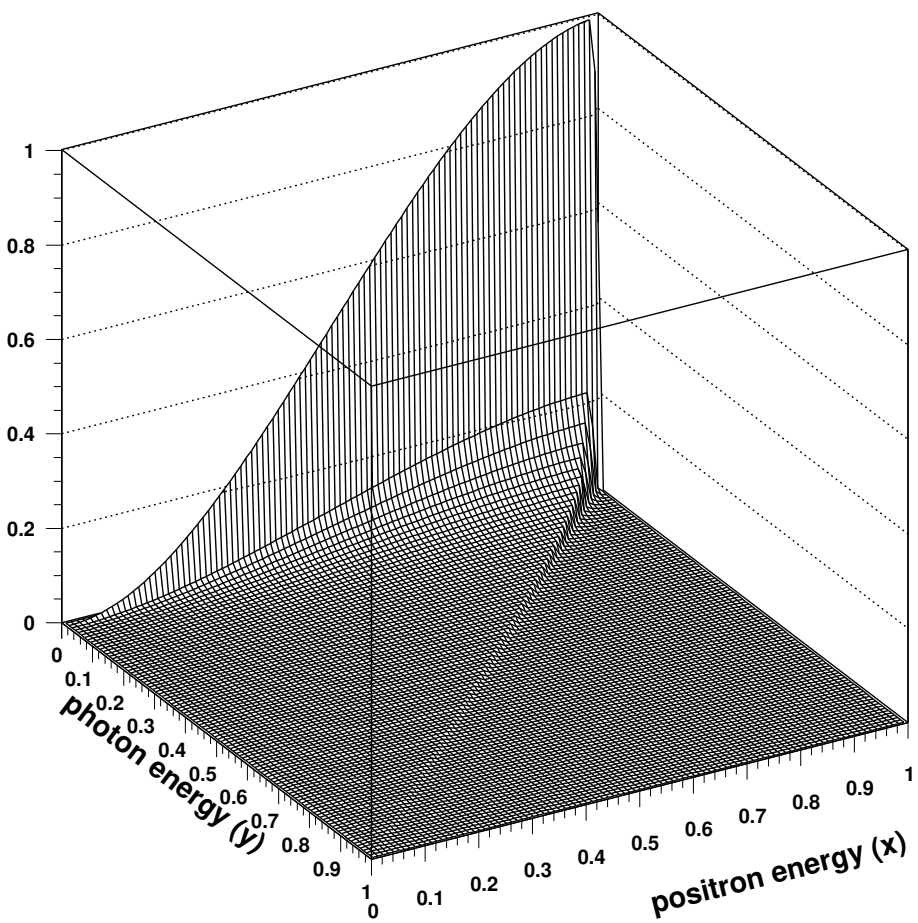

FIG. 4. Decay probability distribution of $\mu^{\pm} \to e^{\pm}\nu\overline{\nu}\gamma$ decay as a function of the $e^{\pm}$ energy ($x \equiv 2E_e/m_\mu$) and photon energy ($y \equiv 2E_\gamma/m_\mu$) for unpolarized muons. The decay probability is high at $x \sim 1$ and $y \sim 0$.

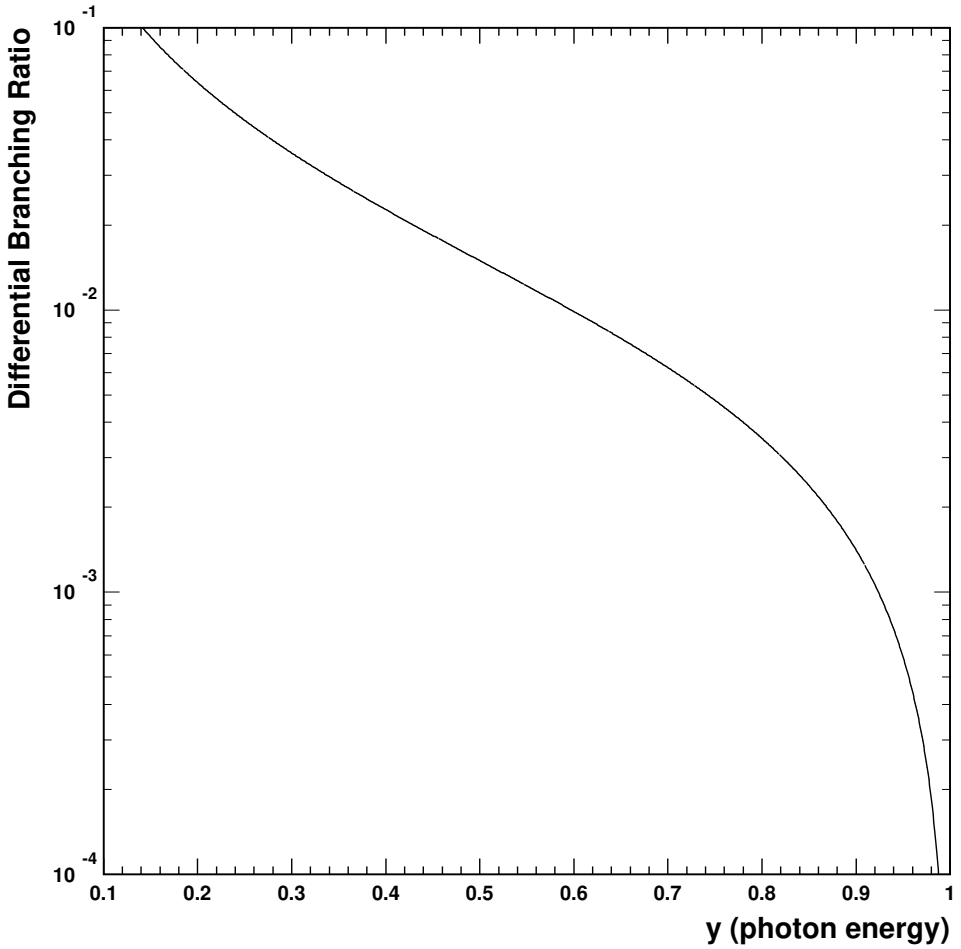

FIG. 5. Differential branching ratio of the $\mu^{\pm} \to e^{\pm}\nu\overline{\nu}\gamma$ decay as a function of the photon energy ($y \equiv 2E_{\gamma}/m_{\mu}$). This branching ratio is obtained by integrating over the e^{+} energy and the angle between an e^{+} and a photon.

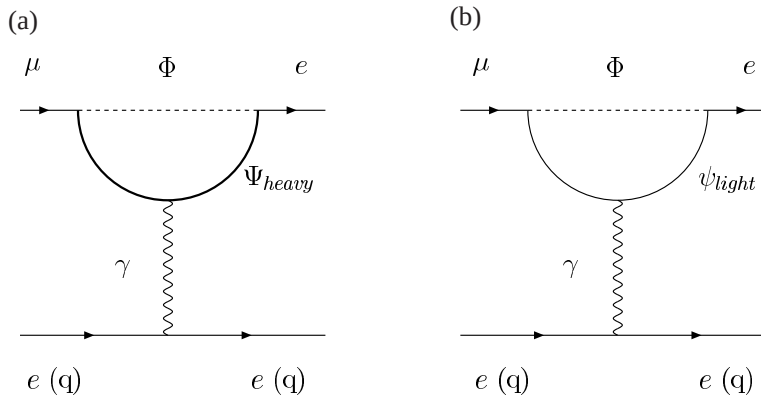

FIG. 6. Photonic penguin diagrams for $\mu - e$ transitions, such as $\mu^+ \to e^+e^+e^-$ or $\mu^- - e^-$ conversion. The cases of (a) a heavy particle (Ψ_{heavy}) in the loop, and (b) a light fermion (ψ_{light}) in the loop are shown. Φ is a scalar field.

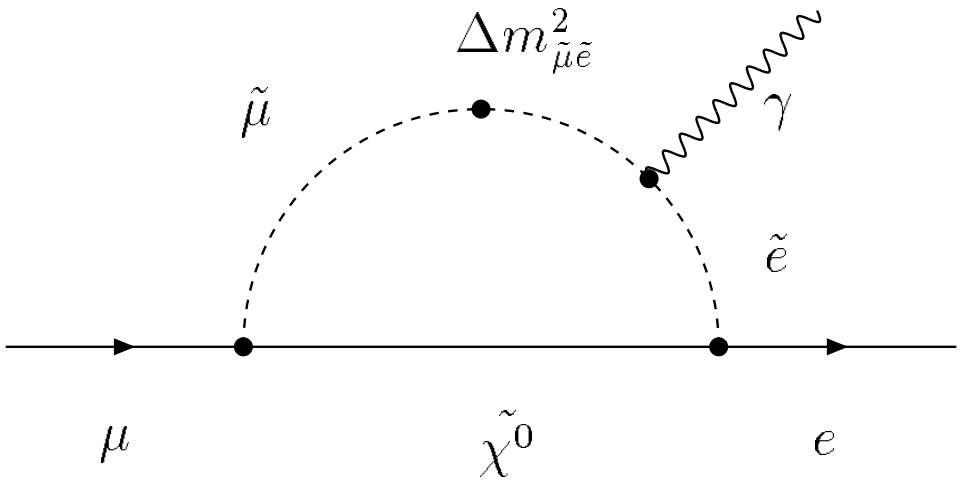

FIG. 7. Feynman diagram for $\mu^+ \to e^+\gamma$ decay induced by slepton flavor mixing ($\Delta m^2_{\tilde{\mu}\tilde{e}}$).

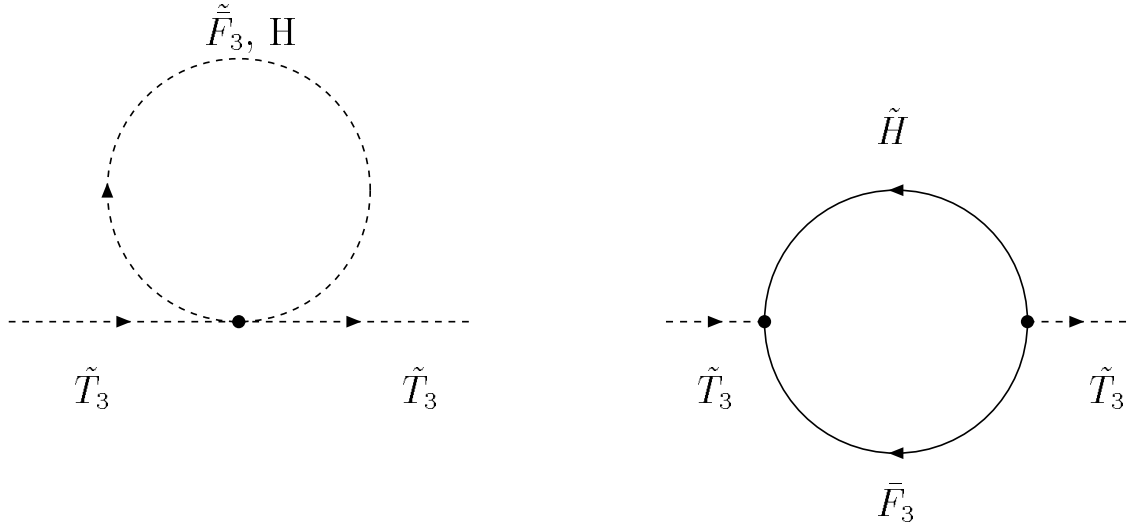

FIG. 8. Feynman diagrams which contribute to the renormalization effect on the slepton masses from the Planck to the GUT energy scales.

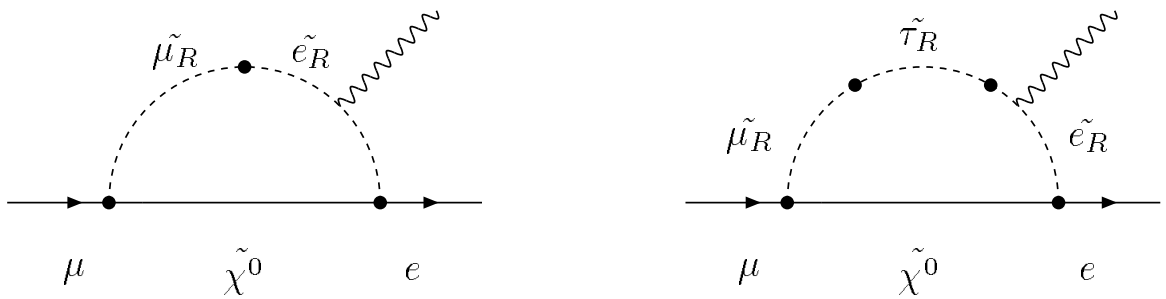

FIG. 9. Feynman diagrams for the $\mu^+ \to e^+\gamma$ decay in $SU(5)$ SUSY GUT. The closed blobs represent the flavor transitions due to the off-diagonal terms of the slepton mass matrices.

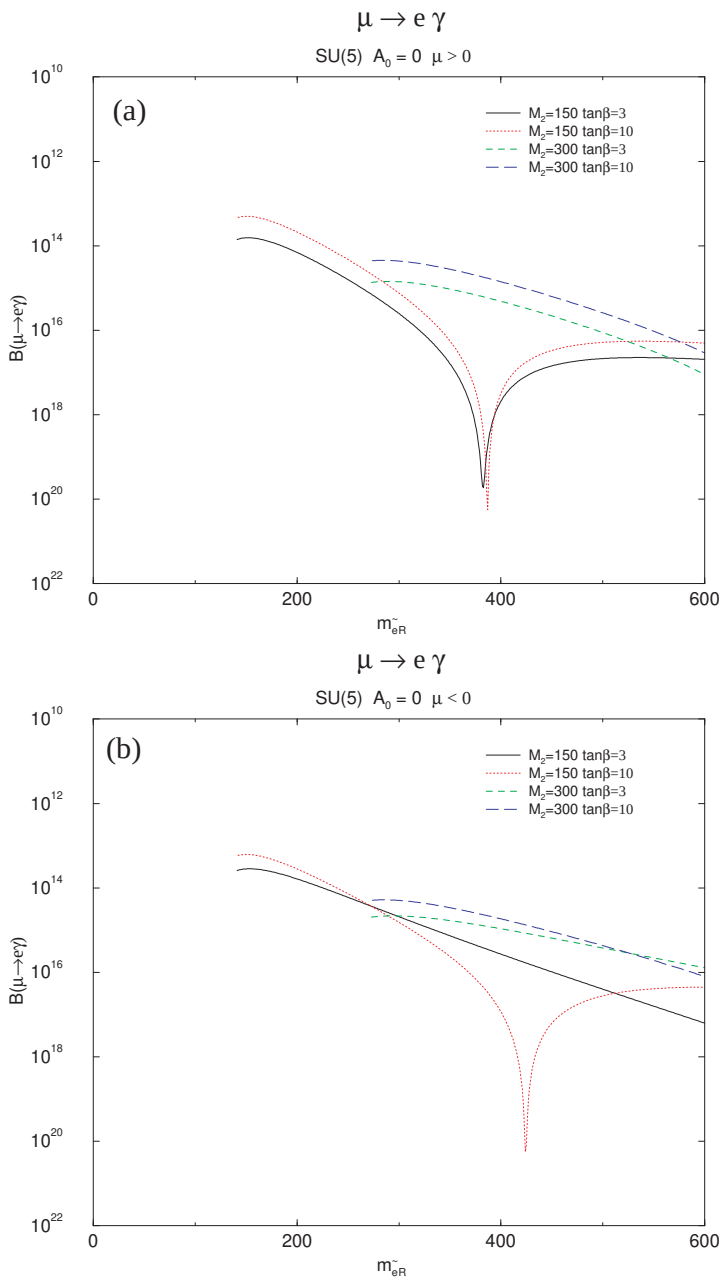

FIG. 10. Predicted branching ratios for the $\mu^+ \to e^+\gamma$ decay in the $SU(5)$ SUSY GUT based on the minimal supergravity model as a function of the right-handed slepton mass for four different sets of the SUSY input parameters of M_2 (the $SU(2)$ gaugino mass) and $\tan\beta$ (the ratio of the two Higgs vacuum expectation values). For the other parameters, the trilinear scalar coupling constant $A_0 = 0$ and $m_t = 175$ GeV. The following CKM matrix elements are used: $|(V_{CKM})_{cb}| = 0.04$ and $|(V_{CKM})_{td}| = 0.01$. (a) and (b) correspond to a positive and negative sign of the higgsino mass parameter μ, respectively.

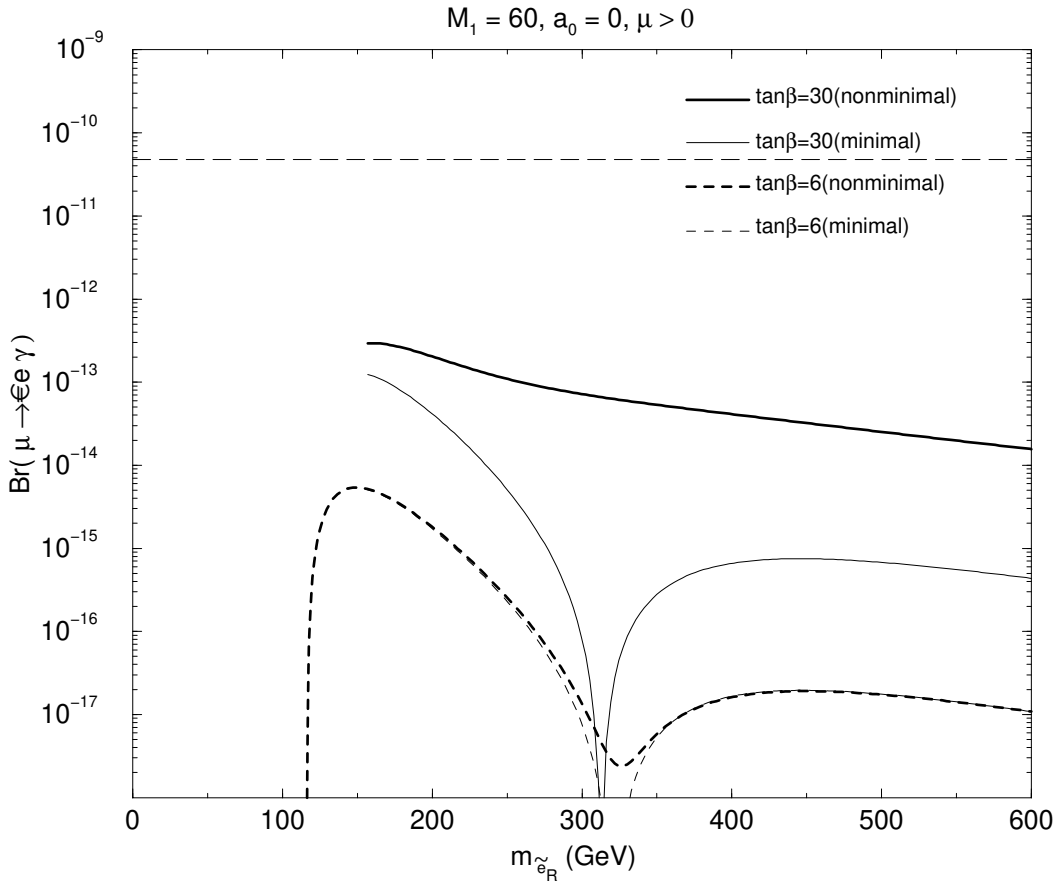

FIG. 11. Predicted $\mu^+ \to e^+\gamma$ branching ratios in the $SU(5)$ SUSY GUT model with higher dimensional operators in the GUT superpotential. The branching ratios are shown as a function of the right-handed selectron mass for $\tan\beta = 6$ (dashed lines) and 30 (solid lines). The thick lines are for the non-minimal case in which $V_{\bar{e}}$ and V_l are the same as V_{CKM}, and the thin lines are for the minimal case in which $V_{\bar{e}} = V_{CKM}$ and $V_l = \mathbf{1}$, where $V_{\bar{e}}$ is the mixing matrix for the right-handed sleptons, and V_l is that for the left-handed sleptons. The bino mass of $M_1 = 60$ GeV/c^2, the trilinear scalar coupling constant of $A_0 = 0$, the positive higgsino mass ($\mu > 0$), and the top quark mass of 175 GeV/c^2 are used. The experimental bound shown in the dashed line is $B(\mu^+ \to e^+\gamma) \leq 4.9 \times 10^{-11}$ (Bolton, *et al.* (1988)), and it is noted that the recent best limit is $B(\mu^+ \to e^+\gamma) \leq 1.2 \times 10^{-11}$ (Brooks, *et al.* (1999)). For detail on the calculations, see Hisano, *et al.* (1998b) (after Hisano *et al.*, (1998b)).

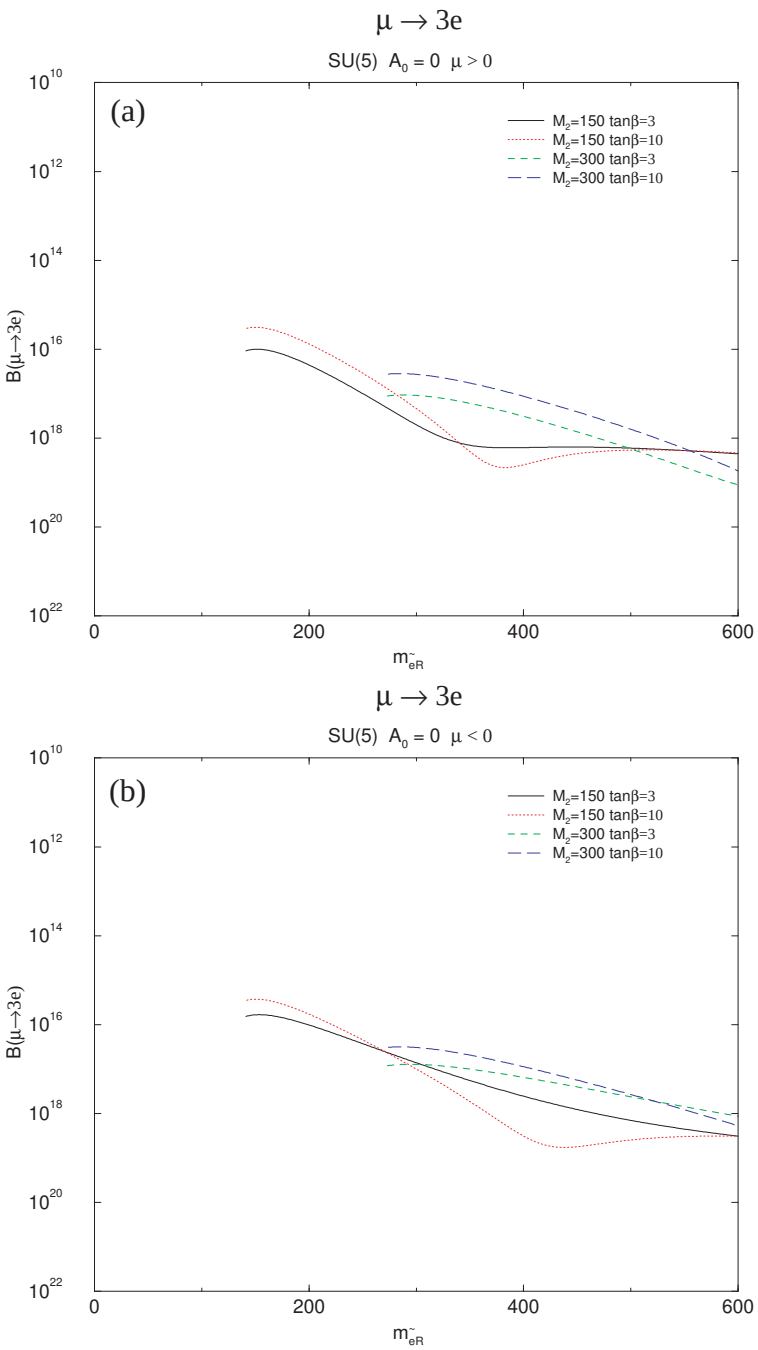

FIG. 12. Predicted branching ratios for the $\mu^+ \to e^+e^+e^-$ decay in the $SU(5)$ SUSY GUT based on the minimal supergravity model. The input parameters are the same as in Fig.9.

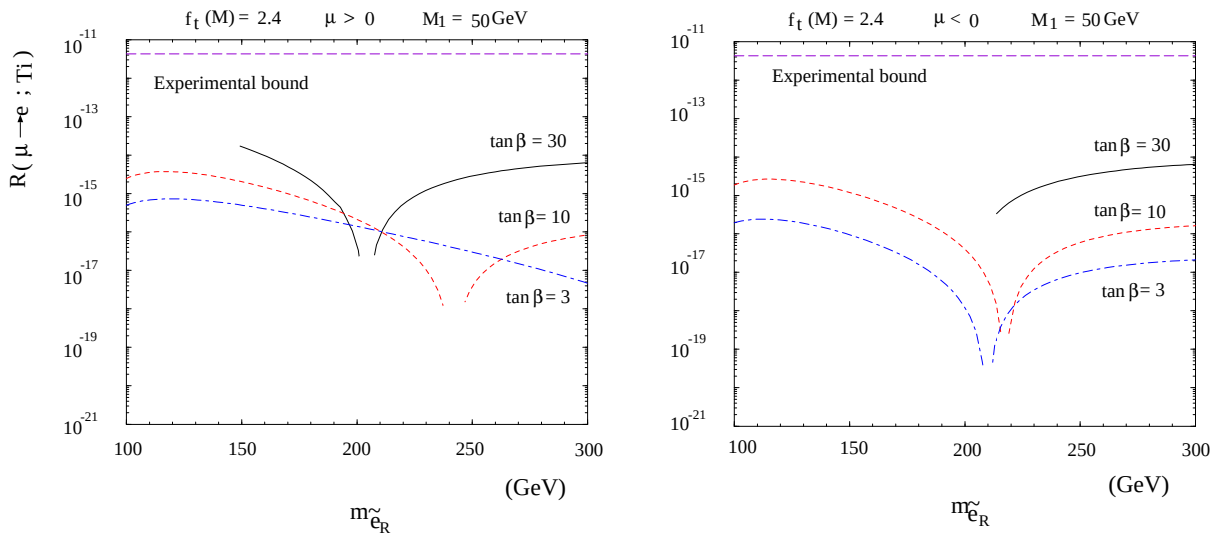

FIG. 13. Predicted branching ratios for the $\mu^- - e^-$ conversion in $SU(5)$ SUSY GUT. The SUSY gaugino mass of $M_1 = 50$ GeV, and the top Yukawa coupling of $f_t(M) = 2.4$ are used. The left and right figures correspond to a positive and negative sign of the higgsino mass parameter μ, respectively. The experimental bound shown is $B(\mu^- Ti \to e^- Ti) \leq 4.3 \times 10^{-12}$ (Dohmen, *et al.* (1993)), and it is noted that the recent best limit is $B(\mu^- Ti \to e^- Ti) \leq 6.1 \times 10^{-13}$ (Wintz (1998)) (after Hisano *et al.* (1997)).

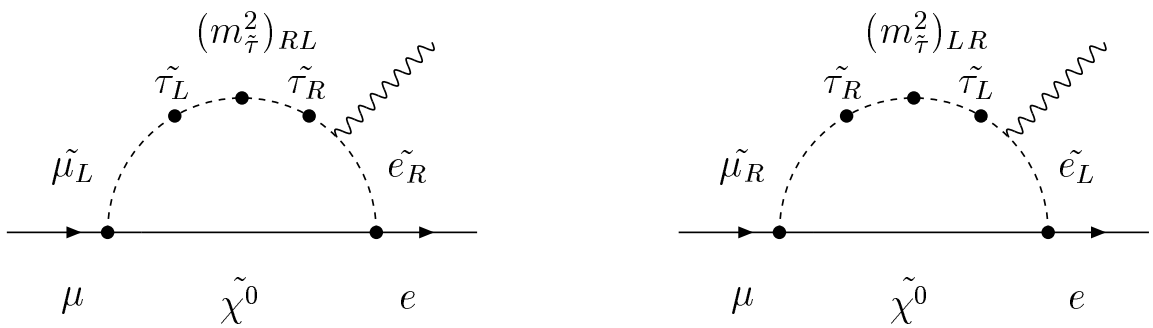

FIG. 14. Feynman diagrams in $SO(10)$ SUSY GUT which give dominant contributions to the $\mu^+ \to e^+\gamma$ process. $(m^2_{\tilde{\tau}})_{RL}$ and $(m^2_{\tilde{\tau}})_{LR}$ are proportional to m_τ.

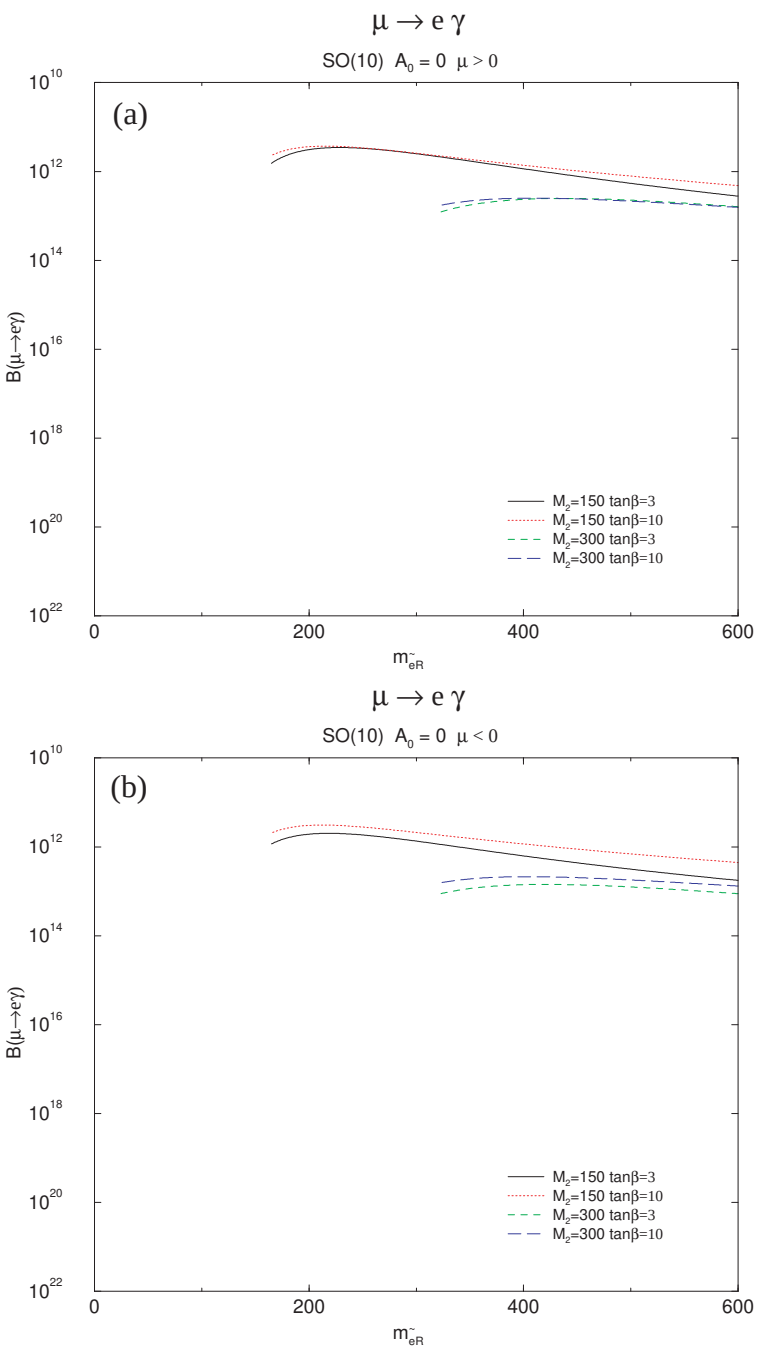

FIG. 15. Predicted branching ratios for $\mu^+ \to e^+\gamma$ decay in the $SO(10)$ SUSY GUT based on the minimal supergravity model. Input parameters are the same as in Fig.9.

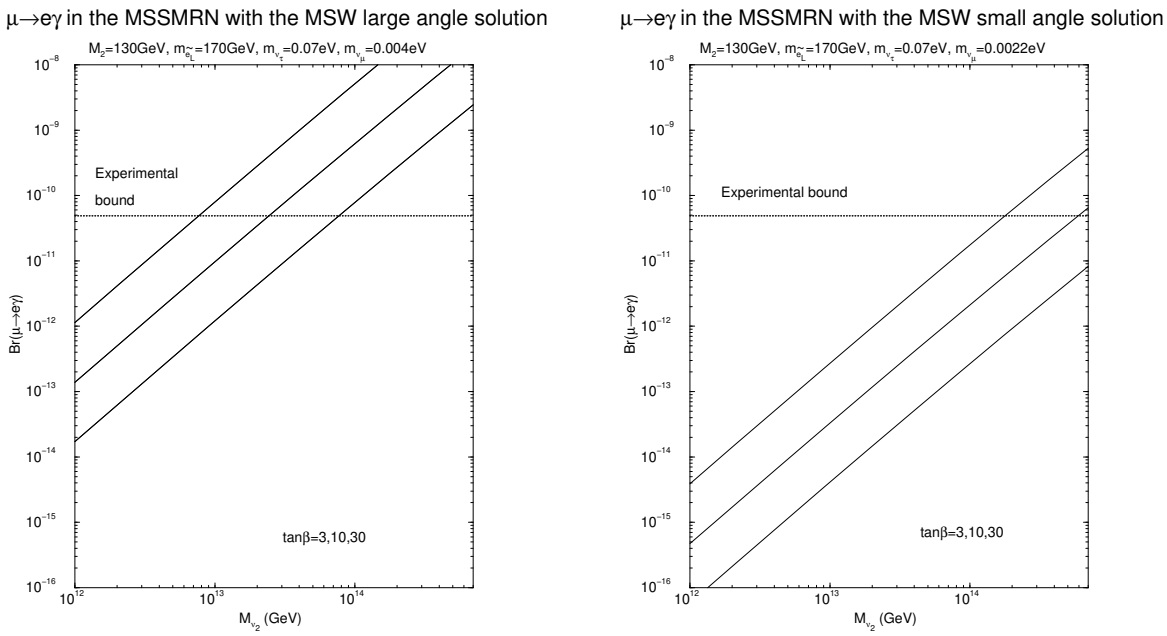

FIG. 16. Predicted branching ratios of $\mu^+ \to e^+\gamma$ decay as a function of the Majorana mass of the second-generation right-handed neutrino (M_{ν_2}) in the MSSM model with right-handed neutrino. They are given for the MSW large angle solution and the MSW small angle solution. The three curves correspond to $\tan\beta = 30$, 10, and 3 from top to bottom for both figures. The other parameters are shown in the top of the figures (after Hisano and Nomura, (1999)).

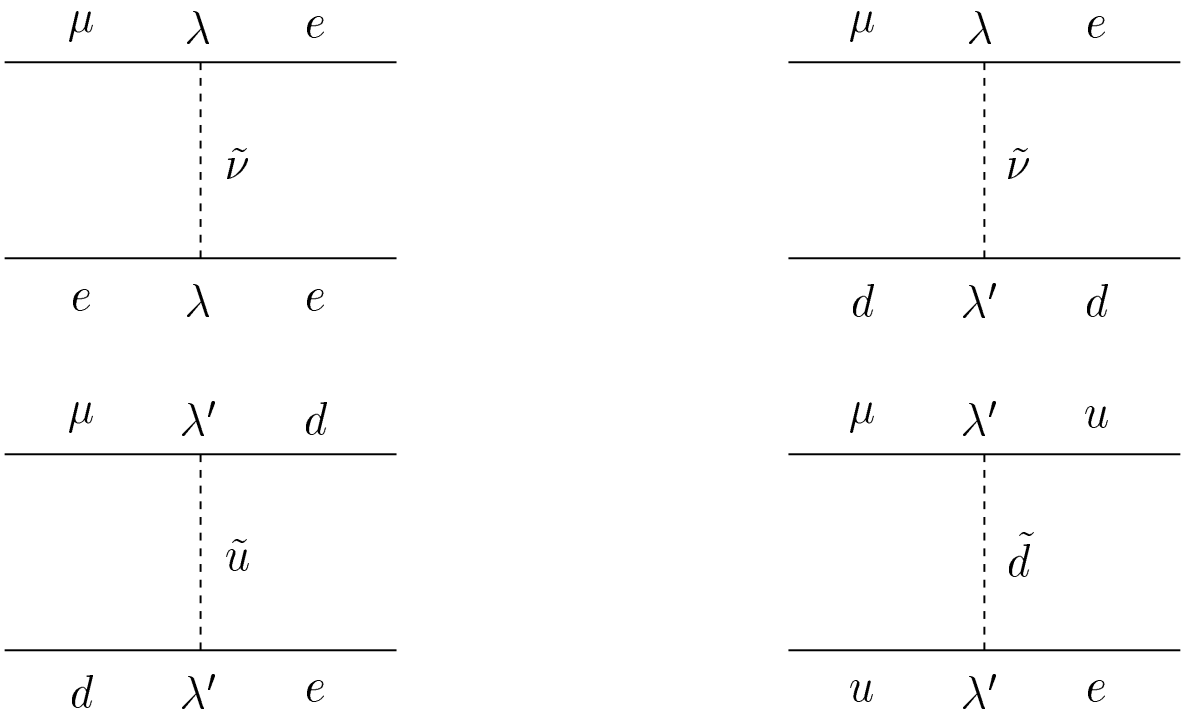

FIG. 17. Tree diagrams for LFV processes in SUSY models with R-parity violation.

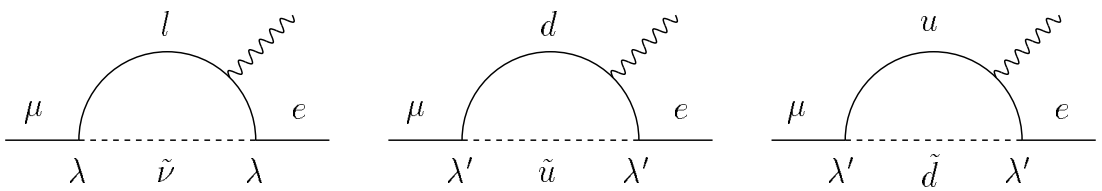

FIG. 18. One-loop diagrams for LFV processes in SUSY models with R-parity violation.

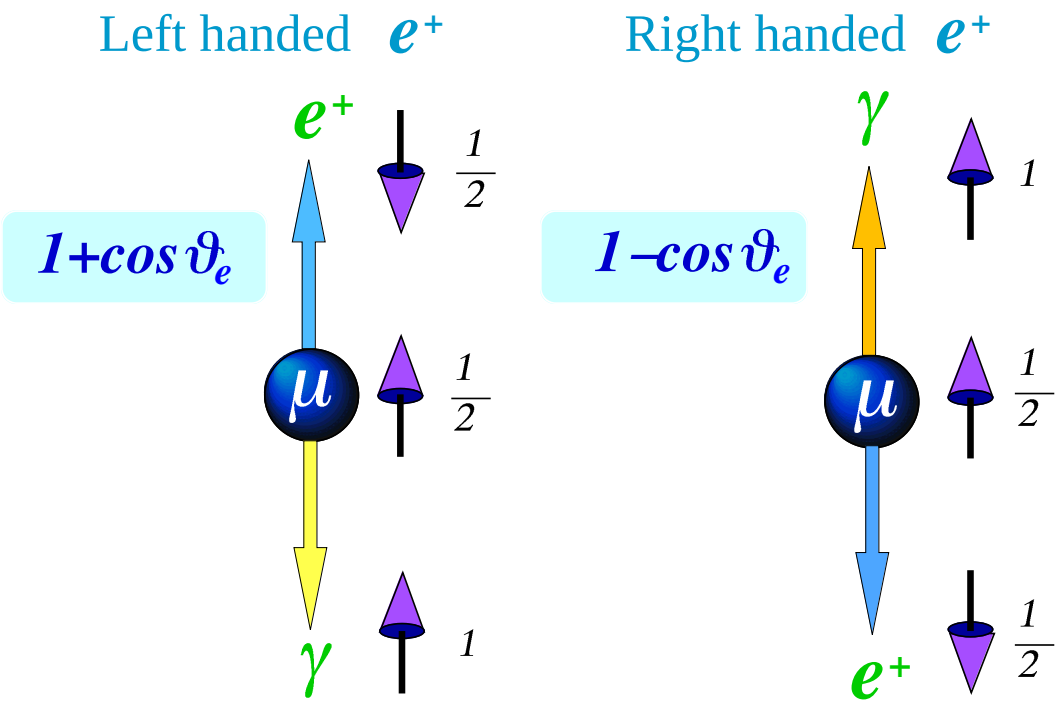

FIG. 19. Angular distribution of e^+ in polarized $\mu^+ \to e^+\gamma$ decay.

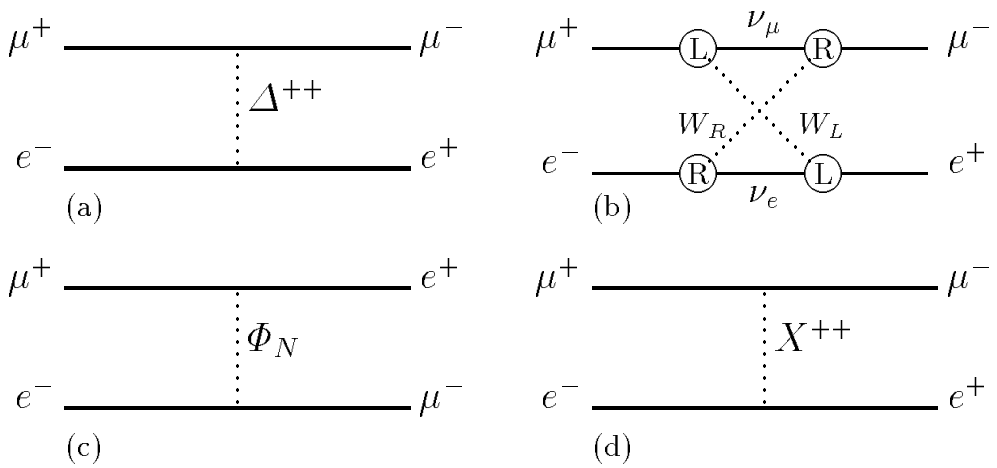

FIG. 20. Examples of theoretical models to induce Mu – $\overline{\text{Mu}}$ conversion. They are mediated by (a) a doubly charged Higgs boson, (b) heavy Majorana neutrinos, (c) a neutral scalar particle like a tau sneutrino, and (d) a bilepton X^{--} (after Willmann, *et al.*, (1999)).

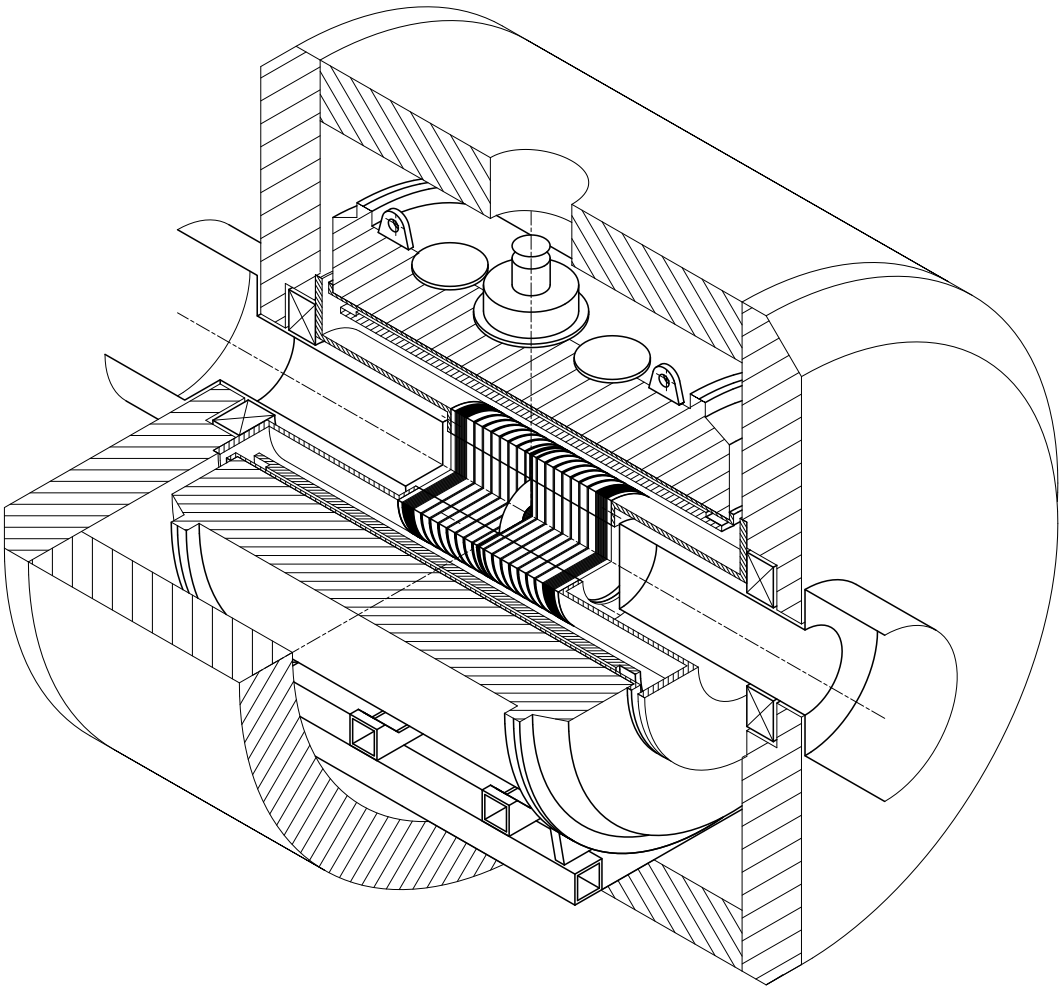

FIG. 21. Schematic view of the E614 detector at TRIUMF (provided by D.R. Gill).

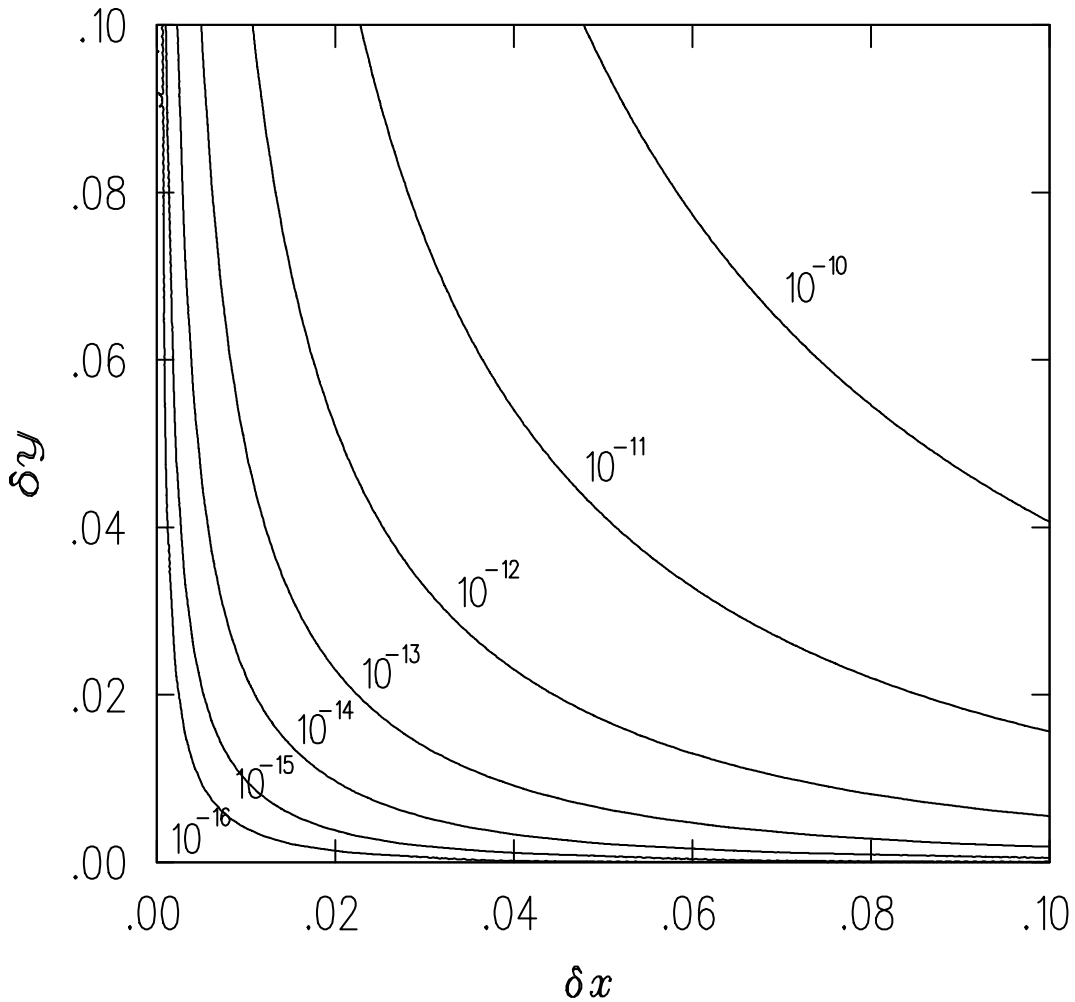

FIG. 22. Effective branching ratio of the physics background from the $\mu^+ \to e^+\nu_e\overline{\nu}_\mu\gamma$ decay as a function of the e^+ energy resolution (δx) and photon energy resolution (δy) (after Kuno and Okada, (1996)).

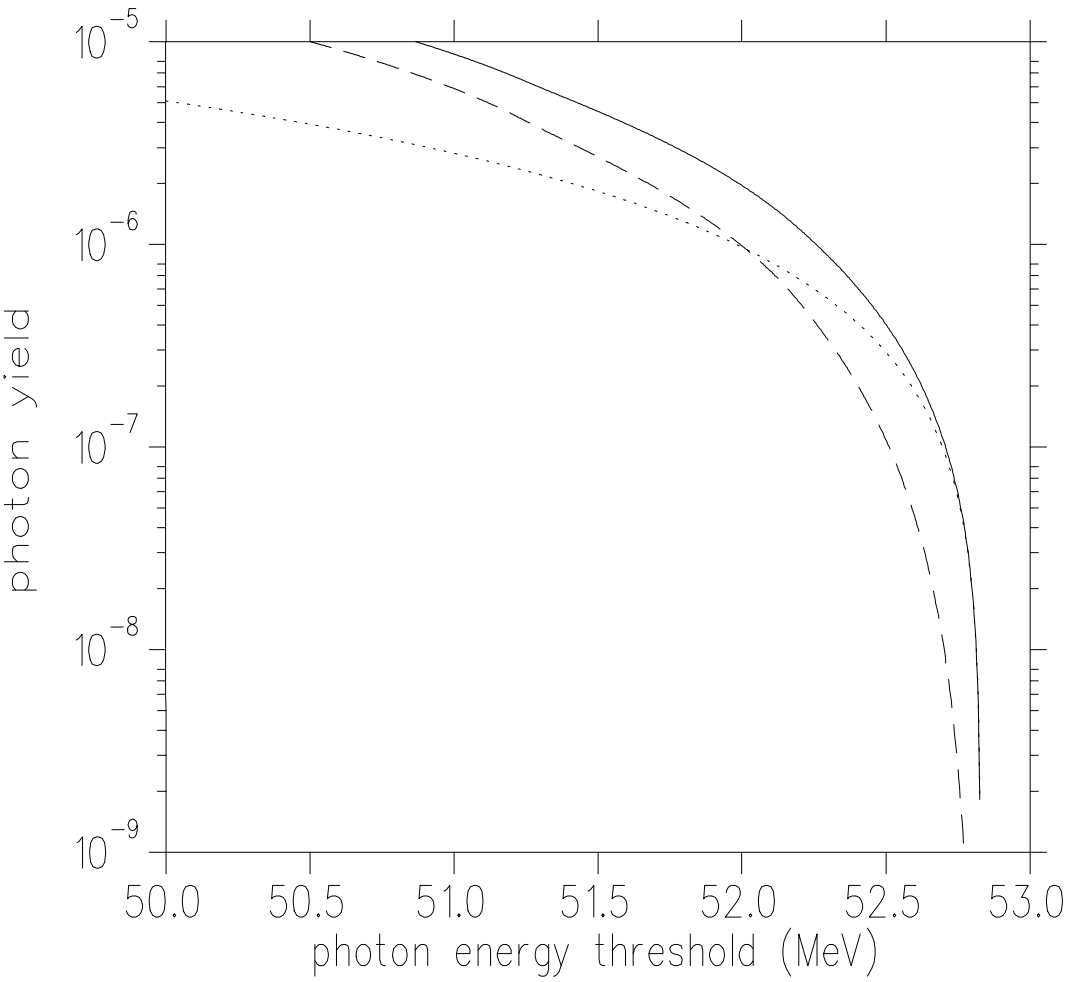

FIG. 23. Integrated rates of backgrounds from annihilation-in-flight (a dotted line) and radiative muon decay (a dashed line) as a function of the photon energy. The sum of the two is shown by the solid line.

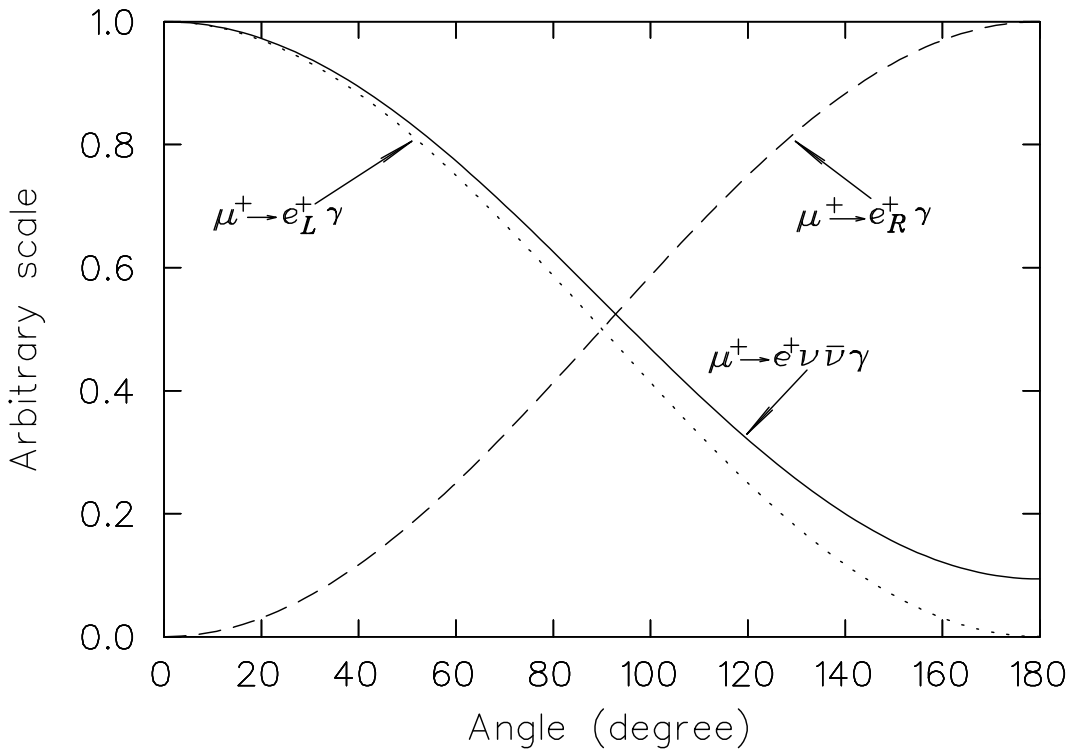

FIG. 24. Angular distribution of the physics background from the $\mu^+ \to e^+ \nu_e \overline{\nu}_\mu \gamma$ decay from polarized muons (a solid line). $\mu^+ \to e_L^+ \gamma$ (a dotted line) and $\mu^+ \to e_R^+ \gamma$ (a dashed line) decays are also shown (after Kuno and Okada, (1996)).

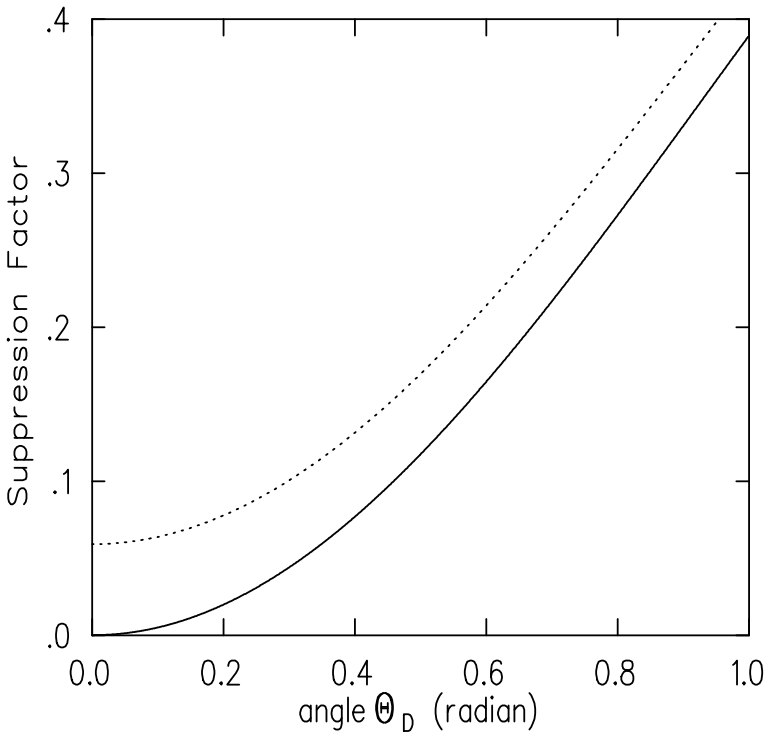

FIG. 25. Suppression factor of the accidental background in a $\mu^+ \to e^+\gamma$ search as a function of (half) the detector opening angle. The solid (dotted) line is for 100% (97%) muon polarization (after Kuno *et al.*, (1997)).

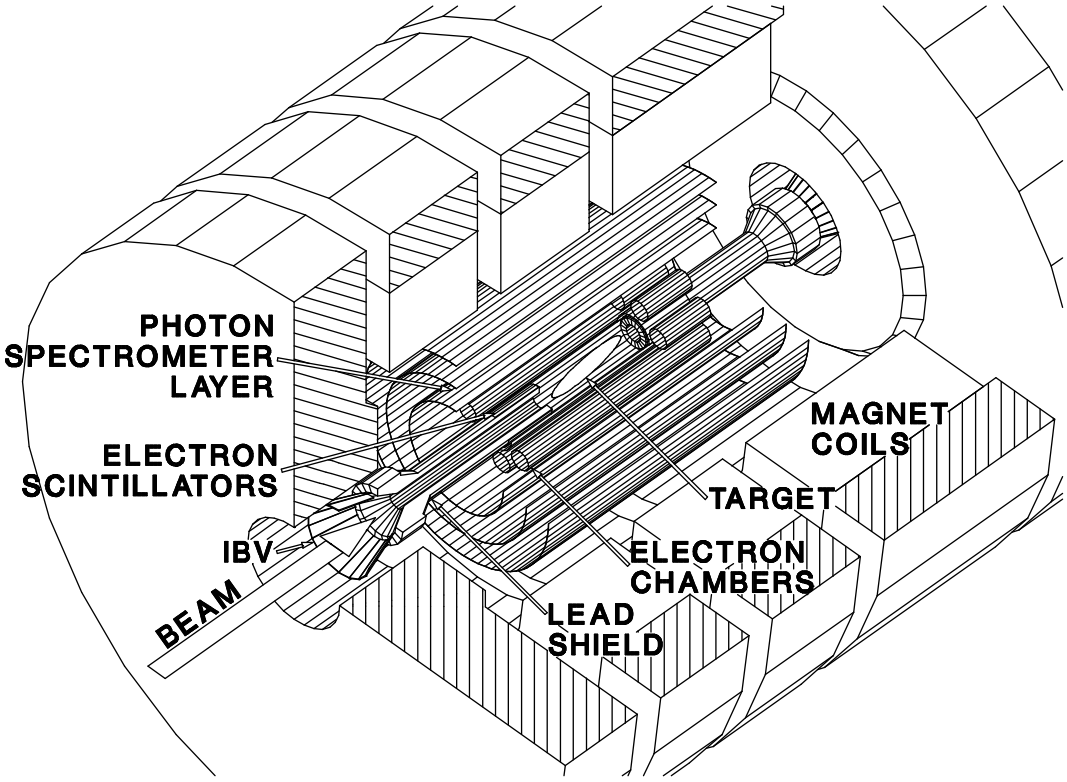

FIG. 26. Schematic layout of the MEGA detector (provided by R. Mischke).

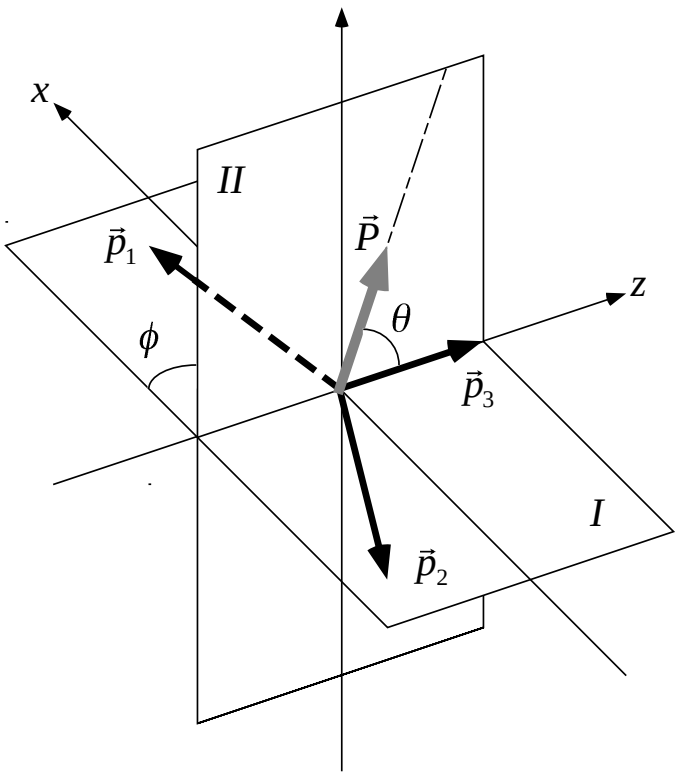

FIG. 27. Kinematics of the $\mu^+ \to e^+e^+e^-$ decay in the muon center-of-mass system, in which $\vec{p}_1, \vec{p}_2$ are the momentum vectors of the two e^+s and $\vec{p}_3$ is that of the e^-, respectively. The plane-I is the decay plane on which $\vec{p}_1$, $\vec{p}_2$, and $\vec{p}_3$ lie. The plane-II is the plane in which the muon polarization vectors, $\vec{P}$ and $\vec{p}_3$, are located (after Okada, *et al.*, (1999)).

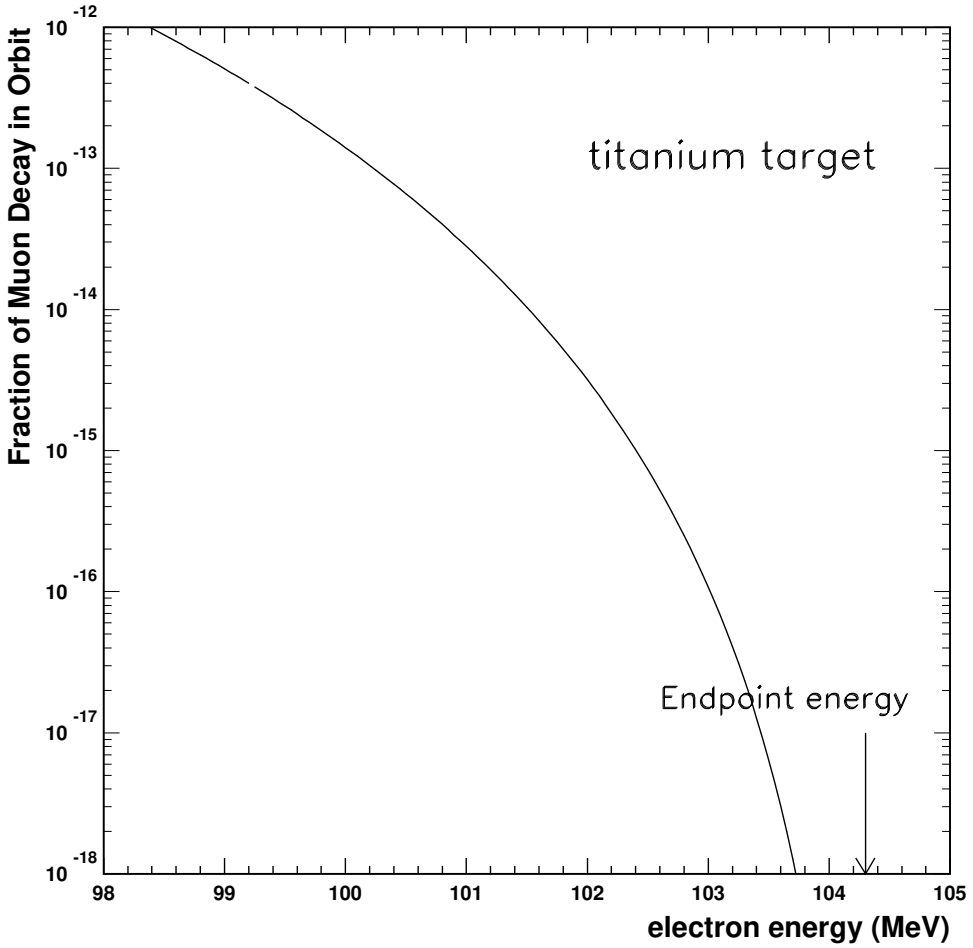

FIG. 28. Fraction of muon decay in orbit normalized to the total nuclear muon capture rate as a function of the e^- energy for a titanium target. It represents an effective branching ratio of muon decay in orbit as a background to the $\mu^- - e^-$ conversion. It was calculated by Shanker's formula in Eq.(147). The energy of the $\mu^- - e^-$ conversion signal in a titanium target is $E_{\mu e}$=104.3 MeV.

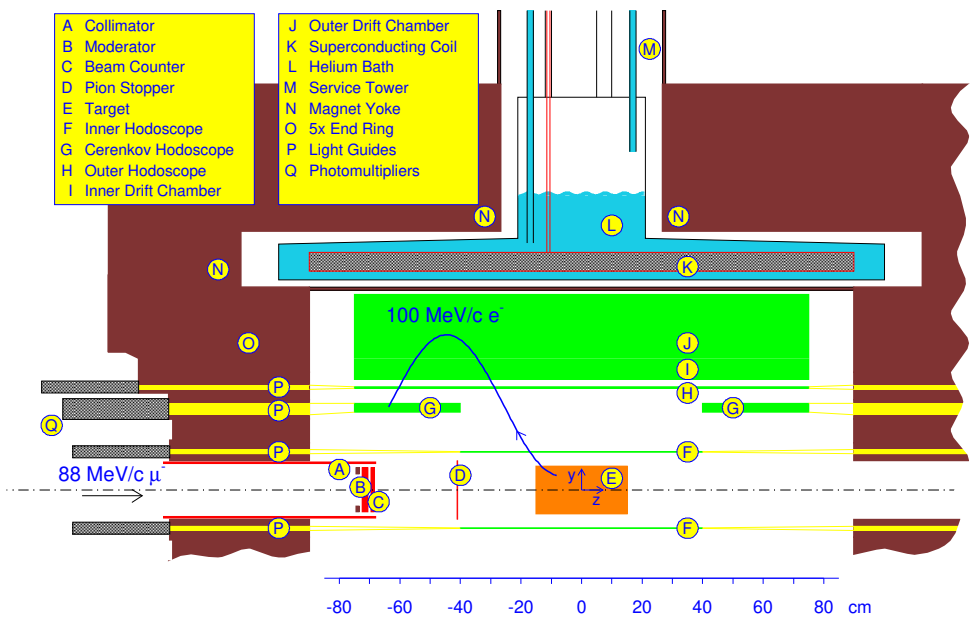

FIG. 29. Schematic layout of the SINDRUM-II detector (provided by P. Wintz).

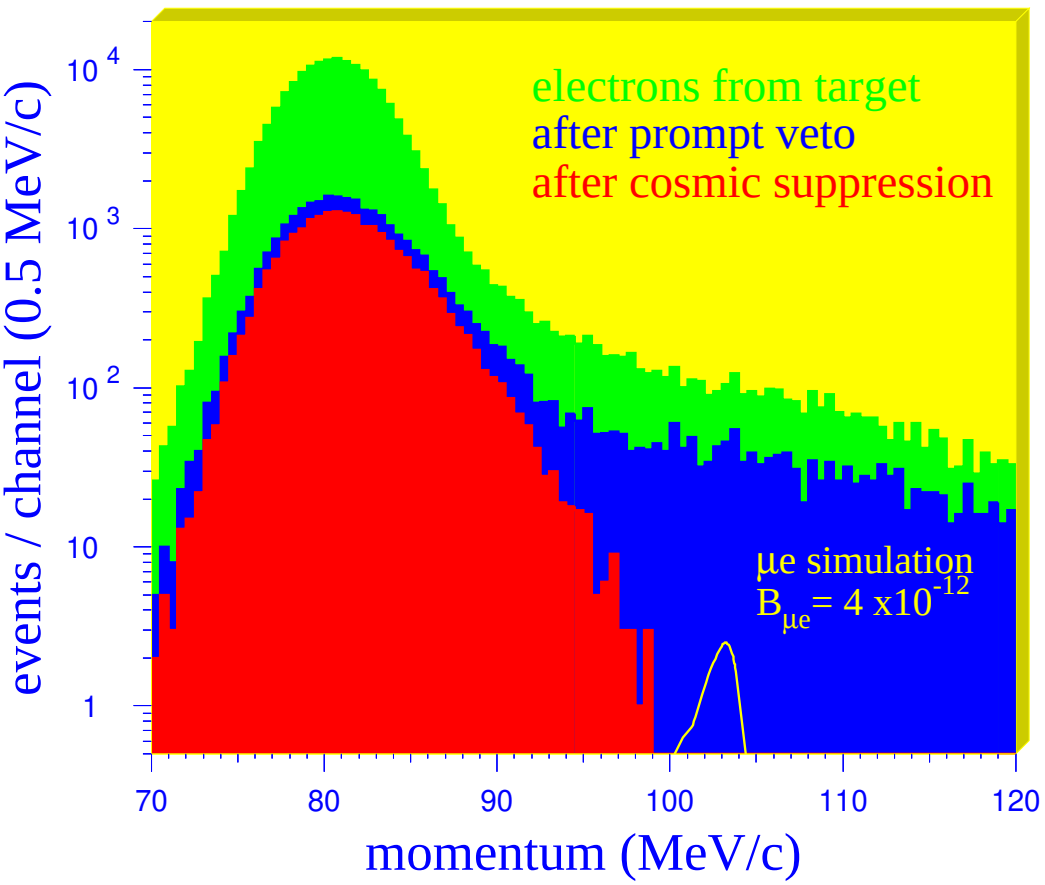

FIG. 30. Electron momentum distributions for the $\mu^- + Ti \to e^- + Ti$ reaction, measured by the SINDRUM-II detector, after the consecutive analysis cuts. The expected signal at $B_{\mu e} = 4 \times 10^{-12}$ is shown (provided by P. Wintz).

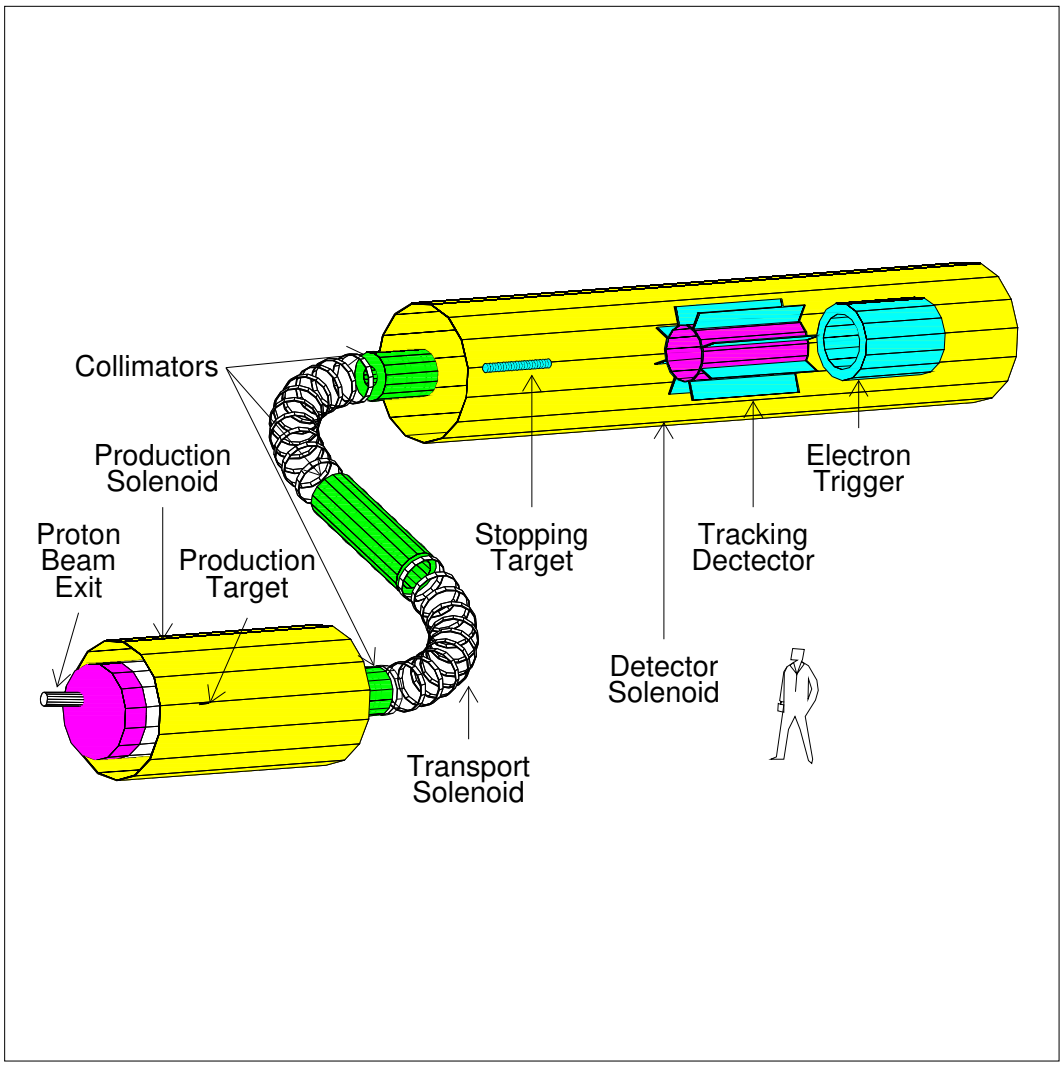

FIG. 31. Schematic layout of the MECO detector (provided by W.R. Molzon).

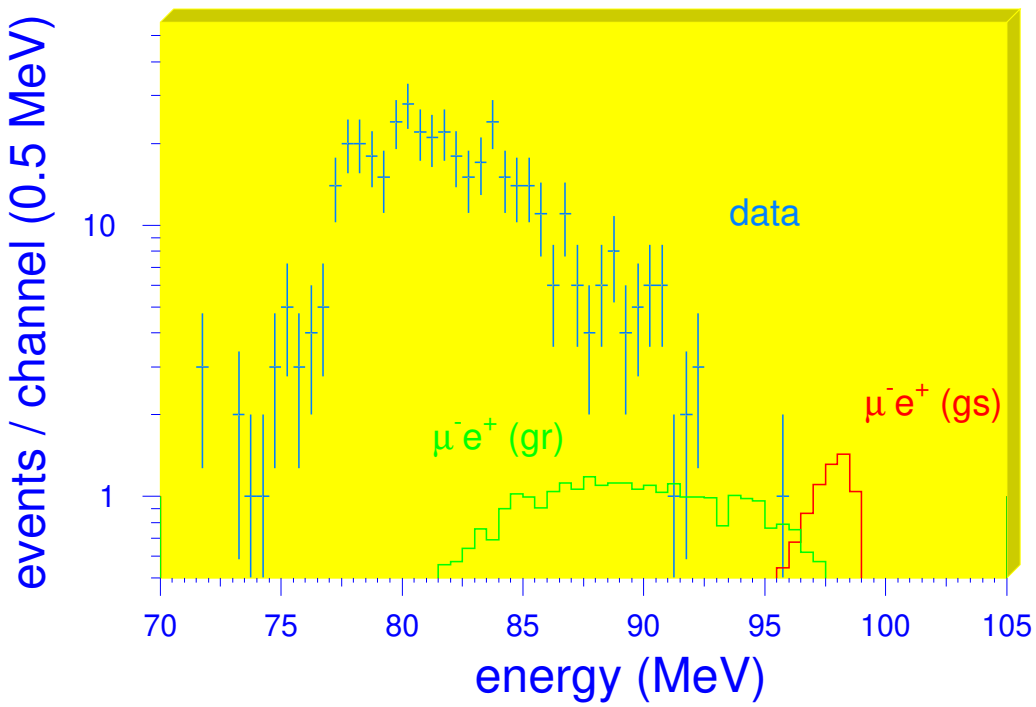

FIG. 32. Positron momentum spectra of the $\mu^- + Ti \rightarrow e^+ + Ca$ reaction. $\mu^- e^+$(gs) and $\mu^- e^+$(gr) are the expected signals for the transitions to the ground state and to the giant dipole resonance states, respectively (provided by P. Wintz).

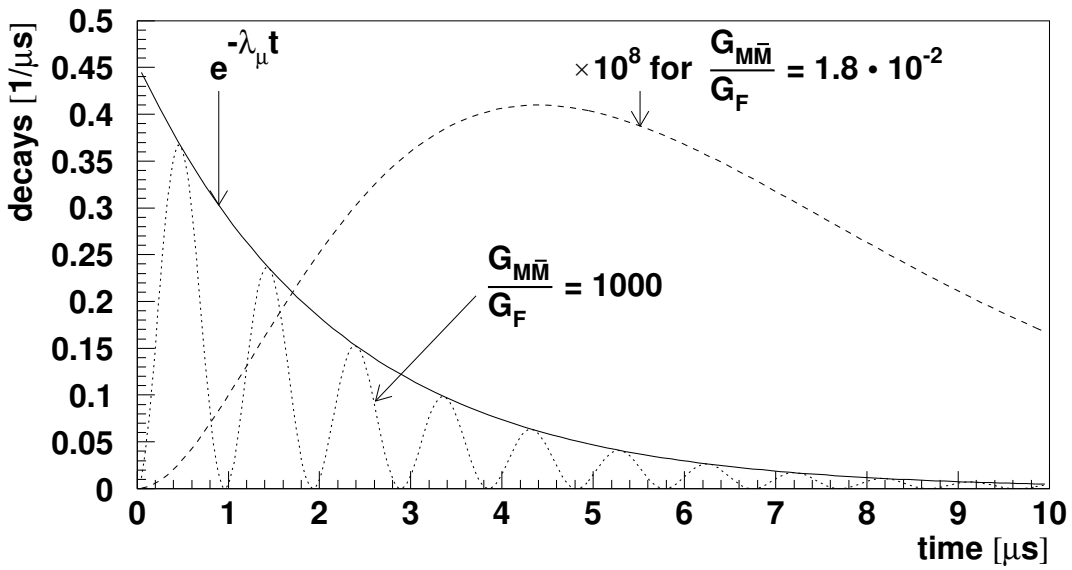

FIG. 33. Time dependence of the probability of anti-muonium decay when a pure muonium atom is created initially. The solid line represents the exponential decay of muonium. The decay probability of anti-muonium is given for $G_{M\overline{M}}/G_F = 1000$ ($G_{M\overline{M}}/G_F = 1.8 \times 10^{-2}$) for the dotted line (for the dashed line). In the latter case, the maximum probability occurs at about twice the muon lifetime (after Willmann and Jungmann, (1998)).

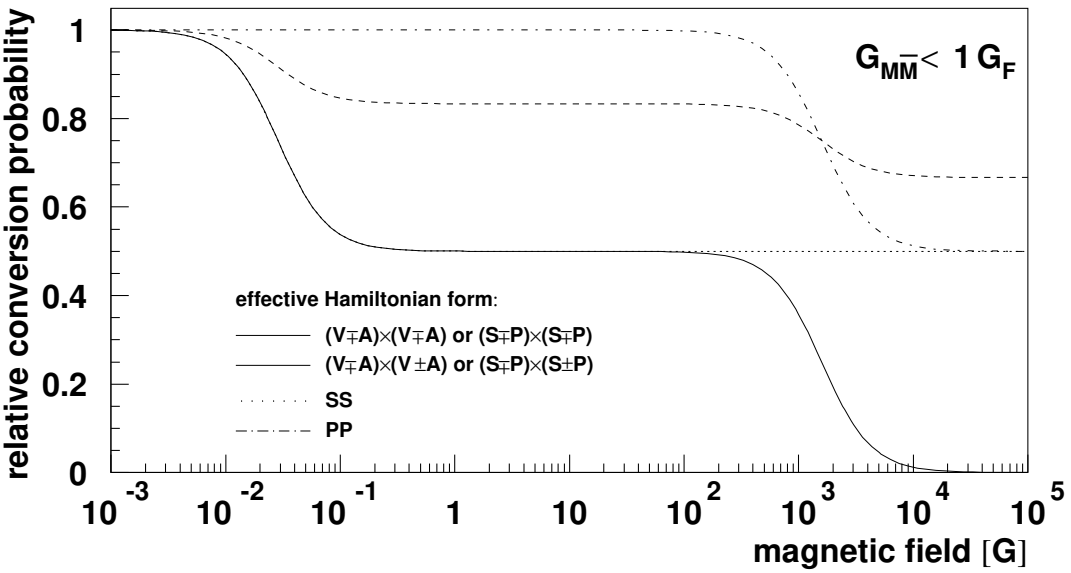

FIG. 34. Mu – $\overline{\text{Mu}}$ conversion rate for different interactions as a function of the external magnetic field (after Willmann and Jungmann, (1998)).

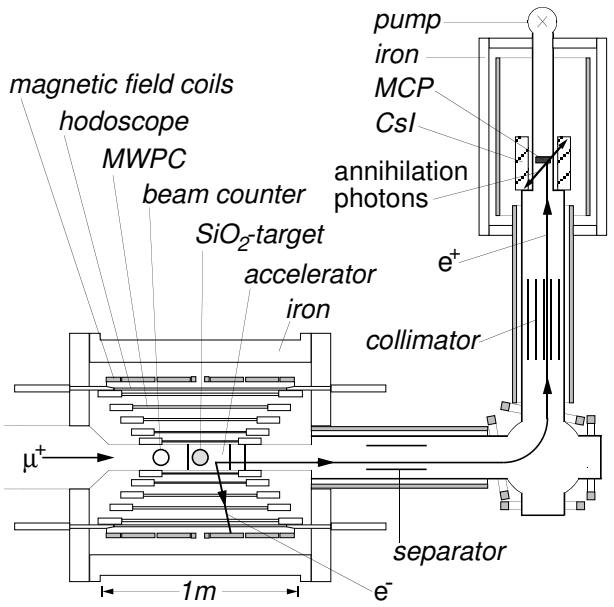

FIG. 35. Schematic layout of the detector for muonium-antimuonium conversion at PSI (after Willmann *et al.*, (1999)).

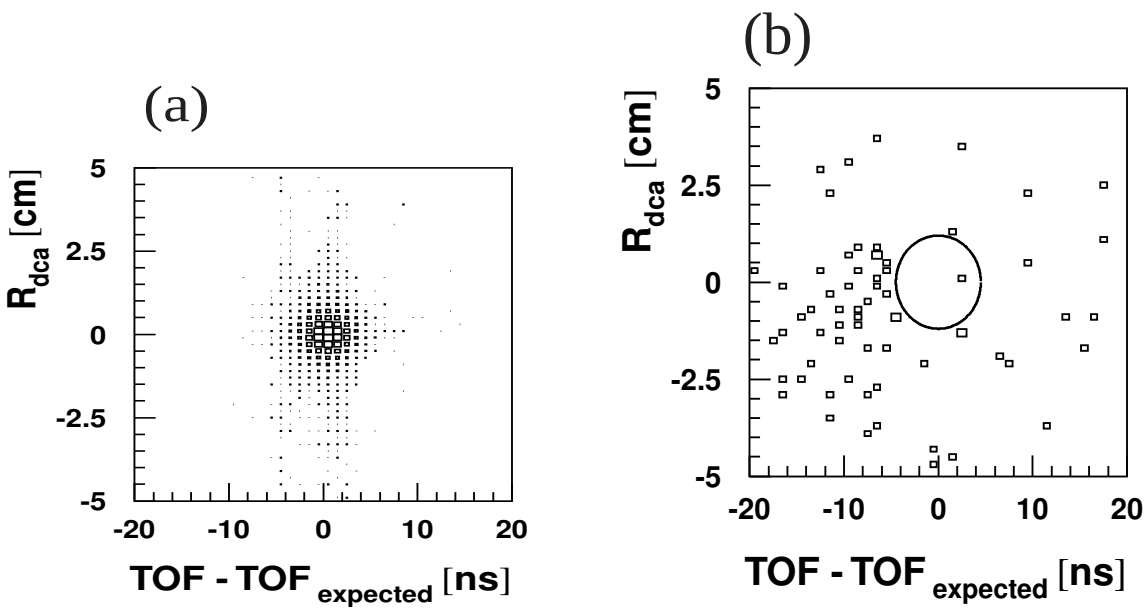

FIG. 36. Distribution of the distance of closest approach between the e^+ track and e^- track versus their timing difference in the experiment to search for Mu $-\overline{\text{Mu}}$ conversion. (a) Monte Carlo data and (b) real data (after Willmann *et al.*, (1999)).

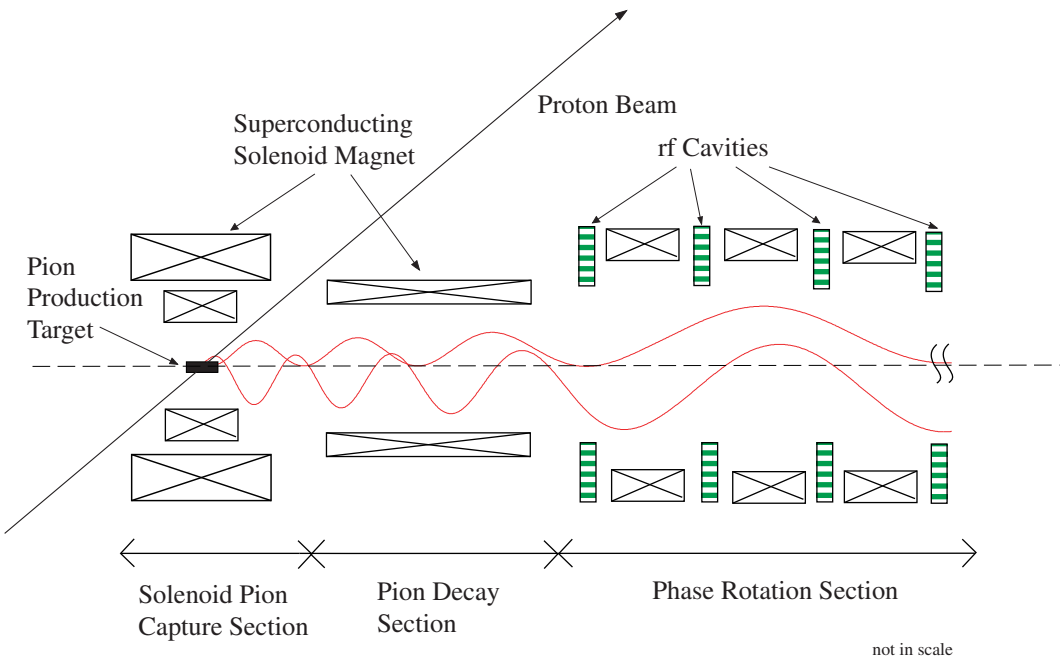

FIG. 37. Schematic layout of a high-intensity muon source.